UNIVERSITÉ DU QUÉBEC À MONTRÉAL

CARACTÉRISATION DE L'ÉTAT BALANCÉ DANS LES MODÈLES NUMÉRIQUES DE PRÉVISIONS DE L'ATMOSPHÈRE À MÉSO-ÉCHELLE

THÈSE

PRÉSENTÉE

COMME EXIGENCE PARTIELLE

DU DOCTORAT EN SCIENCES DE L'ENVIRONNEMENT

PAR

CHRISTIAN PAGÉ

MARS 2006

À

Peter Zwack

Ami et collègue.

REMERCIEMENTS

Je tiens à remercier et à rendre hommage à Peter Zwack, professeur au département des sciences de la Terre et de l'atmosphère de l'UQAM, pour la direction de ma thèse et son soutien financier. Peter Zwack m'a aidé à obtenir une meilleure interprétation physique de certains résultats et a contribué à la définition de la méthodologie ainsi qu'à la rédaction des articles. Il est décédé des suites du cancer ce 8 novembre 2005. J'adresse un remerciement particulier à Luc Fillion, de la division de la Recherche en Prévision Numérique d'Environnement Canada, pour sa grande disponibilité à discuter des résultats et analyses découlant de ma thèse, de ses conseils très pertinents pour la publication des articles, et pour sa contribution appréciée lors de la rédaction du dernier article. Je remercie Nicolas Chapelon, stagiaire de Météo-France, qui a aidé significativement à la première partie de ma thèse par des discussions et des questionnements en profondeur au sujet des résultats et analyses. Je remercie également plusieurs autres chercheurs, collègues et professeurs pour leur aide ponctuelle au cours de cette thèse. Parmi eux : René Laprise, Enrico Torlaschi, Daniel Caya, Amin Erfani, Yves Chartier, Jean-François Caron, mes collègues du groupe SCA, Claude Desrochers. Je remercie aussi Richard Harvey et Anne Armstrong pour les corrections de l'orthographe et de la syntaxe de cette thèse. Je tiens à remercier, en particulier, Jean-Louis Brenguier, du groupe GMEI/MNP du Centre National de Recherche Météorologique (CNRM) à Météo-France qui, lors de mon séjour de 11 mois au CNRM en 2001, m'a convaincu de faire une thèse de doctorat.

Je remercie également la Fondation canadienne pour les sciences du climat et de l'atmosphère (FCSCA) pour son appui financier par l'intermédiaire de bourses de recherche doctorale.

Un merci tout particulier et chaleureux à ma femme, Sandra Turner, de même qu'à mes deux enfants, Simon et Soline, pour leur soutien, leurs encouragements et leur compréhension. Merci également à mes parents pour leur soutien et leurs encouragements.

Finalement, je remercie tous ceux, amis, famille, collègues, étudiants, du Canada, de la France, qui sont restés présents avant, pendant et après le doctorat.

TABLE DES MATIÈRES

LISTE DES TABLEAUX

LISTE DES FIGURES

RÉSUMÉ

La présente recherche se propose de caractériser l'équilibre dynamique à méso-échelle, c'est-à-dire l'équilibre entre les forçages dynamiques et physiques et ce, pour des phénomènes météorologiques ayant une échelle horizontale de l'ordre de 15 à 150 km. Elle combine des simulations numériques et la théorie de la balance non-linéaire autant dans un contexte de simulations idéalisées que dans celui d'une simulation d'un cas réel. Elle s'inscrit dans un objectif à plus long terme d'améliorer les prévisions à court terme des quantités de précipitations, en développant une méthode permettant de contraindre l'état initial de la dynamique du modèle à un état de balance dynamique dans un contexte où les données de précipitations sont inclues au temps initial.

Dans un premier temps, l'étude porte sur l'identification précise de la suite des processus physiques impliqués dans l'ajustement vers un état balancé dans les modèles numériques en lien avec la théorie classique d'ajustement linéaire et ce, autant à petite qu'à grande échelle (phénomènes météorologiques d'un diamètre de 15 à 1500 km). Les analyses démontrent que, lorsque la taille du réchauffement est à petite échelle : (a) la latitude (force de Coriolis) n'a qu'une influence très limitée sur les mécanismes et sur l'état balancé ; (b) le temps d'ajustement vers l'état balancé est très réduit par rapport aux simulations à plus grande échelle ; (c) la stabilité statique de l'atmosphère a une influence significative sur le temps d'ajustement ainsi que sur l'état balancé lui-même ; (d) ces résultats sont en accord avec la théorie classique d'ajustement linéaire ; (e) il est possible d'utiliser l'équation de balance non-linéaire en combinaison avec une équation complète décrivant le mouvement vertical pour déterminer le vent divergent balancé à petite échelle.

Dans un deuxième temps, la méthodologie est appliquée à un cas réel tel que simulé par le modèle Global Environnemental Multi-Échelle (GEM) en mode aire limitée à une résolution horizontale de 2.5 km. Ce cas réel est caractérisé par de la convection profonde d'été en absence de baroclinicité et de dynamique en altitude significatives. Parmi les conclusions dégagées de l'analyse, il a été montré que : (a) le type de balance à cette échelle est principalement relié à la divergence horizontale ; (b) l'information apportée par les vents divergents dans la prévision à court terme du mouvement vertical (et donc de la précipitation) est très importante ; (c) il est possible de calculer les vents divergents balancés, à cette échelle, en utilisant une équation du mouvement vertical complète en combinaison avec l'équation de balance non-linéaire et en utilisant les tendances de température, causées par la convection, directement issues du modèle numérique ; (d) en imposant que les vents divergents soient balancés au temps initial, les prévisions de précipitations (évaluées par l'intermédiaire du mouvement vertical) sont remarquablement similaires par rapport à une simulation de contrôle.

En conclusion, le travail réalisé a permis principalement de développer une méthodologie appropriée pour caractériser l'état balancé dans les modèles numériques de prévision à méso-échelle pour des phénomènes météorologiques ayant un diamètre aussi petit que de l'ordre de 15 km, et utiliser des relations de balance dynamique dans les modèles numériques à une résolution horizontale de 2.5 km. Les contributions les plus importantes sont : (a) l'identification précise de la suite des processus physiques impliqués dans l'ajustement vers un état balancé dans les modèles numériques en lien avec la théorie classique d'ajustement linéaire ; (b) la caractérisation de l'état balancé à méso-échelle dans des simulation numériques idéalisées ; (c) la caractérisation de l'état balancé à méso-échelle dans un contexte de simulation réaliste d'un cas de convection profonde d'été ; (d) l'importance de l'information apportée par les vents divergents pour les prévisions de précipitations à méso-échelle ; (e) la démonstration qu'il est possible d'utiliser les tendances de température issues de la convection dans le modèle en combinaison avec l'équation de balance non-linéaire et une équation complète décrivant le mouvement vertical, afin de déterminer des vents divergents balancés ayant une bonne précision. Ainsi, le présent projet est innovateur pour l'utilisation des relations impliquant une balance non-linéaire à petite échelle, ainsi que pour l'utilisation des tendances de température issues directement de la convection du modèle dans des équations représentant un type de balance dynamique à cette échelle.

Les limites de la recherche portent principalement à la fois sur certains aspects des simulations idéalisées, de la méthode d'évaluation des vents divergents balancés et sur le type de situation réelle présentée ici. Des études complémentaires permettraient d'approfondir quelques-unes des limites identifiées.

SUMMARY

The current research aims at providing a characterisation of dynamical balance at mesoscale, i.e., the balance between the dynamical and physical forcings, for meteorological phenomena having a horizontal scale on the order of 15 to 150 km. It combines numerical simulations with the nonlinear balance theory in the context of idealized simulations as well as in a real case simulation. The longer term objective is to improve quantitative precipitation forecasts by developing a methodology in which the initial state of the numerical model's dynamics is constrained to a state of dynamical balance in the context where precipitation data is included at initial time.

First, the research identifies the precise sequence of physical processes involved in the adjustment toward a balanced state in numerical models, by making comparisons with the classical linear adjustment theory, from small to large scales (meteorological phenomena with diameters on the order of 15 to 1500 km). The analysis demonstrates that when the heating occurs at small scales : (a) latitude variations (Coriolis force) have a very limited impact on the mechanisms and the balanced state; (b) the adjustment time toward the balanced state is much reduced when compared to simulations at larger scales; (c) atmospheric static stability has a significant impact on the adjustment time and balanced state itself; (d) these results are in agreement with classical linear adjustment theory; (e) it is possible to use the nonlinear balance equation in combination with a complete vertical motion equation to determine the balanced divergent wind at small scales.

Second, the methodology is applied to a real case as simulated by the Global Environmental Multi-Scale (GEM) model in limited-area configuration at a horizontal resolution of 2.5 km. This real case is characterised by summer deep convection in the absence of significant baroclinicity and upper-level dynamics. Among conclusions resulting of the analysis of this case, it has been shown that : (a) the type of balance at this scale is mostly related to horizontal divergence; (b) information given by divergent winds from short-term forecasts of vertical motion (and thus precipitation) is very important; (c) it is possible to calculate balanced divergent winds at this scale by using a complete vertical motion equation in combination with the non-linear balance equation, and by using temperature tendencies generated by the model convection that are output directly by the numerical model; (d) when imposing a balance of the divergent winds at initial time, precipitation forecasts (evaluated from vertical motion) are remarkably similar when compared to a control numerical simulation.

To conclude, the research proposes an appropriate methodology to characterise a balanced state in mesoscale numerical forecast models for meteorological phenomena

having a diameter as small as 15 km, and to use dynamical balance relationships in numerical models using a horizontal resolution of 2.5 km. The most important contributions of this work are : (a) a characterisation of the precise sequence of physical processes involved in the adjustment to a balanced state in numerical models as related by the classical linear adjustment theory ; (b) the characterisation of balanced state at mesoscales in idealized numerical simulations ; (c) the characterisation of balanced state at mesoscales in the context of a simulated real case summer deep convection ; (d) the importance of information brought by divergent winds for the precipitation forecasts at mesoscales ; (e) the demonstration that it is possible to use model-generated convective temperature tendencies in combination with the non-linear balance equation and a complete vertical motion equation, in order to determine balanced divergent winds with a good accuracy. Thus, the current project is innovative in its use of equations involving a non-linear balance at small scales, as well as in its use of model-generated convective temperature tendencies in equations involving a dynamical balance at this scale.

Limits of this research deal primarily with certain aspects of idealized simulations, the methodology used to evaluate the balanced divergent winds and the type of real case simulated here. Further research may take into account parts of these caveats.

CHAPITRE I

INTRODUCTION GÉNÉRALE

Résumé

Le travail réalisé se propose de caractériser la balance dynamique à méso-échelle en utilisant des simulations numériques. Des simulations idéalisées, de même qu'une simulation d'un cas réel, sont utilisées. Cette caractérisation est rendue nécessaire car les modèles numériques de prévision auront très prochainement une résolution horizontale très fine, de l'ordre de 3 km, et il devient impératif de ré-évaluer les hypothèses de balance dynamique qui sont utilisées à plus grande échelle. La présente recherche s'insère dans un objectif d'améliorer les prévisions à court terme des quantités de précipitation en développant une méthode permettant de contraindre l'état initial de la dynamique du modèle à un état balancé en incluant la précipitation. Les objectifs spécifiques sont : la caractérisation de l'état balancé à méso-échelle en effectuant des simulations numériques idéalisées avec le Modèle régional canadien du climat (MRCC), en comparant avec l'analyse de simulations à l'échelle synoptique ; l'analyse de la suite de processus physiques intervenant dans le processus de l'ajustement à l'état balancé dans ces simulations numériques idéalisées ; la caractérisation de l'état balancé dans une simulation réaliste par le modèle Global Environnemental multi-échelle (GEM) avec une résolution horizontale de 2.5 km, et la détermination de l'impact sur la prévision de la précipitation, à méso-échelle, de l'utilisation de vents divergents balancés au temps initial. La méthodologie utilisée pour chacune des étapes est détaillée dans les chapitres correspondants aux articles publiés ou soumis pour publication.

Abstract

The current research aims at providing a characterisation of dynamical balance at mesoscale, using numerical simulations. Idealized simulations, along with a simulated realistic case, are used. This balance characterisation is now necessary because numerical forecast models will have quite soon very high horizontal resolutions, on the order of 3 km. Consequently, a re-evaluation of the dynamical balance hypothesis used in lower resolution configurations of these models must be performed. This research seeks, as its

main objective, to improve short-term quantitative precipitation forecasts by developing a method of constraining the initial state of the model's dynamics to a balanced state, when precipitation is included at initial time. The specific objectives are: characterisation of balanced state at the mesoscale using idealized numerical simulations of the Canadian Regional Climate Model (CRCM), by comparing numerical simulations analysis at synoptic scale; analysis of the sequence of physical processes which are involved in the balance adjustment process in idealized simulations; characterisation of the balanced state in a realistic case as simulated by the Global Environmental Multiscale (GEM) model using a horizontal resolution of 2.5 km, and identification of the impacts of using balanced divergent winds in the analysis on precipitation forecasts at mesoscale. The detailed methodology is presented in each chapter corresponding to published or submitted articles.

1.1 Problématique et contexte de la recherche

Les prévisions des précipitations à court terme (prévision de moins de 12h) présentent actuellement un défi de taille pour les modèles numériques de prévision météorologiques. Ces prévisions sont cruciales au niveau environnemental à plusieurs niveaux, par exemple pour les prévisions connexes comme celles de la pollution des cours d'eau et des nappes phréatiques par le ruissellement, les phénomènes d'érosion, les inondations affectant les écosystèmes, les crues subites (qui ont un impact significatif sur la pollution au niveau hydrologique), la dispersion des panaches de pollution atmosphérique par les vents et le lessivage de ceux-ci par la précipitation. Également, les événements extrêmes de précipitations intenses sont encore très mal prévus par les modèles numériques.

Un programme pan-canadien a été créé en 1999, pour une durée initiale de 5 ans, afin d'améliorer la prévision des situations météorologiques extrêmes. Ce programme est le « Programme canadien de recherche météorologique » (PCRM), qui regroupe le Service Météorologique du Canada (SMC) et plusieurs universités canadiennes dont l'UQAM et McGill. Ce programme est financé en grande partie par la « Fondation canadienne pour les sciences du climat et de l'atmosphère » (FCSCA). Ce programme se fait en collaboration avec le « World Weather Research Program » (WWRP) et le « United States Weather Research Program » (USWRP). Un des objectifs principaux de ce programme de recherche est l'amélioration de la qualité des quantités de précipitations prévues. Ce projet de recherche s'intègre à cette initiative.

La prévision numérique de l'atmosphère est principalement un problème de conditions initiales. En partant d'un estimé de l'état de l'atmosphère, exprimé en terme des variables d'un modèle numérique de prévision qui calcule les équations connues de la physique, celui-ci simule l'évolution temporelle de l'état de l'atmosphère. Il calcule aussi la précipitation et d'autres propriétés importantes pour les prévisions publiques du temps. La détermination de l'état initial (l'analyse) pour un modèle numérique de prévisions se nomme l'assimilation de données.

Un des problèmes importants pour la précision des prévisions de précipitations à court terme est l'assimilation des données de précipitation par les systèmes d'analyses opérationnels. Plusieurs groupes de scientifiques travaillant dans le domaine de l'assimilation de données y consacrent d'ailleurs leurs efforts. Il y a encore un débat dans la communauté scientifique pour trouver le moyen de correctement initialiser ces modèles numériques avec la précipitation observée afin de minimiser le temps d'ajustement (spin-up) des modèles. Ce temps d'ajustement est relié au fait qu'il existe un équilibre entre la masse et le vent dans l'atmosphère, et que si celui-ci n'est pas précisément représenté par un modèle numérique au temps initial, il en résulte un ajustement qui crée des oscillations artificielles dans la prévision du modèle numérique. Présentement, ce temps d'ajustement est trop important et cela affecte significativement la précision des prévisions à court terme, plus précisément les prévisions des précipitations. De plus, avec l'augmentation constante de la résolution horizontale des modèles numériques, cette problématique s'inscrit dans un autre contexte, celui de l'initialisation, de l'analyse et de la prévision à méso-échelle (d'environ 2 à 50 km de résolution horizontale).

Ainsi, plusieurs questions se posent afin de déterminer une méthode qui permettra éventuellement d'assimiler correctement les données de précipitation au temps initial des simulations des modèles numériques dans le but d'améliorer les prévisions à court terme. Ces données de précipitations doivent être représentées par les variables des modèles numériques, par l'intermédiaire d'un schéma de convection paramétrée ou explicite. Il faut donc ajuster les variables qui influencent la convection afin que le modèle numérique génère la précipitation observée. Ces variables sont principalement reliées à la température, l'humidité et les vents divergents. Il faut aussi que cette précipitation, obtenue de façon diagnostique ou prognostique, continue à évoluer à partir de l'état initial dans les simulations numériques sans créer d'oscillations indésirables causées par l'ajustement de l'atmosphère analysée aux équations du modèle numérique. Cela implique que l'état initial du modèle soit dans un état équilibré dit « balancé ». L'état balancé représente un état de l'atmosphère dynamique où les champs atmosphériques ne varient que lentement et ne causent pas d'excitation d'oscillations rapides et de forte amplitude.

L'approche de la présente recherche est de caractériser cet état balancé dans les simulations numériques à méso-échelle (environ 2 à 50 km de résolution horizontale), dans un contexte de modèles numériques à aire limitée. Cette caractérisation se fera en comparant avec des analyses de simulations idéalisées à l'échelle synoptique. Cela nécessitera principalement la détermination de la structure dynamique des champs atmosphériques à l'état balancé, de même que la série des processus physiques qui sont responsables de l'ajustement vers cet état balancé. L'influence de différents paramètres sur l'état balancé et l'ajustement vers celui-ci devra aussi être déterminés, tels que l'influence de la rotation de la Terre et de la taille horizontale du réchauffement. Cette caractérisation de l'état balancé permettra ensuite de déterminer une méthode afin d'utiliser cette information de balance pour déterminer l'état initial.

1.2 Objectifs

La présente recherche consiste donc à caractériser l'état balancé à méso-échelle dans les simulations numériques, au moyen des modèles numériques MRCC (Caya et Laprise, 1999) et GEM (Côté et al., 1998) dans un but de déterminer une méthode permettant de contraindre l'état initial de la dynamique du modèle à cet état balancé en incluant la précipitation, dans un contexte d'analyse simplifiée dans un premier temps, puis par la suite dans le contexte d'un cas réel. Le modèle MRCC sera utilisé pour effectuer des simulations dans un environnement très simplifié, de même que des simulations à plus grande échelle (synoptique), alors que le modèle GEM sera utilisé pour produire des simulations réalistes.

Les *objectifs à long terme* de ce projet de recherche sont de : (a) améliorer les prévisions à court terme des quantités de précipitation ; (b) développer une méthode permettant de contraindre l'état initial de la dynamique du modèle à un état balancé en incluant la précipitation, dans un contexte d'analyse variationnelle, c'est-à-dire une analyse multivariée.

Les *objectifs à court terme* sont articulés autour des objectifs spécifiques suivants :

- Effectuer des simulations numériques idéalisées avec le modèle MRCC, afin de caractériser l'état balancé à méso-échelle, en comparaison avec une analyse à l'échelle synoptique.
- Déterminer la séquence de processus physiques intervenant dans le processus de l'ajustement à l'état balancé dans ces simulations numériques.
- Caractériser le type de balance dans une simulation réaliste effectuée par le modèle GEM à une résolution de 2.5 km.
- Déterminer l'impact sur la prévision de précipitation, dans un cas réaliste tel que simulé par le modèle GEM, d'une initialisation avec les vents divergents balancés à méso-échelle.

1.3 Méthodologie générale

Étant donné que la présente thèse a été réalisée sous forme d'articles, la méthodologie utilisée pour chacune des étapes est détaillée dans les chapitres correspondant aux articles soumis pour publication (chapitres II, III et IV). Afin d'éviter toute répétition, seule la méthodologie générale est présentée ici.

Les objectifs spécifiques de la recherche mettent en évidence trois volets méthodologiques développés pour atteindre les objectifs. D'abord, des simulations idéalisées, réalisées avec le modèle MRCC développé à l'UQAM, permettent de caractériser l'état balancé à méso-échelle en comparant avec des analyses à l'échelle synoptique, de même que d'étudier les oscillations transitoires générées par l'ajustement du modèle numérique. Ce modèle a d'ailleurs déjà été utilisé précédemment (Thurre, 1998) pour l'étude de l'onde de Lamb dans ce même contexte de simulations idéalisées sans rotation. Ces simulations sont donc effectuées dans un contexte simplifié, ce qui permet de mieux isoler les processus physiques en jeu. Seule la partie dynamique du MRCC est utilisée (la partie des paramétrages physiques est désactivée). Le modèle est forcé par un réchauffement constant durant toute la simulation. Ce réchauffement est introduit directement et artificiellement dans la boucle interne d'intégration du modèle. Les caractéristiques de la distribution du réchauffement et l'état initial du modèle (taille horizontale du réchauffement, distribution

de température, vents initiaux) sont variées, de même que la configuration du modèle : différentes valeurs du plan-f (rotation de la Terre) et différentes résolutions horizontales. Ceci permet de caractériser l'état balancé atteint par le modèle numérique selon ces différentes conditions initiales et configurations du modèle, ainsi que d'évaluer l'impact sur les processus d'ajustement. De plus, les vents divergents et le mouvement vertical balancés sont diagnostiqués par l'intermédiaire d'une équation d'oméga non-linéaire balancée (Caron et al., 2006) incluant le terme de tendance du tourbillon agéostrophique (la seule hypothèse, à part l'hypothèse de balance non-linéaire, étant l'hydrostatisme). Ces diagnostics permettent d'évaluer les termes de ces équations balancées qui sont importants lors des processus d'ajustement.

Dans un deuxième temps, un cas réaliste est simulé par le modèle GEM à une résolution horizontale très fine de 2.5 km. Le modèle GEM a été développé à la Division de Recherche en Prévisions Numériques (RPN) à Environnement Canada, et a maintenant été étendu à une version en aire limitée, nommée GEM-LAM (Gravel et al., 2004; Erfani et al., 2005). Le modèle GEM est celui qui est actuellement utilisé pour effectuer les prévisions opérationnelles au Canada. Par conséquent des outils d'initialisation (filtre digital) et d'analyse variationnelle y sont intégrés, ceci justifie alors l'utilisation de ce modèle pour l'analyse d'un cas réaliste dans le cadre de la présente étude. En utilisant les résultats des simulations idéalisées réalisées avec le MRCC, la balance à cette échelle peut être mieux caractérisée dans le cas réaliste. Le mouvement vertical balancé est également comparé avec un mouvement vertical auquel un filtre digital est appliqué.

Dans un dernier temps, l'impact sur les prévisions de précipitations d'une initialisation dynamique balancée dans la simulation du cas réaliste est déterminé. Ces impacts sont mis en relief en comparant avec une simulation de contrôle ainsi qu'avec une simulation où les vents divergents sont mis à zéro.

1.4 Plan

La thèse est composée de cinq chapitres dont trois correspondent aux articles publiés ou soumis pour publication. Les chapitres I et II ont été combinés et soumis en un seul article pour des fins de publication. Le chapitre IV a été soumis en un seul article. Le *présent chapitre* introduit la pertinence du travail effectué en présentant la problématique, les objectifs, le plan et le contexte général de la recherche.

Les aspects plus théoriques de la recherche sont présentés principalement aux *chapitres II et IV*. Plus particulièrement, le chapitre II présente une mise en contexte exhaustive de la présente recherche par rapport aux méthodes d'assimilation de données en modélisation numérique de prévision du temps, de même que par rapport aux recherches déjà effectuées au niveau de la compréhension des phénomènes de balance. La suite du *chapitre II* ainsi que le *chapitre III* présentent en détail la suite de processus physiques qui sont impliqués lors de l'ajustement du modèle à partir d'un état initial au repos vers un état balancé lorsqu'un réchauffement idéalisé constant est appliqué, à l'échelle synoptique et à méso-échelle. L'impact de différents paramètres sur les processus d'ajustement ainsi que sur l'état balancé lui-même sont également évalués. Ceci permet également de caractériser l'état balancé. Les paramètres principaux qui sont évalués sont la dimension horizontale du réchauffement, la stabilité statique de l'atmosphère, ainsi que la latitude. De plus, la validité des approximations de balance non-linéaire est déterminée pour les simulations avec un réchauffement de plus petite échelle, c'est-à-dire d'environ 150 km (résolution horizontale du modèle de 3 km).

Le *chapitre IV* présente un cas réaliste tel que simulé par le modèle numérique GEM-LAM, ayant une résolution horizontale de 2.5 km. Le type de balance présent à cette échelle est déterminé et analysé. Dans un premier temps, il est évalué s'il est possible d'utiliser une équation de balance non-linéaire afin de déterminer la partie divergente du vent, tout en considérant le réchauffement produit par la convection tel que déterminé directement par le modèle numérique. Cette évaluation se fait également en comparaison avec l'application d'un filtre digital. Finalement, une validation de l'approche est effec-

tuée en comparant l'évolution des prévisions de précipitations (par l'intermédiaire du mouvement vertical) lorsque la partie divergente du vent au temps initial est balancée, par rapport à une simulation de contrôle ainsi qu'une simulation où la partie divergente du vent au temps initial est mise à zéro.

Bibliographie

Caron, J.-F., P. Zwack, et C. Pagé, 2006 : « DIONYSOS : A diagnostic tool for numerically-simulated weather systems ». *Atmos.-Ocean*, submitted. Technical related document see http ://www.dionysos.uqam.ca/doc/Dionysos.pdf.

Caya, D. et R. Laprise, 1999 : « A semi-implicit semi-Lagrangian regional climate model : The Canadian RCM ». *Mon. Wea. Rev.*, **127**, 341–362.

Côté, J., J.-G. Desmarais, S. Gravel, A. Méthot, A. Pantoine, M. Roch, et A. Staniforth, 1998 : « The operational CMC-MRB Global Environmental Multiscale (GEM) model. Part I : Design considerations and formulation. ». *Mon. Wea. Rev.*, **126**, 1373–1395.

Erfani, A., J. Mailhot, S. Gravel, M. Desgagnés, P. King, D. Sills, N. McLennan, et D. Jacob, 2005 : « The high resolution limited area version of the Global Environmental Multiscale model (GEM-LAM) and its potential operational applications ». *Preprints, 11th Conference on Mesoscale Processes, 24-28 October 2005*, Amer. Meteor. Soc., Albuquerque, NM, 1M.4.

Gravel, S., A. Erfani, et U. Gramann, 2004 : « A comparison of an interactive and non-interactive approach to mesoscale forecasting using the IOP-2B of MAP ». *Preprints, 11th Conference on Mountain Meteorology and the Annual Mesoscale Alpine Program (MAP), 20-25 June 2004*, Amer. Meteor. Soc., Bartlett, NH, 17.4.

Thurre, C., 1998 : « Étude de l'ajustement hydrostatique suite à un forçage diabatique dans un modèle pleinement élastique ». Thèse de Doctorat, McGill University, 124 pp.

CHAPITRE II

ANALYSIS OF DYNAMIC BALANCE ADJUSTMENT PROCESSES PART I : ROTATIONAL EFFECTS

Christian Pagé and Peter Zwack

Abstract

Dynamical balance is very important for a proper initialisation of numerical models. Since the introduction of primitive equation numerical models, the analysis is not necessarily in dynamic balance unless enforced. This holds true in the context of both 3D and 4D-var data assimilations. Furthermore, since the horizontal resolution of operational numerical models is evolving to resolutions ranging from 3 to 15 km, it is not clear what type of dynamical balance should be used at these scales, while at large scale it is well known. To address these issues, we propose here numerical experiments aiming at a better understanding of the mechanisms involved in dynamical balance adjustments and gravity wave excitation. As well, we examine the impact on these mechanisms of important parameters, such as static stability, rotation and higher scale (mesoscale) diabatic heating. Experiments are therefore performed on two scales: synoptic and mesoscale. Experimental results are also compared to classical theory.

First, underlying theory is briefly introduced, followed by an analysis of idealized simulations using a limited-area mesoscale model for two cases. The first case involves no rotation and the second has typical mid-latitude rotation. A synthetic heating is imposed in the model from the initial time step. An ω equation, based on nonlinear balance (NLB), is used to compare the modelled resulting balance to NLB theory. Time series of important parameters most influenced by balanced state adjustments are analyzed and compared to NLB as well as to classical theory. A description and an analysis of the mechanisms related to the dynamically balanced state adjustments are then presented, along with links to classical linear adjustment theory. An objective analysis technique is also developed here to determine the time when the model is in a near balanced state.

Résumé

La balance dynamique est très importante pour l'initialisation des modèles numériques. Depuis l'introduction des équations primitives dans la formulation des modèles numé-

riques, l'analyse utilisée comme état initial pour ces modèles n'est pas nécessairement en balance dynamique avec celui-ci, si elle n'est pas forcée. Cela est vrai également dans les contextes d'analyses variationnelles 3D et 4D. De plus, avec l'augmentation de la résolution horizontale des modèles numériques de prévisions opérationnelles, vers des valeurs de l'ordre de 3 à 15 km, il n'est pas certain quel type de balance dynamique devrait être utilisé à ces échelles, contrairement à la grande échelle où le type de balance est bien connu. Afin d'aborder cette problématique, la présente recherche propose des expériences numériques ayant comme but une meilleure compréhension des mécanismes impliqués lors des ajustements vers un état de balance dynamique, ainsi que lors de la génération d'ondes de gravité produites par ces ajustements. De même, l'impact sur ces mécanismes de paramètres importants tels que la stabilité statique, la rotation de la Terre et un réchauffement diabatique de fine échelle est examiné. En conséquence, de telles expériences sont faites à deux échelles spatiales : synoptique et méso-échelle. Les résultats des expériences sont également comparés à la théorie classique de l'ajustement géostrophique.

Après l'introduction brève de la théorie, une analyse de simulations idéalisées, qui utilisent un modèle numérique à méso-échelle, est présentée pour deux cas. Le premier est un cas sans rotation, tandis que le second est un cas avec une rotation typique des latitudes moyennes. Un chauffage idéalisé est imposé dans le modèle à partir du temps initial. Une équation diagnostique du mouvement vertical utilisant l'approximation de balance non-linéaire est utilisée afin de comparer la balance observée dans le modèle à la théorie de la balance non-linéaire. Par la suite, une description et une analyse des mécanismes reliées aux ajustements reliés à la balance dynamique sont présentés, en effectuant des liens avec la théorie classique de l'ajustement linéaire. Une technique d'analyse objective est également développée afin de déterminer le moment où le modèle est à l'état quasi-balancé.

2.1 Introduction

When using numerical models based on primitive equations, the analysis used as input is not in dynamic balance unless enforced. There is a scale separation between acoustic or gravity waves and the motions of interest, which are significant for weather forecasts. The motions of interest can be highly contaminated by unbalanced motions (including spurious gravitational oscillations generated artificially by numerical models in response to imbalances that can be present in the analysis) permitted by primitive equations. As a result, controlling gravitational oscillations in data assimilation with hydrostatic models has been under investigation over the last decade. Daley (1991) showed that initialisation is essential since it is required to generate a suitably balanced background field for the next analysis in a data assimilation cycle.

Several initialisation techniques were developed to control these gravity waves. One of the first was dynamic initialisation which was introduced in the late 1960s (digital filters). This technique integrates a model forwards and backwards with artificial damping terms and requires several hours of integration. It requires a timescale separation between gravity waves and the motions of interest, which is difficult to define at mesoscale. Another technique which was widely used was that of normal mode initialization. At first, linear normal mode schemes were developed, but then nonlinear schemes were needed to be successful in suppressing inertia-gravity oscillations.

Until recently, nonlinear normal modes have been used to control gravitational oscillations and to study balance in numerical models. In this context, the very well known Machenhauer balance condition (Machenhauer, 1977) has been widely used to control gravitational modes. However, according to Daley (1991), balance conditions like Machenhauer used as initialization constraints should be weak since these constraints define a region of the phase space where inertia-gravity activity is weak but not zero.

More recently, Zou et al. (1993) proposed a simple penalty method in an adiabatic 4D-var context. They show that gravitational oscillations can be controlled by a much simpler

procedure than penalty terms using the nonlinear model normal modes.

As stated in Daley (1991), balanced atmosphere and model states each satisfy different nonlinear multivariate relationships and therefore "the analyzed fields may not be well balanced when the analysis increments are large". This implies that the balance in numerical model space is not necessarily the same as the balance in observational space. A thorough analysis of balance (quasi-geostrophic and non-linear) has been performed by Errico (1990) using normal modes. He analyzed the degree of balance in numerical models at mesoscale-β ($20 - 200\ km$; $30\ mins - 6\ hrs$) and found that it is primarily a function of vertical scale and mostly adiabatic. Furthermore, he concludes that it is not highly dependant on the synoptic situation. However, we show in this present work that quasi-geostrophic and non-linear balance are both applicable at mesoscale-β, but that they can only be applied to the largest vertical scales and that non-linear and diabatic processes must be considered. Indeed, when these processes are taken into account to assimilate precipitation data in a 3D-Var data assimilation, Fillion (2002) has shown that unbalanced gravity waves can be excited. Also, he noted that gravity wave imbalance appears early in the minimisation process.

Using the forecast model as a strong constraint in 4D-Var data assimilation does not completely solve the balance problem. Polavarapu et al. (2000) have shown that 4D-Var still requires initialization. This is due to high-frequency spurious noise being generated if observations contain errors (Courtier and Talagrand, 1990). To overcome this, it is proposed to use a digital filter approach.

The Ensemble Kalman Filter (EnKF) technique can also be used to produce a balanced analysis. However, as Mitchell et al. (2002) demonstrate, the Schür product localisation must be relaxed. However there are still small imbalances left, which implies a requirement of a large ensemble. If the errors are small enough, it follows that their dynamics are approximately linear and then the resulting analyses are nearly balanced.

Some recent studies have also investigated the impact of high-frequency gravity waves generated by convective storms on general circulation of the middle atmosphere. Such

a study was performed by Alexander et al. (1995) in the context of a simulation of a 2D squall-line in a fully compressible numerical model.

The studies briefly presented thus far show that dynamic balance is important and must be considered, even in 3D-Var and 4D-Var data assimilation contexts. Many studies have focused on the balanced state itself or on varying aspects of the adjustment towards balance. Bannon (1996) examined the energetics of the final equilibrium of Lamb's nonlinear hydrostatic adjustment, while very recently, Chagnon and Bannon (2001) examined the initial and steady-state response of localized heating in a compressible atmosphere to evaluate compressibility approximations. Chagnon and Bannon (2001) used an analytic approach to determine the energy released (kinetic, elastic, potential, acoustic and gravity waves) and the remaining energy at steady state. They also studied the impact of boundary conditions and a rigid lid. The balanced (semigeostrophic) atmospheric response in an idealized case has also been studied in the context of a 2D squall line by Schubert et al. (1989). Their study uses a potential vorticity (PV) approach demonstrating that when a squall line propagates, the large-scale balanced flow is modified permanently. They clearly show that the modification to the large-scale flow depends on the ratio of the convective overturning time to the squall line passage time. Another study using the "PV-viewpoint" and a similar idealized setup of the present study was performed by Delden (2003). They nicely reproduced classical geostrophic balance response to tropospheric heating/cooling. They found that the question of whether the adiabatic adjustment time is shorter than the timescale of the applied heating is not relevant for the balanced state. They have also shown that the region outside of the heating is hardly permanently affected by the adjustment, even if the amplitude of the gravity wave oscillations are significant.

Some studies have also analyzed the mechanisms responsible for gravity wave excitations. It is important to understand well these mechanisms in order to be able to develop a proper methodology which will include balance at mesoscale when initialising numerical models. For instance, Shutts and Gray (1994) have studied the geostrophic adjustment process for a deep convection plume in a 2D simulation for a non-rotating and a highly

rotating (artificially high to reduce computer cost) atmosphere. They have calculated the energy budget for the final quasi-balanced state. They also developed an analytic model for the balanced state. A more detailed research on the mechanisms has been done by Fovell et al. (1992), who have identified that mechanical forcing of transient oscillating updrafts within a convective system is a process which generates vertically propagating gravity waves.

We propose here an analysis of the fully nonlinear dynamically balanced state and its adjustment processes and mechanisms in idealized simulations using a 3D numerical model. The model is based on the complete elastic Euler equations. The goal of this analysis is to understand the series of physical processes or mechanisms leading to a dynamically balanced state in 3D numerical model simulations. One of the main focus here is to understand the differences between balance and adjustment mechanisms at synoptic-scale vs. mesoscale within the context of operational data assimilations. One of the goals here is to analyze the series of physical processes by which gravity waves are generated; consequently they will not be filtered at the synoptic-scale. In the current context of high horizontal resolution operational forecasts and data assimilation, acoustic and Lamb waves are not important and will therefore not be discussed.

In part I, idealized simulations are run using a limited-area mesoscale model for two cases; one involving no rotation and the second, a typical mid-latitude rotation. The nonlinear balance ω equation, described in section 2.3, is used to compare the model resulting balance to nonlinear balance theory. Results are then presented in section 2.4 in terms of the time series of several fields which are most influenced by balance state adjustments. A description and an analysis of the mechanisms involved in the dynamically balanced state adjustments are then presented, along with comparisons to classical linear theory. The analysis technique developed here is used in part II to assess the effects of varying the diabatic heating horizontal size, static stability, as well as the presence of a background wind, on the dynamically balanced state and its adjustment mechanisms.

2.2 Numerical simulations

The numerical model used here for the simulations is the dynamical core of the Canadian Regional Climate Model (CRCM) as described in Caya and Laprise (1999). This core is based on the same formulation as that of the Mesoscale Compressible Community Model (MC2) (Benoit et al., 1997). This dynamical core was developed by Tanguay et al. (1990) and is based on the complete elastic Euler non-hydrostatic equations, using semi-implicit, semi-lagrangian schemes (SISL). The model does not enforce monotonicity constraints on SL advection, and a ∇^4 horizontal diffusion operator is applied.

The experimental setup is based on that of Thurre (1998), who studied the hydrostatic adjustment without rotation. Thus, in order to simplify the analysis and isolate the dynamics of the problem, the physics package of the model is put offline during these simulations, and the atmosphere is dry. Since the model's physics is not activated, there is no horizontal diffusion, friction, convection scheme nor topography. An f-plane and a horizontal plane projection are used to eliminate β and projection effects. The model has a rigid upper lid at 29654.5 m. The integration time-step used is 60 seconds and data is output every 15 minutes. Two special simulations were also performed with much shorter integration time-steps; 1 second and 5 seconds, in order to achieve a very detailed representation of the dynamics involved in the first 15 minutes and 30 minutes of the simulations since fields are varying very fast during this time period. Also, some important features and structures of the adjustment and balanced state are established during this time period.

To study the non-linear balanced state and its adjustment mechanisms, an artificially imposed localised diabatic heating is forced into the model at the first timestep and kept constant (in pressure coordinates) throughout the simulation, as done in earlier studies (Bretherton, 1988; Nicholls et al., 1991; Pandya et al., 1993). Two scales are studied: synoptic-scale and mesoscale with two different imposed heatings; one which is of the same order (dimensions and amplitude) as a synoptic-scale convection zone and another as an extensive mesoscale convective complex (MCC). This potential diabatic heating is

sinusoidal in the vertical and Gaussian in the horizontal. The heating amplitude at the maximum is set at a value of $21.6K/day$ ($2.5 \times 10^{-4}K/sec$). The heating is imposed from 300 to 800 hPa, which is more realistic than a heating that encompasses all of the troposphere. This heating is meant to represent the result of convection, and therefore does not generate instabilities itself with a proper stratification. The heating equation is as follows:

$$L_\theta = L_\theta \; exp\Big\{ - \Big[(\frac{x - m_x}{a_0})^2 + (\frac{y - m_y}{b_0})^2 \Big] \Big\} \sin \Big\{ \frac{-\pi(p - \tau)}{e} \Big\}, (\tau + e) > p > \tau \quad (2.1)$$

where $L_\theta = d\theta/dt$, e is the vertical extent in p coordinates, $L_\theta = 0$ when $(\tau + e) \leq porp \leq \tau$, $m_x = m_y$ are the grid points locating the center of the domain, $a_0 = b_0 = 6$ are the number of grid points representing the half-width of the Gaussian, τ is the pressure at the top of the heating.

To further simplify the experiment, the reference simulation (hereafter F0), with f, the Coriolis parameter, equal to zero is run with the configuration and initial conditions presented in table 2.1. The simulation with typical mid-latitude rotation ($f = 10^{-4}\ s^{-1}$), hereafter F4, uses the same configuration and initial conditions, except for the simulation length which is 24h. The heating horizontal size is defined as the diameter which encompasses all values which exceed 10% of the maximum value. The horizontal distribution of the imposed diabatic heating is shown in figure 2.1. Geography and latitude-longitude lines are shown only for reference, since the actual projection is cartesian and an f-plane is used in the simulations.

According to Courant numbers, the SISL numerical scheme will not slow down waves in the horizontal. Extensive verifications were performed to ensure that the model configuration is indeed suitable for the present experiments. Simulations were performed with a doubled grid size to ensure that there were no boundary effects outside the sponge. This ensured that the horizontal lateral extent of the domain is much larger than the lateral extent of the imposed diabatic heating, which in turn ensures that the gravity waves are generated correctly and not influenced by the horizontal domain size (Browning and Kreiss, 1997). Simulations were also done with a reduced model time-step (5 and

Table 2.1 F0 simulation configuration and initial conditions

Model configuration	
Grid dimensions	92×92
Horizontal resolution	60 km
Horizontal sponge	10 grid points
Vertical sponge depth	15 km
Domain dimensions	5520×5520 km
Vertical levels	30
Coriolis parameter f	0 (non-rotating)
Simulation length	48 h
Initial conditions	
Heating horizontal size	1440 km
Heating vertical extent	300 to 800 hPa
p at heating maximum	522 hPa
Initial horizontal winds	0 m/s
Initial vertical motion	0 m/s
Initial temperature profile	Isothermal at 0 C
Initial mean static stability	10^{-2} s^{-1}
Initial surface pressure	Uniform at 1000 hPa

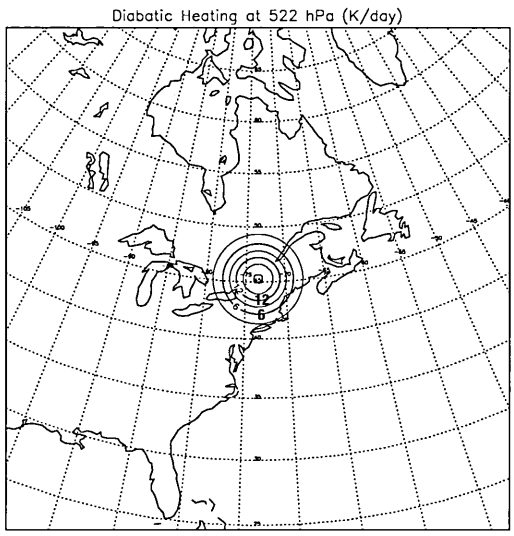

Figure 2.1 Idealized diabatic heating (K/day) for the F0 and F4 simulations at its maximum level (522 hPa). Geography is shown for reference only (f-plane)

30 s instead of 60 s) to assure that the modelled solutions were independent of the integration time-step. Finally, simulations with a finer horizontal resolution (30 km instead of 60 km for the same heating size) and a finer vertical resolution were run to ensure that results were independent of the horizontal and vertical resolutions. All these verifications resulted in differences which were either not significant or non-existent.

2.3 Nonlinear Balance and Diagnostics

2.3.1 The Nonlinear Balance Omega Equation

Rotational Environments

The nonlinear balance (NLB) diagnostic equation can be expressed as follows (note: all equations presented here are defined on pressure vertical coordinates), when rotation is present:

$$\nabla^2\phi - f\zeta + \beta u - 2J(u,v) = 0 \tag{2.2}$$

where ϕ is the geopotential, ζ is the relative vorticity, β is $\frac{\partial f}{\partial y}$, u and v are the horizontal wind components, $J(u,v)$ is the Jacobian of the horizontal winds.

The NLB equation links horizontal winds and geopotential height fields. This equation can also be expressed in another form to directly relate the streamfunction of the non-divergent part of the wind (Ψ) to the geopotential (ϕ):

$$f\nabla^2\Psi + 2\left[\left(\frac{\partial^2\Psi}{\partial x^2}\right)\left(\frac{\partial^2\Psi}{\partial y^2}\right) - \left(\frac{\partial^2\Psi}{\partial x \partial y}\right)^2\right] + \frac{\partial f}{\partial y}\frac{\partial \Psi}{\partial y} = \nabla^2\phi \tag{2.3}$$

The conditions for validity of (2.2) is defined as when the Froude number U/NH is small, where U is the wind scale, N is the Brunt-Väisälä frequency, and H is the height scale. This is equivalent to $U \ll c$, which is the case here since U is initially at rest. Classical linear theory can be used to derive the dispersion relationship, for a base state which is at rest. Thus, the dispersion equation for hydrostatic ($k \ll m$) inertia-gravity waves can be written as follows:

$$\nu^2 = \frac{k^2N^2 + m^2f^2}{m^2} \tag{2.4}$$

where k and m are the horizontal and vertical wavenumbers respectively, and ν is the It follows that the gravity wave frequencies are dependent on N and thus on the static stability. The horizontal phase speed and group velocity are also dependent on N. The equation in non-rotational environments is:

$$c = c_g = \frac{NZ_T}{n\pi} \tag{2.5}$$

where Z_T is the heating depth and n is the vertical mode.

A balance diagnostic package has been developed at Université du Québec à Montréal (UQAM) called DIONYSOS (Caron et al., 2006). It uses a generalized ω equation (Räisänen, 1995)(see equation (2.6)) and the method described in Räisänen (1997).

This omega equation only uses the hydrostatic approximation. In Räisänen (1995), equation (2.6) is solved with the ageostrophic term determined as an independent forcing. In DIONYSOS, this term is determined using the NLB assumption, which is what will be used here to diagnose NLB vertical motion. DIONYSOS can also be used to diagnose NLB vorticity (relative and geostrophic) tendency, temperature tendency, pressure and height tendencies, and horizontal divergence. For a full description, see Caron et al. (2006) :

$$\frac{R}{p}\nabla^2 S\omega + f(f+\zeta)\frac{\partial^2\omega}{\partial p^2} - f\omega\frac{\partial^2\zeta}{\partial p^2} - f\frac{\partial}{\partial p}\left[\frac{\partial\omega}{\partial x}\frac{\partial v}{\partial p} - \frac{\partial\omega}{\partial y}\frac{\partial u}{\partial p}\right]$$
$$= -\frac{R}{p}\nabla^2\left[-\vec{V}\cdot\vec{\nabla}T\right] - \frac{R}{p}\nabla^2\frac{\dot{q}}{c_p} - f\frac{\partial}{\partial p}\left[-\vec{V}\cdot\vec{\nabla}(f+\zeta)\right]$$
$$- f\frac{\partial}{\partial p}\left[\vec{k}\cdot\vec{\nabla}\times\vec{F}\right] + f\frac{\partial}{\partial p}\left[\frac{\partial\zeta_{ag}}{\partial t}\right] \quad (2.6)$$

where ω is vertical motion, p is the pressure, R is the dry air gas constant, c_p is the specific heat at constant pressure, $\vec{V}$ is the horizontal wind vector, T is the temperature, $\dot{q}$ is the diabatic heating rate, $\vec{F}$ is the frictional forcings, and ζ_{ag} is the ageostrophic vorticity. Equations (2.6) and (2.3) are solved together iteratively (Caron et al., 2006). Balanced state reached in the numerical simulations (defined as discussed below) will be compared to NLB as diagnosed by equation (2.6).

Non-Rotational Environments

For simulations with no rotation, equation (2.2) does not apply since the atmosphere exhibits another type of balance and therefore, (2.6) must be modified. Starting from the complete divergence equation, which can be written as follows (from Holton (1992)):

$$\frac{\partial D}{\partial t} = f\zeta - f\zeta_g + D^2 - 2\left[\frac{\partial u}{\partial x}\frac{\partial v}{\partial y} - \frac{\partial u}{\partial y}\frac{\partial v}{\partial x}\right] - \vec{V}\cdot\vec{\nabla}D$$
$$- \beta u_{ag} - \omega\frac{\partial D}{\partial p} - \left[\frac{\partial\omega}{\partial x}\frac{\partial u}{\partial p} + \frac{\partial\omega}{\partial y}\frac{\partial v}{\partial p}\right] \quad (2.7)$$

Eliminating all β-term (f-plane) and absolute vorticity, divergence tendency can then be written as:

$$\frac{\partial D}{\partial t} = -f\zeta_g + D^2 - 2\left[\frac{\partial u}{\partial x}\frac{\partial v}{\partial y} - \frac{\partial u}{\partial y}\frac{\partial v}{\partial x}\right] - \vec{V}\cdot\vec{\nabla}D \\ - \omega\frac{\partial D}{\partial p} - \left[\frac{\partial \omega}{\partial x}\frac{\partial u}{\partial p} + \frac{\partial \omega}{\partial y}\frac{\partial v}{\partial p}\right] \quad (2.8)$$

Substituting geostrophic vorticity then gives the divergence equation in a non-rotational environment:

$$\frac{\partial D}{\partial t} = -\nabla^2\phi + D^2 - 2\left[\frac{\partial u}{\partial x}\frac{\partial v}{\partial y} - \frac{\partial u}{\partial y}\frac{\partial v}{\partial x}\right] - \vec{V}\cdot\vec{\nabla}D - \omega\frac{\partial D}{\partial p} - \left[\frac{\partial \omega}{\partial x}\frac{\partial u}{\partial p} + \frac{\partial \omega}{\partial y}\frac{\partial v}{\partial p}\right] \\ = -\nabla^2\phi \quad (2.9)$$

Equation (2.6) must also be modified to eliminate all terms multiplied by f. It can then be written as follows:

$$\frac{R}{p}\nabla^2 S\omega = -\frac{R}{p}\nabla^2\left[-\vec{V}\cdot\vec{\nabla}T\right] - \frac{R}{p}\nabla^2\frac{\dot{q}}{c_p} \quad (2.10)$$

For simulations with no rotation, equations (2.9) and (2.10) will be used. (2.10) shows that the type of balance when there is no rotation is an exact balance between the temperature tendency caused by forcings and the adiabatic cooling caused by the vertical motion, omega, and the static stability parameter.

2.3.2 Definition of Balance in Numerical Simulations

A significant problem is to define how it can be determined that balance has been attained in numerical simulations (with static, imposed heating), independent from the use of diagnostic balance equations. It is generally agreed that dynamic balance can be defined as when dynamic and thermodynamic fields in the numerical simulation are either quasi-constant or evolving slowly with a constant tendency, and that the nonlinear balance equation has small or no significant residue. This kind of imprecise definition

leaves plenty of room for subjectivity and leads to the following questions: What is meant by "evolving slowly" or "quasi-constant"? Which field must be used? Which area should be taken into account?

The approach used here tries to be as objective as possible. First, three fields were chosen to determine balance in pressure coordinates: isobaric vertical motion, horizontal divergence, and surface pressure. These fields were chosen since they are all greatly affected by dynamical imbalances. Determining balance using one point only is not sufficient implying that an area must be used and so secondly, to ensure the inclusion of all significant imbalances, an area which is twice the horizontal extent of the Gaussian of the forcing was chosen to be considered here. Thirdly, "significant" imbalances need to be defined. It is difficult to be absolutely objective since absolute or strict dynamical balance is never attained. Here we chose to consider that dynamical balance is attained if the conditions listed next are met. The scale of the field is defined as the absolute maximum tendency of the field during the entire time period of the simulation for the area considered. Thus, to be in balance, the conditions that must be met are that the time tendency of a particular variable must be less than 5% of the order of magnitude of the tendency for: at least three (mesoscale-β) or one (mesoscale-γ) consecutive hour(s); all the vertical levels; and all the points in the horizontal area considered. Balance is defined to be attained at the mid-point of consecutive hours (three for mesoscale-β and one for mesoscale-γ).

2.4 Results

This section presents an in-depth analysis of the numerical simulations. These analyses will first present the balanced state and then the series of processes leading to dynamical balance will be described and analyzed. The F0 and the F4 simulations will be analyzed in subsection 2.4.1. In this analysis the energetics of the generated gravity waves will also be examined, and the resulting balance state achieved by the model will be compared to nonlinear balance diagnostics using DIONYSOS.

It should be noted that the analyses presented here focus on gravity and inertial oscillations. Hydrostatic adjustment, acoustic and Lamb waves are not analyzed here. For complete discussions and analysis on hydrostatic adjustment, acoustic and Lamb waves as a result of an imposed heating, the reader is advised to consult Thurre (1998) and Nicholls and Pielke (1994).

2.4.1 Reference Simulation (F0): No Rotation

Initially, the atmosphere is at rest, with constant temperature, uniform horizontal surface pressure (Table 2.1), and there is no rotation ($f = 0$). Starting during the first integration time-step, an idealized diabatic heating is applied and then kept constant throughout the simulation.

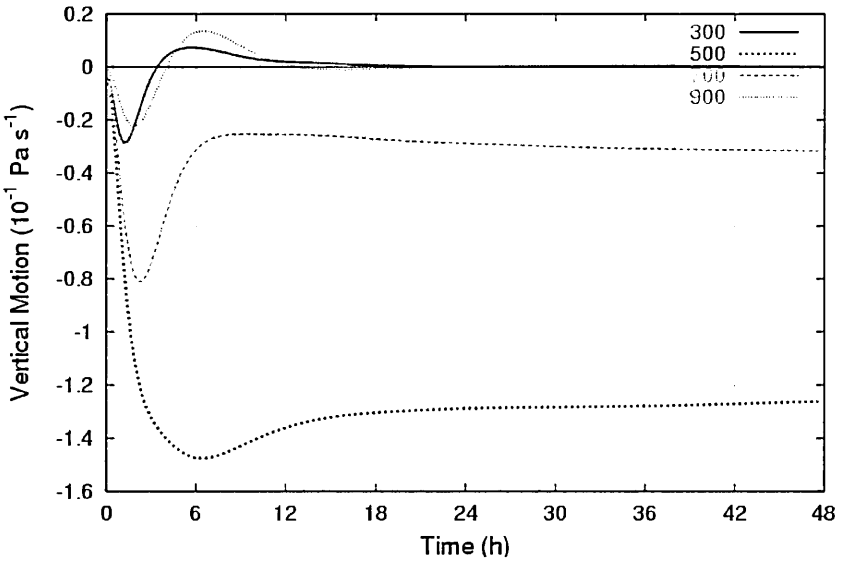

Figure 2.2 Time series of vertical motion (10^{-1} Pa s^{-1}) at the center of the heating for the 300, 500, 700 and 900 hPa vertical levels for the F0 simulation.

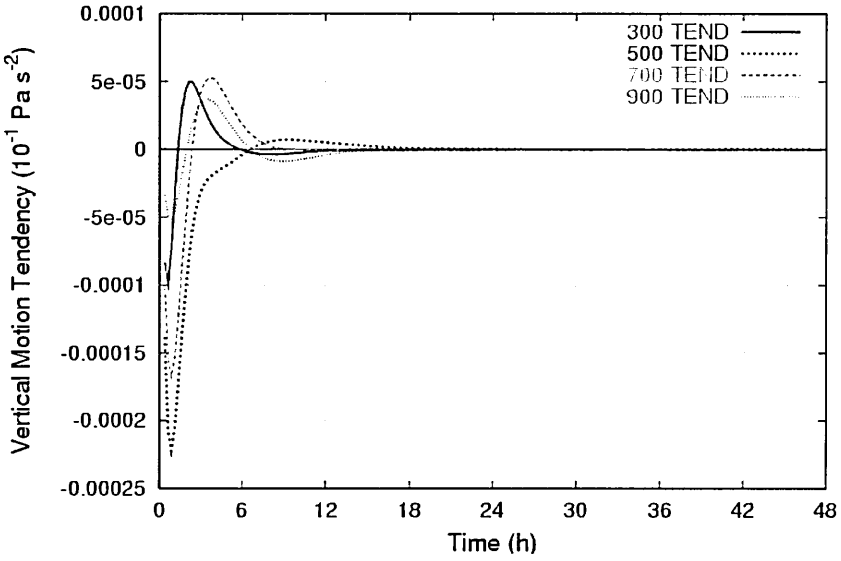

Figure 2.3 Time series of vertical motion tendency (10^{-1} Pa s^{-2}) at the center of the heating for the 300, 500, 700 and 900 hPa vertical levels for the F0 simulation.

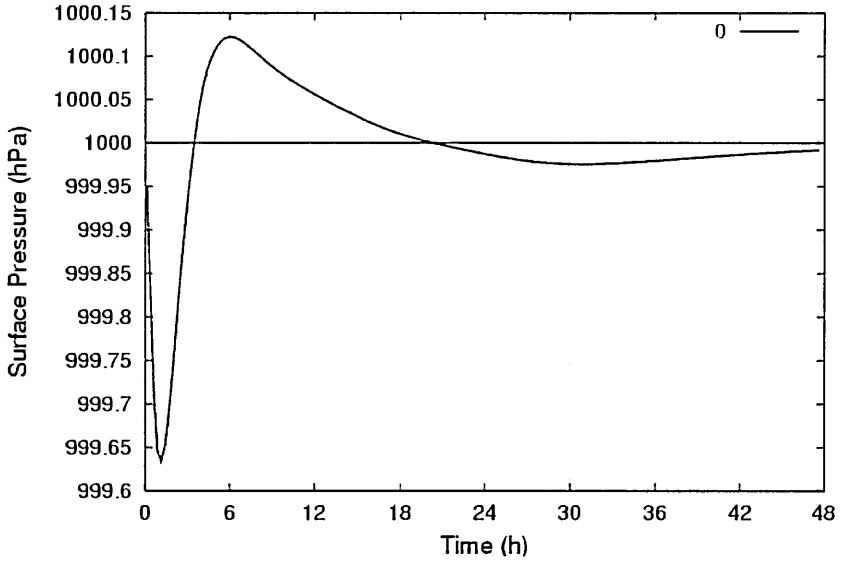

Figure 2.4 Time series of surface pressure (hPa) at the center of the heating for the F0 simulation.

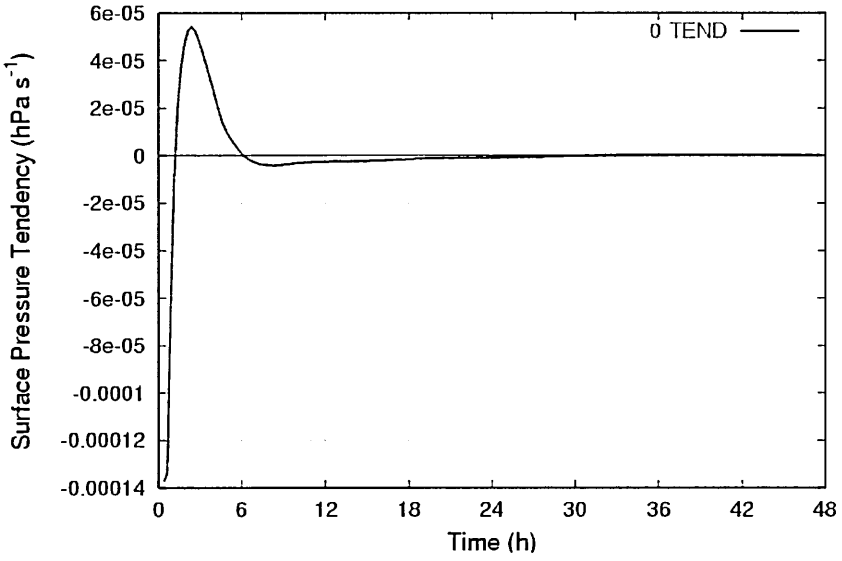

Figure 2.5 Time series of surface pressure tendency ($hPa\ s^{-1}$) at the center of the heating for the F0 simulation.

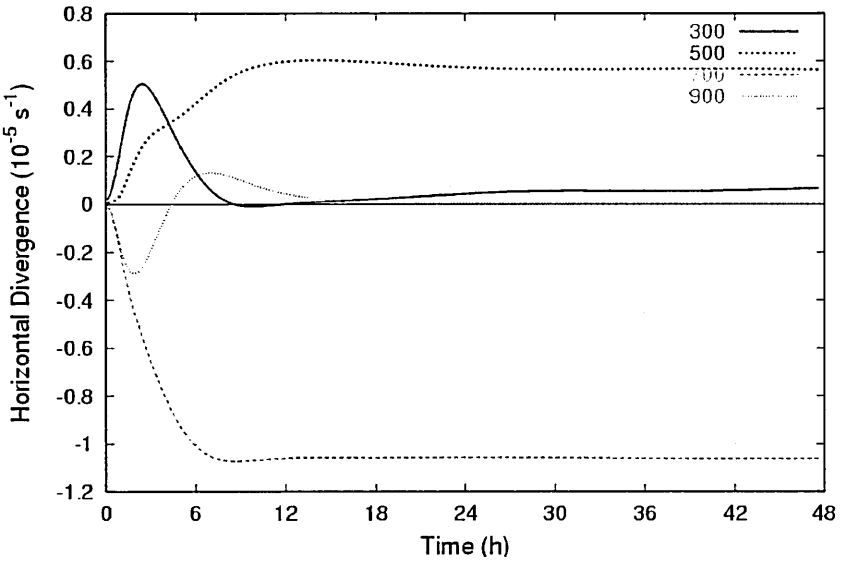

Figure 2.6 Time series of horizontal divergence ($10^{-5}\ s^{-1}$) at the center of the heating for the 300, 500, 700 and 900 hPa vertical levels for the F0 simulation.

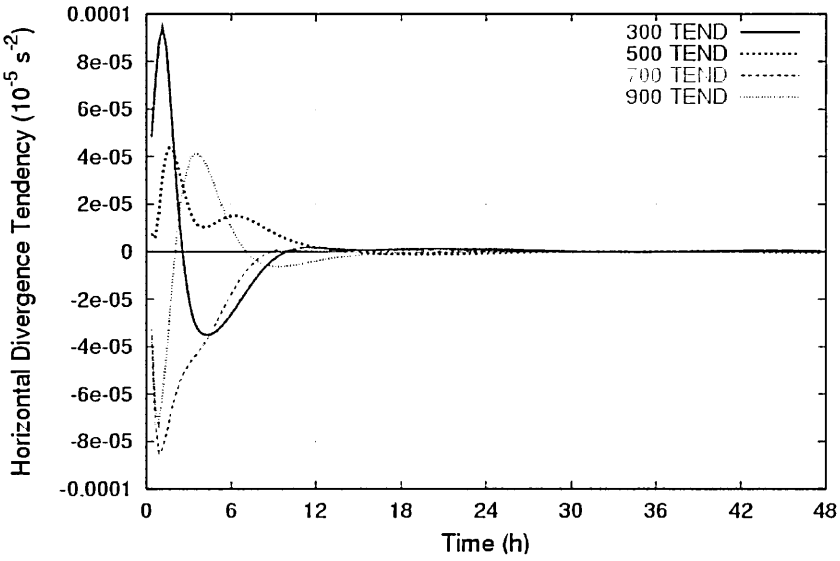

Figure 2.7 Time series of horizontal divergence tendency (10^{-5} s^{-2}) at the center of the heating for the 300, 500, 700 and 900 hPa vertical levels for the F0 simulation.

Balanced State

As defined in section 2.3, balance is determined objectively, using time series of tendencies of vertical motion, horizontal divergence and surface pressure over an area which is twice the size of the Gaussian of the forcing. Using the objective method discussed in the previous section, the simulated atmosphere is very close to the balanced state at all levels by 9h30min for vertical motion (figures 2.2 and 2.3), by 10h30min for surface pressure (figure 2.4 and 2.5), and by 13h30min and for horizontal divergence (figure 2.6 and 2.7). The figures presented here show selected levels at the grid-point where balance is slowest to be attained, which is at the center of the heating. It is noted that a subjective analysis could lead to different results, however here the method is objective and is independent from balance diagnostic equations. A comparison to balance equations is performed in section 2.4.1.

When dynamic balance is reached in this numerical simulation without rotation, the

result is a dynamic and thermodynamic structure quite different from that which develops when a significant Coriolis effect is present. According to Holton (1992, pp. 80-82), with $f = 10^{-4}\ s^{-1}$ there is ridging above the heating and troughing below. Without rotation there is instead a ridge which is maximum at the level of non-divergence at the center of the heating, and no troughing at the maximum convergence below the heating maximum. To understand this structure and why there is convergence below the heating where a ridge is present, we must look more closely at the Laplacian of the geopotential height field (negative identifies a ridge, and positive identifies a trough) and the horizontal winds (figure 2.8). Hence, an analysis of the relative magnitude (using model output) of the x-component of the equation of motion (table 2.2) is required. The analysis will be performed at 650 hPa since it is the level of maximum convergence at the center of the heating (figure 2.9).

In the equation of motion, with rotation present, the dominant term of the left-hand side of the equation is the Coriolis term, while when there is no rotation (table 2.2), the dominant term is the horizontal wind advection. This can be seen at 650 hPa below the heating in figure 2.8 where the horizontal winds are accelerated toward the center of the heating (horizontal convergence) by a trough (solid lines) which encircles the heating center. The winds which continue to converge are then decelerated by the ridge at the center of the heating. This is why we observe convergence where we have a ridge (identified by a negative Laplacian of geopotential height).

It is important to note that divergence values, horizontal winds and the Laplacian of geopotential height are all much weaker here than in cases which involve $f = 10^{-4}\ s^{-1}$, however, they are important since a significant vertical motion is generated.

Table 2.2 Analysis of the relative magnitude of the balanced x-component of the equation of motion at 650 hPa ($10^{-7}\ m/sec^{-2}$)

$\frac{\partial u}{\partial t}$	$+u\frac{\partial u}{\partial x}$	$+v\frac{\partial u}{\partial y}$	$+\omega\frac{\partial u}{\partial p}$	$-fv$	$= -\nabla_{p_x}\Phi$
0.15	40	0.5	14	0	60

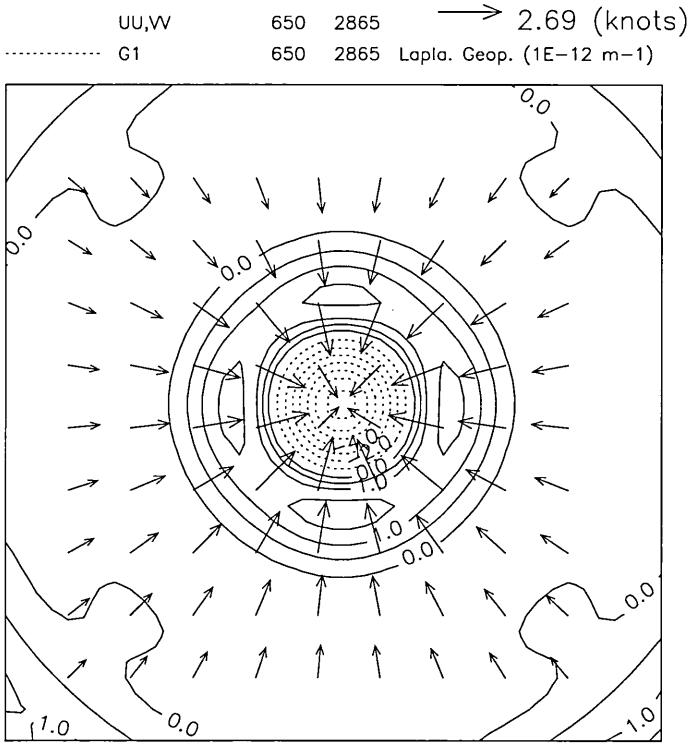

Figure 2.8 Balanced state at 48h in the F0 simulation: Laplacian of geopotential height ($10^{-10}m^{-1}$ black lines, negative contours dotted lines) at 650 hPa with horizontal winds for a region near the center of the domain.

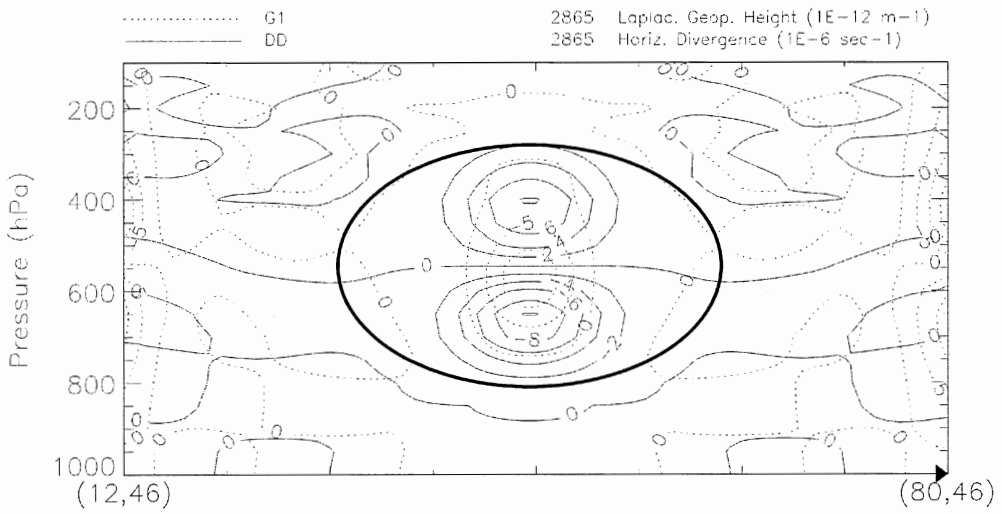

Figure 2.9 Balanced state cross-section at 48h in the F0 simulation: divergence ($10^{-6}s^{-1}$ solid lines, interval 2) and Laplacian of geopotential height ($10^{-10}m^{-1}$ dotted lines, interval 0.05). Region of heating is approximately encircled with a thick black line. Vertical axis: pressure vertical levels. Horizontal axis: cross-section through the center of the heating (numerical sponge areas not included).

In summary for this simulation with $f = 0$, dynamic balance is a steady state with divergence (convergence) above (below) the heating, upward motion in the region of the heating and a maximum at the center of the heating. The surface pressure returns to the background value and then becomes constant. In addition, the adiabatic cooling becomes equal to the diabatic heating and the temperature tendency also becomes zero (not shown). The horizontal geopotential distribution that develops and becomes constant is the distribution that is necessary to produce the balanced state horizontal divergence and convergence. This type of circulation is like a direct thermal (Hadley) circulation.

A crucial question for data assimilation is also how the numerical model adjusts itself to this balance. The mechanisms or series of physical processes involved in the adjustment towards balance must be analyzed in depth to enable a correct assessment of what is important to be considered in data assimilation schemes. It is also important to know what the mechanisms involved in the production of imbalances and spurious high-frequency waves are in order to be able to eliminate or control them. This is what will be presented chronologically in the following subsections.

Initiation of Divergence

The first physical processes to take place are related to the hydrostatic adjustment. From Thurre (1998), it follows that the first processes involved are the elastic mode followed by the Lamb mode. At the heating initiation, $\frac{\partial \rho}{\partial t} = 0$ and $\frac{\partial T}{\partial t} > 0$, and thus $\frac{\partial p}{\partial t} \neq 0$. It follows that $\frac{\partial^2 u}{\partial t^2} \neq 0$, hence mass horizontal divergence is initiated (the magnitude is very small, of the order of $10^{-10}\ s^{-1}$). This divergence is maximum horizontally at the center of the heating. At the same time, horizontal convergence occurs at the edge of the heating and convergence occurs below the heating, the latter being several orders of magnitude less than the divergence aloft. Figure 2.10 shows the divergence profiles in the first 15 seconds of the simulation at the center of the heating.

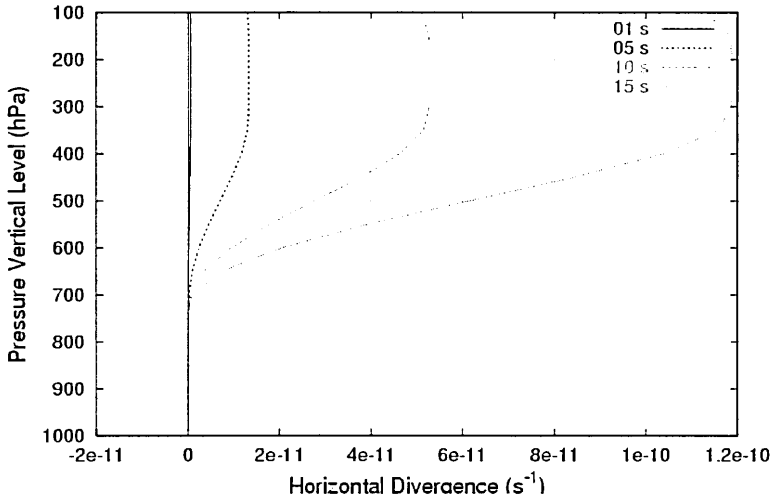

Figure 2.10 Vertical profiles of divergence (s^{-1}) at the center of the heating for the first 15 seconds of the simulation. A numerical integration time-step of 1 second is used in this F0 simulation.

Initiation of Falls in Pressure and Convergence

The gravity mode oscillation mechanisms take place after the Lamb mode, which will generate the first external gravity wave. Since horizontal divergence is taking out mass in the column at the horizontal center of the heating, falls in pressure are initiated at the surface and below the heating maximum. These localized pressure falls produce low pressure below the heating which induces horizontal convergence. They reach a maximum at the bottom edge (750 hPa) of the heating since this is where the cumulative effects of divergence aloft are also at a maximum. This process happens in the first 5 to 11 minutes of the simulation. It is important to note here that there is a time lag between the increase in the convergence below the heating and an increase in the divergence aloft. This is shown in the figure 2.11.

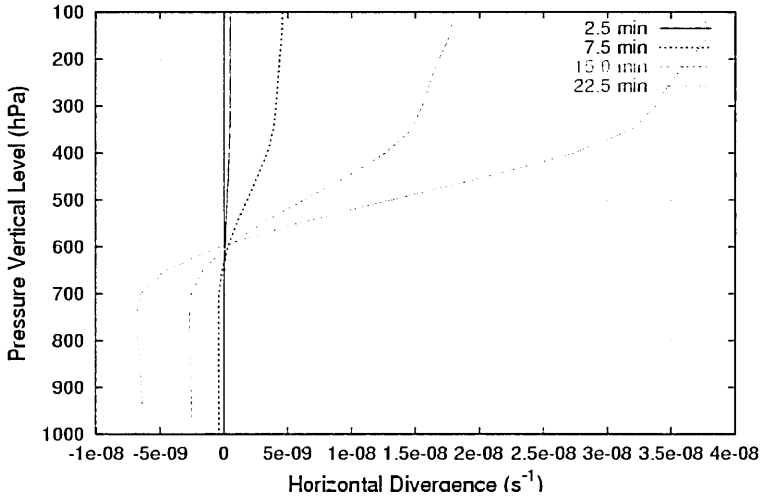

Figure 2.11 Vertical profiles of divergence (s^{-1}) at the center of the heating for the first 22.5 minutes of the simulation. A numerical integration time-step of 15 seconds is used in this F0 simulation.

Initiation of Vertical Motion

By continuity (assuming an anelastic approximation), vertical motion can be calculated from this divergence (convergence) aloft (below) the heating maximum. Due to the stability of the atmosphere, this vertical motion produces adiabatic cooling which begins to counteract the diabatic heating. Since the heating does not encompass all of the troposphere (heating is applied between 300 and 800 hPa in the F0 simulation), this vertical motion also produces cooling below and above the heating. This cooling is much stronger aloft since the stability parameter in the upper troposphere is much stronger in an isothermal atmosphere. However, since there is ridging above the heating, this cooling produced by vertical motion reduces this ridging, while below the heating, it enhances the troughing already occurring.

Overshoots and Balance

During the adjustment process, there are several overshoots in the dynamic and thermodynamic fields. These overshoots are the generators and the signatures of gravity waves. These waves are creating pressure perturbations through several interactions and retroactions between dynamic and thermodynamic fields. In this section, an in-depth analysis is performed to determine how these oscillations are generated and how they evolve.

There are two main overshoots (positive and negative) in the dynamic and thermodynamic fields, however, only one overshoot is visible in the vertical motion at the center of the heating at 500 hPa (figure 2.2). From classical theory, it is known that the first wave emitted is an external gravity wave, followed by internal waves. The single overshoot in the vertical motion can be separated into two series of distinct physical processes, related to the external and internal gravity waves. We can clearly see the two distinct overshoots in the surface pressure (figure 2.4) and also in the vertical motion at 250 and 900 hPa (figure 2.2). These two overshoots are not simultaneous at all vertical levels, but are however still the results of two distinct mechanisms.

The first of these two overshoots in the vertical motion is caused by the overshoot in the fall in surface pressure that occurs at the beginning of the simulation, which can be identified as an external gravity wave. The lowest value of pressure is attained after 1h. This overshoot in the fall in pressure is caused by the fact that divergence aloft is much greater than convergence below the heating at the beginning of the simulation since convergence below lags in time. This is because pressure falls take time to develop: divergence aloft must have already occurred to produce the surface pressure falls which induce convergence below. Furthermore, since the stability parameter is much higher aloft, once the upward vertical motion is produced, the strong adiabatic cooling aloft quickly weakens the ridging and reduces the divergence aloft while, on the other hand, convergence below the heating becomes larger in reaction to the strong pressure and the falls in height which have already occurred. The result is that in the column, convergence below becomes stronger than divergence aloft. This process then increases surface

pressure back up to a point where the pressure is almost the same as the surrounding pressure (and initial conditions) as can be seen in figure 2.4. These processes generate the external gravity wave.

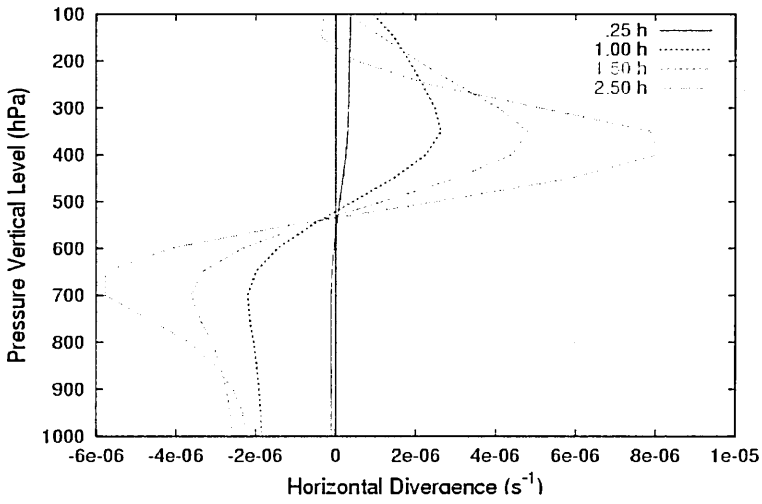

Figure 2.12 Divergence vertical profiles (s^{-1}) at the center of the heating at 15 min, 1h, 1h30 and 2h30 for the F0 simulation.

The second overshoot is caused by the fact that the heating does not encompass all of the troposphere, it is restricted from 300 hPa to 800 hPa. This heating configuration results in an oscillation in the vertical motion below (800 hPa) and above (300 hPa) the heating (figure 2.2). This oscillation is due to vertical motion generated throughout the atmospheric column at the beginning of the simulation which produces adiabatic cooling below and above the heating. The effect of this adiabatic cooling is crucial, and it is highly dependent on the static stability profile and the heating configuration. The adiabatic cooling will enhance convergence below by increasing the troughing through the cooling of the layer between the surface and the heating. On the contrary, it will decrease divergence aloft by decreasing the ridging above the heating through the cooling, which is quite strong due to the strong static stability parameter value aloft as compared to near the surface. The net result will then be an increase in convergence in the column,

and a decrease of the divergence (figure 2.13), which then results in a strong surface pressure rise coming greater than the surrounding pressure, effectively creating a high pressure at the surface. Thus, these mechanisms are generating an internal gravity wave.

With the two overshoots described, we once again note that these overshoots do not take place simultaneously at all vertical levels. Nor do they take place in all the model variables, which means that there is a superposition of gravity wave frequencies. This is confirmed by classical theory, which states that the oscillation modes which are generated are dependent on the heating depth. A superposition of modes is expected due to the fact that the imposed heating is only a half-sine period, and since it does not encompass all the vertical extent between the surface and the rigid lid.

Since the balance state requires that the temperature tendency goes to zero, there cannot be any vertical motion, and its associated adiabatic cooling, below or above of the region of heating. In order to reach dynamical balance, adiabatic cooling must totally compensate for the diabatic heating. The high pressure at the surface and below the heating reverses the convergence and hence the vertical motion (figure 2.14), and also heats back up, adiabatically, the lower levels of the atmosphere. At the same time the convergence weakens in the column and becomes equal to the divergence since we no longer have convergence below the heating but rather, a small divergence. The balanced state is reached when there is no divergence, convergence nor vertical motion above or below the heating zone, which is attained nearly perfectly after about 24h. At this time, quasi-constant vertical motion and horizontal divergence is observed. This is the balance, where vertical motion compensates totally the diabatic heating through adiabatic cooling (stability). The balanced state has a mass field (pressure) which has been redistributed in order that the proper divergence/convergence is created to generate a vertical motion which can exactly compensate for the diabatic heating.

It is noted here that the thermodynamic structure (static stability parameter) as well as the 3D heating structure on the dynamic balance adjustment process are of significant importance (figure 2.9).

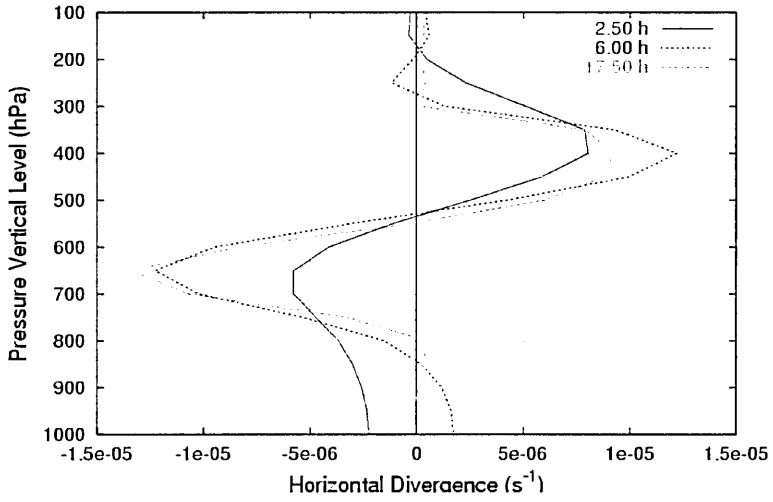

Figure 2.13 Divergence vertical profiles (s^{-1}) at the center of the heating at 2h30, 6h and 17h30 for the F0 simulation.

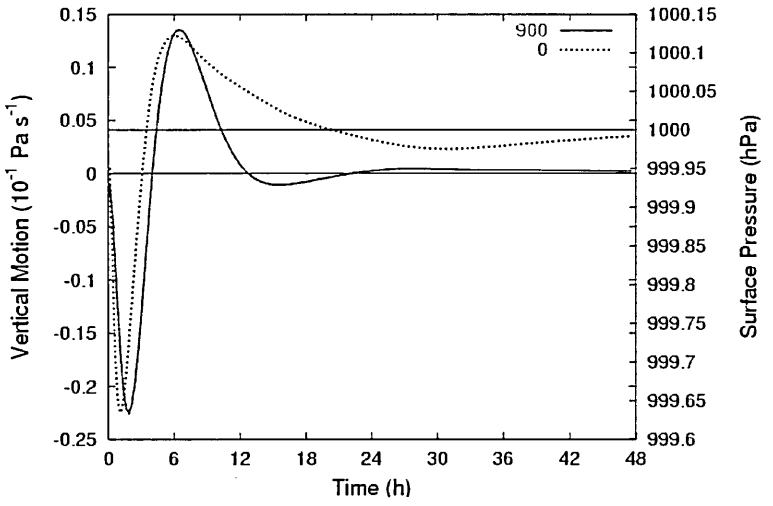

Figure 2.14 Time series of 900 hPa vertical motion ω (10^{-1} Pa s^{-1}) and surface pressure at the center of the heating for the F0 simulation.

Gravity Waves

The gravity waves, which were generated during the dynamic balance adjustment process (external and internal waves), were analyzed. These gravity waves were identified using horizontal divergence, as was done in O'Sullivan and Dunkerton (1995). In the F0 simulation, the atmosphere is isothermal. Hence, the Brünt-Väisälä frequency and the gravity waves speed are constant everywhere for a heating which starts at the surface and extends to a rigid lid (Holton, 1992, pp. 198-203). In this case, several different gravity wave frequencies are to be expected since the heating is restricted in its vertical extent.

This can be verified in figures 2.15 and 2.16, which are cross-sections of horizontal divergence after 3h and 7h, respectively, during the numerical simulation. The first thing to note is that the gravity waves are generated much faster above the heating, where the static stability parameter is stronger. At 3h into the simulation, there are already well-defined gravity waves propagating in the upper troposphere, while in the lower troposphere they are very weakly defined. Secondly, the speed of the gravity waves is much faster in the upper troposphere. This is observed through the identification of positively tilted (in the propagation direction) gravity waves whose tilt increases with time. An animation of this cross-section (not shown) shows this tilt to increase in time. After 24h into the simulation, there remain some residual weak transient gravity waves, mainly in the lower levels where balance is slower to be reached. At balanced state however, it has been calculated (13h30m) that transient gravity waves continue to be strong, but only away from the 3D-cube considered in the balance calculation. This cube only encompasses the main heating center and its immediate surroundings.

Classical theory predicts, using (2.5), that if the heating were to be of the same depth but confined between the surface and a rigid lid, the gravity wave speed would be 47 m/s for the first mode. This agrees somewhat with the F0 simulation results, which shows the estimated speed of the gravity waves to be on the order of 36 m/s at 300 hPa.

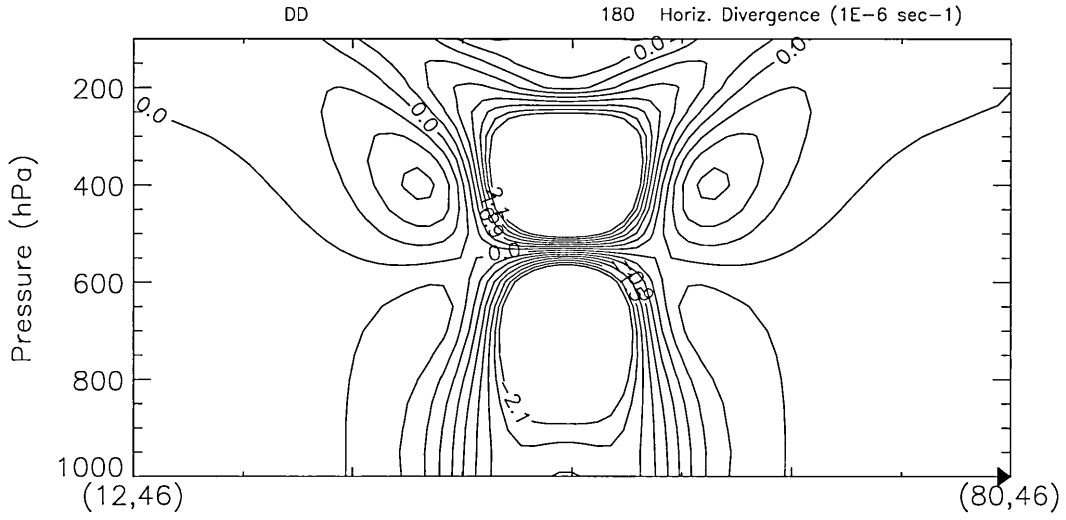

Figure 2.15 Cross-section of horizontal divergence (10^{-6} s^{-1}, intervals 0.3 from -2.1 to 2.1) after 3h into the simulation (F0 simulation) for all the horizontal domain up to the numerical sponge edge. Vertical axes are levels of vertical pressure.

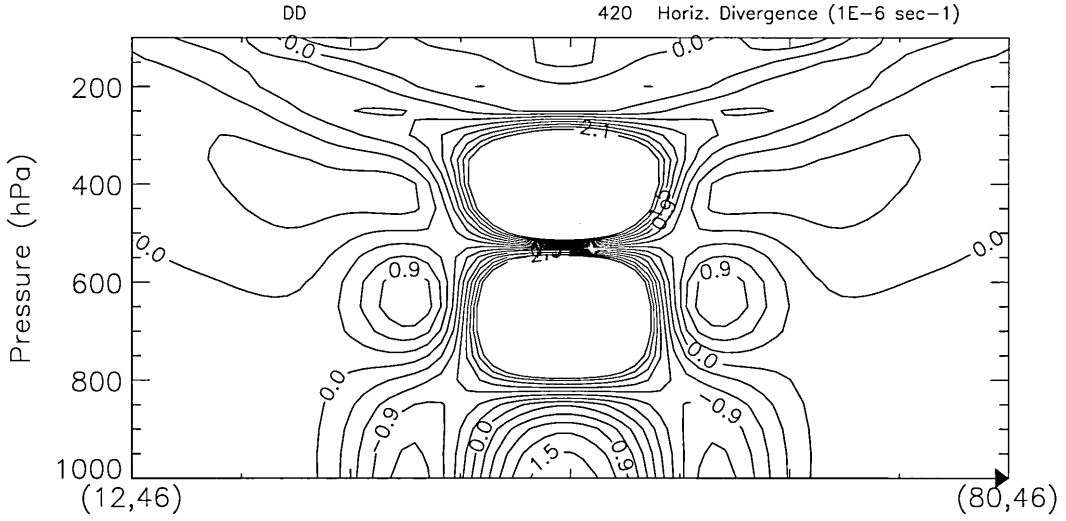

Figure 2.16 Cross-section of horizontal divergence (10^{-6} s^{-1}, intervals 0.3 from -2.1 to 2.1) after 7h into the simulation (F0 simulation) for all the horizontal domain up to the numerical sponge edge. Vertical axes are pressure vertical levels.

The main series of physical processes involved in the dynamic balance adjustment can be summarized as follows. The adjustment is first characterized by the production of divergence aloft with delayed convergence below the heating. This delay, combined with the fact that the adjustment is faster aloft, produces an undershoot in surface pressure (which correspond to the first external gravity wave) immediately followed by an overshoot (first internal gravity wave). Divergence oscillates rapidly above and below the heating, generating the gravity waves. These oscillations are due to the vertical motion which heats and cools the atmosphere according to the static stability parameter combined with the surface pressure oscillations. Dynamical balance is reached when divergence and vertical motion vanish above and below the heating.

Balance Diagnostics

Now that the balanced state and its adjustment have been analyzed for this F0 simulation, we must compare the balanced vertical motion reached in the numerical simulation to the diagnosed balanced vertical motion (equation 2.10). We only compare vertical motion (figure 2.17) for the simulation with no rotation due to the fact that the NLB equation (2.2) does not apply here since $f = 0$. Note that (2.10) would not be valid in the presence of vorticity. Balance was calculated objectively to be attained at 13h30m in the simulation. The difference between the model and the diagnosed balanced vertical motion at 13h30m are 6% and 16% at 500 and 700 hPa respectively. After 24h, the differences are smaller, 4% and 6% respectively, and after 48h, the differences are only 3% and 2% respectively. This means that the model, in this F0 simulation, rapidly eliminates strong imbalances, while smaller amplitude imbalances take much more time to be eliminated. Also, the dynamic balance diagnostics represent very well the balance state of the numerical model.

Summary: Reference Simulation (F0)

This completes the analysis of the F0 simulation. We have seen that the static stability parameter is very important in the dynamic balance adjustment and balanced state

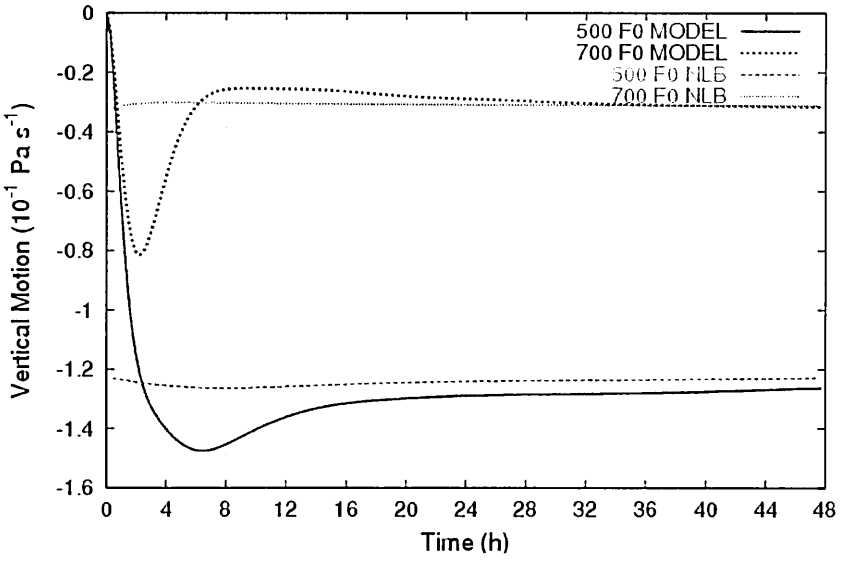

Figure 2.17 Time series of vertical motion ω (10^{-1} Pa s^{-1}) at 500 and 700 hPa comparing model vs NLB vertical motion for the F0 simulation.

itself. Two main distinct series of physical processes were identified during the adjustment phase, being the mechanisms by which the first external and internal gravity waves are generated. Since the simulation was done in the absence of rotation, the only horizontal force is the pressure force, hence vertical motion must compensate totally the diabatic heating through adiabatic cooling and exact balance is nearly reached during the simulation (static stability parameter tendency is near zero after balance is reached). The balance state structure was also analyzed, and it has been shown that the structure is quite different from cases with rotation. This is due to the fact that the main term in the equation of motion is no longer the term which involves Coriolis, but rather many other terms, which are generally several orders of magnitude less. This is why the particular 3D structure is generated (subsection 2.4.1). The vertical motion balanced equation (2.10) is valid at this scale.

2.4.2 Effect of Latitude (Coriolis)

Several numerical simulations were done with different values of f (plane) to assess the effects and the importance of latitude (or Coriolis effect) in the balance adjustment processes and balanced state itself. The F0 simulation uses no rotation, while the other simulations were performed with values of $f = 10^{-4}\ s^{-1}$ (latitude 45°), $10^{-5}\ s^{-1}$ (latitude 4°) and $10^{-6}\ s^{-1}$ (latitude 0.4°). Results with $f = 10^{-6}\ s^{-1}$ will not be shown here since they are very close to those of the simulation with no rotation, while results with $10^{-5}\ s^{-1}$ were much weaker but similar in structure to $f = 10^{-4}\ s^{-1}$. This means that, for the forcing scales examine here, Coriolis effects are important for dynamical balance only for mid and high latitudes. In this section, we analyse the simulation F4 with $f = 10^{-4}\ s^{-1}$ and compare it to the F0 simulation (no rotation). The balanced state will be first described followed by an analysis of the adjustment. The analysis will focus on the center of the heating since this is the location within the domain where the reaction of the atmosphere is the strongest and where balance is slower to be reached.

Balance State

Compared to the F0 simulation (no rotation), the F4 simulation (using $f = 10^{-4}\ s^{-1}$) has a very different dynamically balanced state. In terms of vertical motion ω at the center of the heating, shown in figure 2.18, the effect of Coriolis is quite important. The balanced state vertical motion is also constant but 25% smaller than that of the F0 simulation.

As was done with the F0 simulation, we can calculate when the balanced state is reached in the numerical simulation. For vertical motion, balance is reached at 10h45m, for surface pressure, it is reached at 13h15m and for horizontal divergence, it is reached at 16h45m. As is the case with no rotation, horizontal divergence is the most sensitive field to the imbalances; hence it is the field which takes the longest amount of time to reach balance.

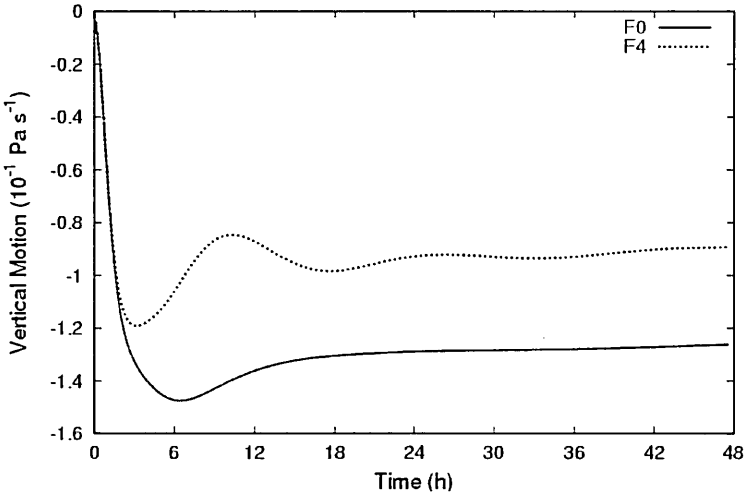

Figure 2.18 Vertical motion ω $(10^{-1}\ Pa\ s^{-1})$ vertical profiles at the center of the heating for simulations using $f = 0$ (F0) and $f = 10^{-4}\ s^{-1}$ (F4).

The dynamical structure of the balanced state is also quite different with rotation as compared to the simulation with no rotation. The structure of divergence, geopotential and vertical motion is well known: with a ridge, negative vorticity and divergence above the heating and a trough, positive vorticity and convergence below the heating with an upward motion maximum in the center of the heating. There is also divergence and vertical motion above and below the heating region (above 300 hPa and below 800 hPa). Contrary to the F0 simulation (no rotation), the balanced state is not a steady state. The ridging and negative vorticity (troughing and positive vorticity) above (below) the heating are constantly intensifying. The balanced divergence and vertical motion are almost constant and are evolving slowly due to the change in the static stability parameter (explained below).

Balanced State Adjustment

Now that the balanced state has been analyzed, we analyse how Coriolis affects the adjustment processes. The Rossby radius of deformation can be calculated to predict

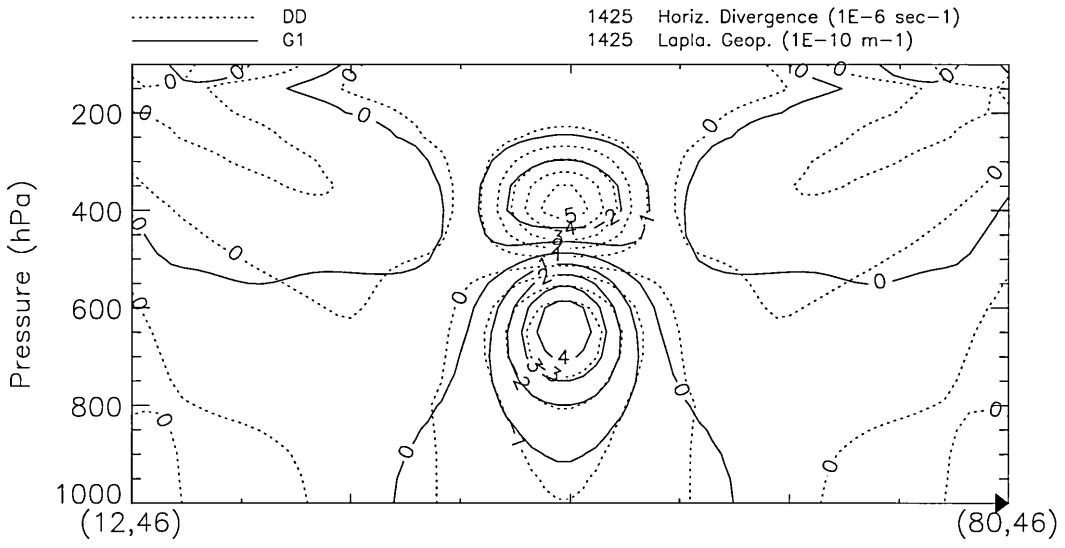

Figure 2.19 Balanced state cross-section at 24h in the F4 simulation: divergence ($10^{-6}s^{-1}$ solid lines) and Laplacian of geopotential height ($10^{-10}m^{-1}$ dotted lines). Vertical axis: pressure vertical levels. Horizontal axis: cross-section through the center of the heating (numerical sponge areas not included).

the effect of Coriolis. If the forcing scale is comparable to or larger than the radius of deformation, rotational effects will be important. For $f = 10^{-4}\ s^{-1}$ the radius is on the order of 450 km, and for $f = 0$ it is infinite. Thus, we would expect that for the 1440 km heating diameter Coriolis effects will be significant, while for the 144 km heating diameter Coriolis effects will not be important.

The adjustment processes of the first 3 hours of this simulation are near exactly as described previously for the F0 simulation (subsections 2.4.1 to 2.4.1). Even the first overshoot (the external gravity wave) is near identical (described in subsection 2.4.1). These similarities are due to the fact that it takes time to generate a significant vorticity which will affect the adjustment process.

However, after the first overshoot has occurred, the simulation diverges significantly from the F0 simulation. This can be seen in the figure 2.20, where there is no longer the development of a high pressure at the surface during the adjustment towards dynamical balance. Furthermore, once the balanced state is achieved, the surface pressure continuously falls, but at a constant rate. The question now arises as to why the surface pressure evolution is different when there is rotation? What happens after the first overshoot? This is answered below.

The answer is strongly related to the vertical profile of the static stability parameter. This can be seen in figure 2.22, where divergence vertical profiles for both simulations are shown at 3h, which is 1h after significant differences in the surface pressure appears between the two simulations (figure 2.20). The fact that the static stability parameter is much stronger aloft is crucial. Since the effect of Coriolis is distributed equally throughout the vertical column and divergence above the heating is shallower than convergence below, its effect is to reduce more convergence in the column than divergence. Hence surface pressure increases less when there is rotation compared to the F0 simulation. This can be seen after roughly 3 hours of simulation. Furthermore, Coriolis effects become more important after that because vorticity increases with time. The net result is that there is never a high pressure at the surface and that pressure tendency is stronger

with rotation. Hence, from classical theory, the Coriolis force generates an inertial wave which superimposes itself on the internal waves.

This also demonstrates that the slow but constant increase in vorticity for the rotating case (figure 2.21) is significant in the adjustment process. It takes time to generate significant values of vorticity (around 2 hours into the simulation to attain the same order as the geostrophic vorticity), and this fact is also significant in the adjustment process. This is related to the Rossby radius of deformation, as discussed above.

Now, we answer the question of whether or not the gravity waves generated are affected by rotation. Since the most energetic transient gravity waves are generated in the first part of the adjustment process (in the first 3 hours of the simulation), the gravity waves structures and intensities are very close (not shown) to what was shown for the F0 simulation (figures 2.15 and 2.16). Hence, rotation has a very limited effect on gravity waves generated during the adjustment process, which could have been predicted by the dispersion relationship of the classical linear adjustment theory.

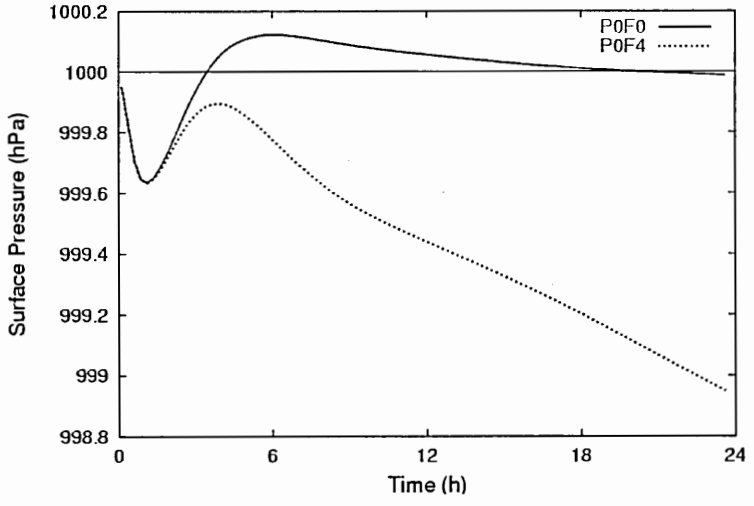

Figure 2.20 Surface pressure (hPa) at the center of the heating for F0 and F4 simulations.

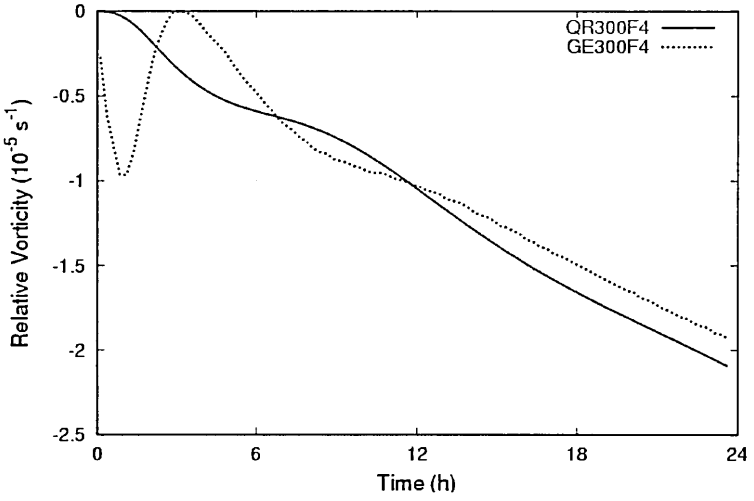

Figure 2.21 Relative and geostrophic vorticity (10^{-5} s^{-1}) at 300 hPa at the center of the heating for the F4 simulation.

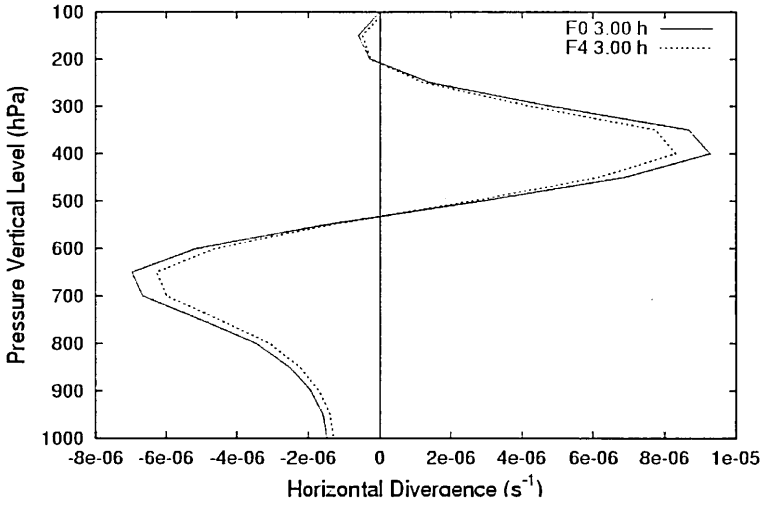

Figure 2.22 Divergence (s^{-1}) vertical profiles at the center of the heating for F0 and F4 simulations, after 3h of simulation, at the beginning of significant differences between the two simulations.

Balance Diagnostics

Now we can compare the balance reached in the numerical simulation to the balance diagnosed by NLB equations (section 2.3), as we have done with the F0 simulation. We are comparing vertical motion at 500 and 700 hPa (figure 2.23) at the center of the heating. Furthermore, since rotation is present, we are also comparing relative vorticity tendency at 400 and 700 hPa (figure 2.24). Also, in order to compare non-linear to geostrophic balance validity, figure 2.25 is a plot of relative vorticities issued from the model, the NLB equation and the geostrophic balance.

The time series of vertical motion have several important characteristics. First, as in the F0 simulation, there is a very good agreement in the F4 simulation between the numerical simulations and the NLB diagnosed values at both of these vertical levels once balance is achieved. Inspecting figures 2.24 and 2.25, it can be seen that at the center of the heating, the numerical simulation is very close to NLB by 15h, however, the simulation never attains an exactly balanced state during the first 24h. Interestingly, a period of 16h can be easily identified, which corresponds to mixed inertio-gravity waves created by the initial imbalance (Holton, 1992, Sect. 7.5). Fillion (2002, Fig. 5b) has identified similar oscillations created by imbalance caused by the adjustment of convection in a 3DVAR analysis using adiabatic first-order implicit normal mode.

The above subjective estimation of the NLB period adjustment (15h) agrees well with the objective determination of 16h45. Also, NLB diagnostics show a diagnosed vertical motion which evolves slowly in time. This indicates that static stability has a non-null tendency. This occurs mostly due to the fact that the temperature profile and, thus, the static stability, which is important in the omega equation, also evolve slowly. The time series of vorticity tendency also shows that the numerical model and the NLB diagnostic are very close, confirming what has been seen in the vertical motion time series.

The comparison of the relative vorticities at 400 hPa is quite interesting (figure 2.25). The NLB equation is used linking the vorticity to the mass field. By definition the dia-

gnosed NLB vorticity is in balance with the mass field. When the curvature is negligible, the diagnosed NLB vorticity is identical to the geostrophic vorticity. At the beginning of the simulation, the wind field is not in balance with the mass distribution resulting from the heating forcing, so the diagnosed NLB vorticity is different from the model vorticity. Starting from 15h, the wind field is almost in balance with the mass distribution and hence the vorticity is also in balance. Both the diagnosed NLB vorticity and the model vorticity are then almost equal. On the other hand, geostrophic vorticity diverges from the model vorticity in time, after balance is reached. This is related to the second order term (the jacobian term) in the NLB equation (2.2). The jacobian term is not taken into account in the geostrophic vorticity definition, and this term increases in time in the simulation together with the rotational wind. The balanced state of the model is then better represented by the NLB as compared to the geostrophic balance.

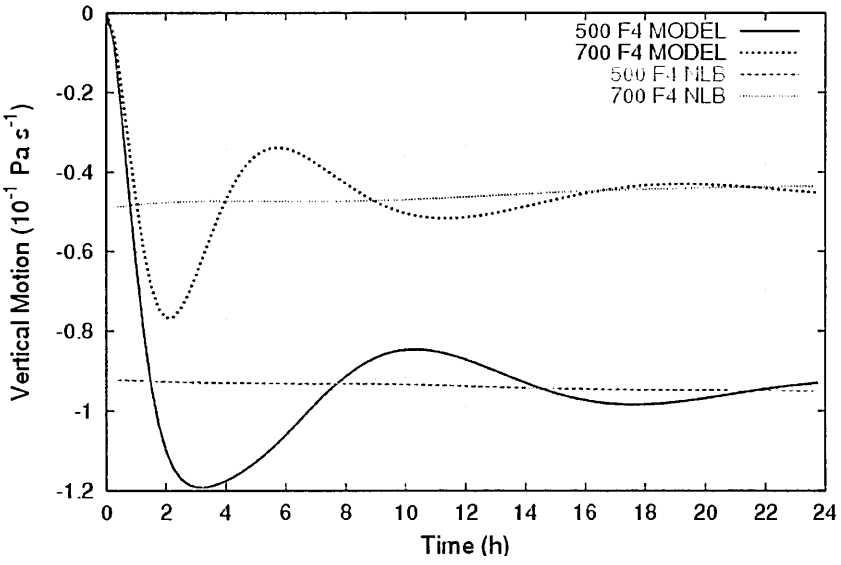

Figure 2.23 Time series of vertical motion ω (10^{-1} Pa s^{-1}) at 500 and 700 hPa comparing model vs NLB vertical motion for the F4 simulation. NLB vertical motion is identified as NLB in the figure legend.

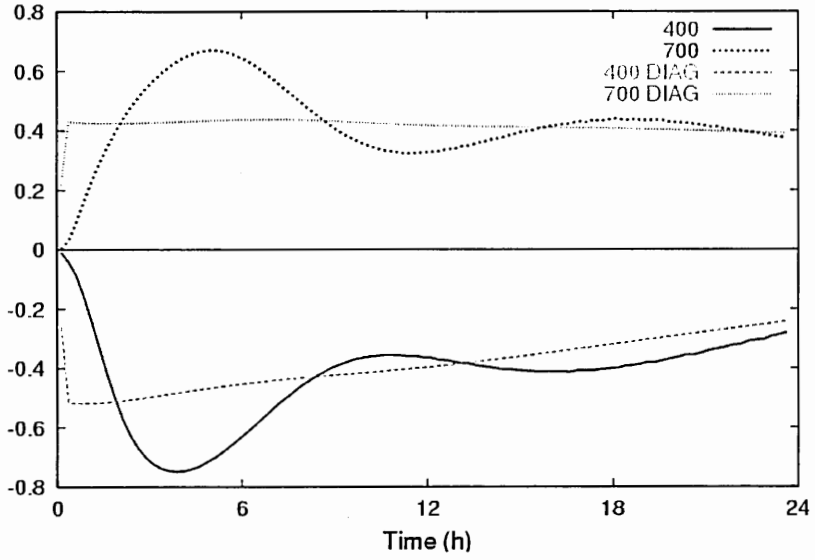

Figure 2.24 Time series of vorticity tendency (10^{-9} s^{-2}) at 400 and 700 hPa comparing model vs NLB vorticity tendency for the F4 simulation.

Summary

In summary, the effect of Coriolis is very important to achieve balance in numerical models, not only because it affects the balanced state itself as previously discussed, but also the adjustment processes and spin-up time, and consequently the characteristics of gravity waves generated. Here, since we initially have no vorticity, it takes about 2h for Coriolis to have a significant effect on the dynamics, which is consistent with the Rossby radius of deformation and classical theory.

Also, as was the case for the F0 simulation (no rotation), the numerical model and the NLB diagnostics agree very well, implying that the balanced state is closely approached by the model, and that NLB is quite closely respected at these scales. An important point is that NLB better represents the balance of the model than geostrophic balance due to the jacobian supplemental term, which is linked to the rotational winds and the curvature of the wind field.

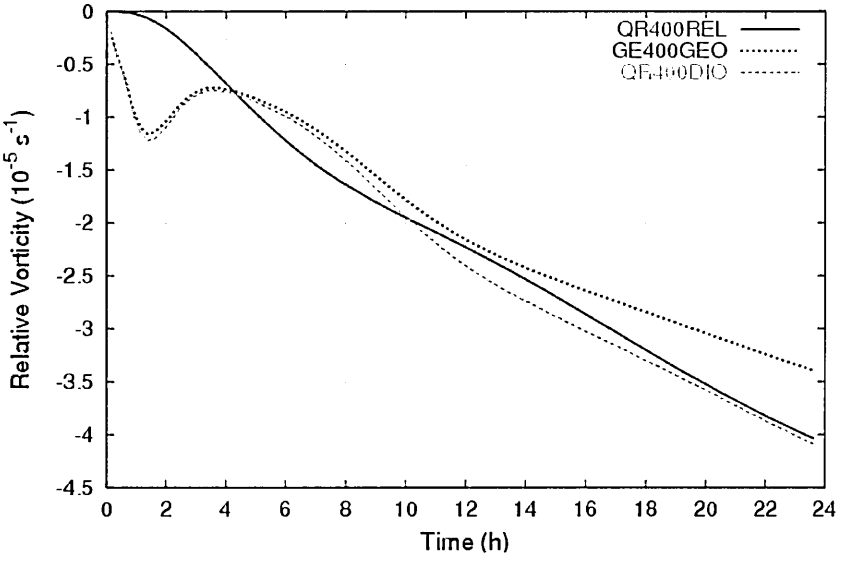

Figure 2.25 Time series of relative vorticity (10^{-5} s^{-1}) at 400 hPa, comparing model (solid black line), NLB (dashed gray line) and geostrophic (dotted black line) for the F4 simulation.

2.5 Conclusions

The analysis of the dynamically balanced state and that of the adjustment processes reveal several important characteristics. Classical theory predicts that the spectrum of gravity waves that are excited depend on the heating depth and stability. When the heating is confined in the vertical, results have shown here that the adjustment is faster above the heating, and that gravity wave group velocity and phase speed are also faster. This is linked to the static stability parameter, which is stronger in the upper atmosphere; as well it is linked to the absence of heating in the same part of the atmosphere. It has been shown that these oscillations are caused by adiabatic cooling/warming, and that they are generated faster (faster atmospheric response), hence resulting in higher gravity wave frequencies and more efficient unbalanced energy propagation away from the heating source. This also shows that the vertical and horizontal structure of the static stability parameter is crucial along with the heating depth.

Rotation also has a significant effect on the physical processes themselves. It is known from classical theory that the effect of Coriolis will depend on the Rossby radius of deformation, and that gravity wave frequencies and speed will depend on heating depth and stability. It has been shown that for a synoptic scale tropospheric heating, the Coriolis force is not equally distributed in the vertical during the balance adjustment. This leads to an impact on divergence/convergence which is not distributed equally in the vertical. The cause of this differential vertical distribution is the speed at which the adjustment occurs. This effect is significant during the adjustment process due to the experimental conditions used here in which a second overshoot in the surface pressure was prevented in the F4 simulation compared to the F0 simulation. The balanced state is also strongly affected, the presence of a Coriolis force will produce vorticity (hence a non-null vorticity tendency), which is also present outside the heating in the vertical column. This will lead to non-null tendencies of divergence and temperature, since vorticity is always increasing.

An important note about the balanced state is that, when there is no rotation, the dy-

namic and thermodynamic structure is quite different from the structure which develops when a significant Coriolis effect is present, as in Holton (1992, pp. 80-82), with ridging above and troughing below the heating source. Instead there is a ridge which is a maximum at the level of non-divergence, and no significant troughing below the heating. This is because when Coriolis is null, other terms in the equation of motion then become important.

An objective method has been developed to calculate when the balance is reached in these idealized numerical simulations. It has been used as a method independent of the NLB equations (2.2 and 2.6) since one of the goals was to compare the balance reached by the model (which is not necessarily described by the NLB) with a principally NLB vertical motion ω (equation 2.6). This method was successful in determining when balance is reached in the simulation as compared to a subjective analysis of the time series.

This work can be extended in many ways. Energetics analysis can be extended significantly. Specifically, gravity waves energetics and spectra can be calculated and fully analyzed. Also, total energy could be calculated and partitioned. Conclusions drawn here can be used as a basis to study NLB in real cases in 3D-Var or 4D-Var contexts. These cases should be chosen at first for their similarity with the idealized cases described here, such as a real summer isolated MCC in the absence of a moderate/strong pressure and temperature gradients.

The analysis described does have its limitations. The case studied here are idealized with a dry atmosphere and with a prescribed diabatic heating. It is likely that different initial conditions can have a strong impact on the balance adjustment and on the balanced state itself. However, conclusions drawn here are still valid and important since they identify many of the important aspects of dynamical balance. These aspects should be taken into account when defining balance at higher mesoscale horizontal resolutions, e.g. mesoscale-γ, in 3D and 4D-var data assimilation contexts.

Acknowledgements. Any comments/questions should be emailed to page.christian@uqam.ca. Luc Fillion and Nicolas Chapelon have helped with several discussions during the course of this work. This work was funded by the CWRP for research aimed at improving short-term QPF for extreme events. It is part of the Ph.D. Thesis of the first author.

Bibliographie

Alexander, M. J., J. R. Holton, and D. R. Durran, 1995 : « The gravity wave response above deep convection in a squall line simulation ». *J. Atmos. Sci.*, **52**, 2212–2226.

Bannon, P. R., 1996 : « Nonlinear hydrostatic adjustment ». *J. Atmos. Sci.*, **53**, 3606–3617.

Benoit, R., M. Desgagné, P. Pellerin, S. Pellerin, Y. Chartier, and S. Desjardins, 1997 : « The Canadian MC2 : A semi-Lagrangian, semi-implicit wide-band atmospheric model suited for fine-scale process studies and simulation ». *Mon. Wea. Rev.*, **125**, 2382–2415.

Bretherton, C. S., 1988 : « Group velocity and the linear response of stratified fluids to internal heat or mass sources ». *J. Atmos. Sci.*, **45**, 81–93.

Browning, G. L. and H.-O. Kreiss, 1997 : « The role of gravity waves in slowly varying in time mesoscale motions ». *J. Atmos. Sci.*, **54**, 1166–1184.

Caron, J.-F., P. Zwack, and C. Pagé, 2006 : « DIONYSOS : A diagnostic tool for numerically-simulated weather systems ». *Atmos.-Ocean*, submitted. Technical related document see http ://www.dionysos.uqam.ca/doc/Dionysos.pdf.

Caya, D. and R. Laprise, 1999 : « A semi-implicit semi-Lagrangian regional climate model : The Canadian RCM ». *Mon. Wea. Rev.*, **127**, 341–362.

Chagnon, J. M. and P. R. Bannon, 2001 : « Hydrostatic and geostrophic adjustment in a compressible atmosphere : Initial response and final equilibrium to an instantaneous localized heating ». *J. Atmos. Sci.*, **58**, 3776–3792.

Courtier, P. and O. Talagrand, 1990 : « Variational assimilation of meteorological observations with the direct and adjoint shallow-water equations ». *Tellus*, **42A**, 531–549.

Daley, R., 1991 : *Atmospheric Data Analysis*. Cambridge University Press, 457 pp.

Delden, A. V., 2003 : « Adjustment to heating, potential vorticity and cyclogenesis ». *Quart. J. Roy. Meteor. Soc.*, **129**, 3305–3322.

Errico, R. M., 1990 : « An analysis of dynamic balance in a mesoscale model ». *Mon. Wea. Rev.*, **118**, 558–572.

Fillion, L., 2002 : « Variational assimilation of precipitation data and gravity wave excitation ». *Mon. Wea. Rev.*, **130**, 357–371.

Fovell, R., D. Durran, and J. R. Holton, 1992 : « Numerical simulations of convectively generated stratospheric gravity waves ». *J. Atmos. Sci.*, **49**, 1427–1442.

Holton, J. R., 1992 : *An introduction to dynamic meteorology*. Academic Press, Inc., 511 pp.

Machenhauer, B., 1977 : « On the dynamics of gravity oscillations in a shallow water model with application to normal mode initialization ». *Contrib. Atmos. Phys.*, **50**, 253–271.

Mitchell, H. L., P. L. Houtekamer, and G. Pellerin, 2002 : « Ensemble size, balance, and model-error representation in an Ensemble Kalman Filter ». *Mon. Wea. Rev.*, **130**, 2791–2808.

Nicholls, M. E. and R. A. Pielke, 1994 : « Thermal compression waves. Part II : Mass adjustments and vertical transfer of total energy ». *Quart. J. Roy. Meteor. Soc.*, **120**, 333–359.

Nicholls, M. E., R. A. Pielke, and W. R. Cotton, 1991 : « Thermally forced gravity waves in an atmosphere at rest ». *J. Atmos. Sci.*, **48**, 1869–1884.

O'Sullivan, D. and T. J. Dunkerton, 1995 : « Generation of inertia-gravity waves in a simulated life cycle of baroclinic instability ». *J. Atmos. Sci.*, **52**, 3695–3716.

Pandya, R., D. Durran, and C. Bretherton, 1993 : « Comments on "thermally forced gravity waves at rest" ». *J. Atmos. Sci.*, **50**, 4097–4101.

Polavarapu, S., M. Tanguay, and L. Fillion, 2000 : « Four-dimensional variational data assimilation with digital filter initialization ». *Mon. Wea. Rev.*, **128**, 2491–2510.

Räisänen, J., 1995 : « Factors affecting synoptic-scale vertical motions : A statistical study using a generalized omega equation ». *Mon. Wea. Rev.*, **123**, 2447–2460.

———, 1997 : « Height tendency diagnostics using a generalized omega equation, the vorticity equation, and a nonlinear balance equation ». *Mon. Wea. Rev.*, **125**, 1577–1597.

Schubert, W. H., S. R. Fulton, and R. A. Hertenstein, 1989 : « Balanced atmospheric response to squall lines ». *J. Atmos. Sci.*, **46**, 2478–2483.

Shutts, G. J. and M. E. B. Gray, 1994 : « A numerical modelling study of the geostrophic adjustment process following deep convection ». *Quart. J. Roy. Meteor. Soc.*, **120**, 1145–1178.

Tanguay, M., A. Robert, and R. Laprise, 1990 : « A Semi-implicit Send-Lagrangian Fully Compressible Regional Forecast Model ». *Mon. Wea. Rev.*, **118**, 1970–1980.

Thurre, C., 1998 : « Étude de l'ajustement hydrostatique suite à un forçage diabatique dans un modèle pleinement élastique ». PhD. Thesis, McGill University, 124 pp.

Zou, X., I. M. Navon, and J. Sela, 1993 : « Control of gravitational oscillations in variational data assimilation ». *Mon. Wea. Rev.*, **121**, 272–289.

CHAPITRE III

ANALYSIS OF DYNAMIC BALANCE ADJUSTMENT PROCESSES PART II : HEATING SIZE, STABILITY AND BACKGROUND WIND EFFECTS

Christian Pagé and Peter Zwack

Abstract

In this paper we continue the description and analysis of the sequence of physical processes leading to an adjusted dynamical balanced state in 3D idealized numerical simulations initiated in part I. Special emphasis is put on the effect on dynamical balance when varying the diabatic heating horizontal size, static stability, as well as the presence of a background wind. In particular, an analysis of two simulations with a diabatic heating of meso-β size (with $f = 0$ and $f = 10^{-4}\ s^{-1}$) is presented.

Résumé

Dans cet article, nous présentons la description et l'analyse de la série de processus physiques impliqués lors des ajustements vers un état de balance dynamique dans les simulation numériques 3D idéalisées présentées dans la partie I. Une attention particulière est appliquée aux effets sur la balance dynamique d'une variation de la dimension horizontale du réchauffement, de la stabilité statique, de même que de la présence d'un vent de base. En particulier, une analyse de deux simulations qui utilisent un réchauffement diabatique à méso-échelle-β,ayant des valeurs de $f = 0$ et $f = 10^{-4}\ s^{-1}$ respectivement, est présentée.

3.1 Introduction

Dynamical balance issues are still currently of great interest in data assimilation (Fillion, 2002; Polavarapu et al., 2000; Lorenc, 2003; Mitchell et al., 2002), especially at higher model resolutions, e.g. mesoscale-γ ($\sim$ 5 km). The analysis which is presented here goes along those lines, where dynamical balance is defined as the balance of the forces acting on the model's dynamical fields. In part I, nonlinear balance (NLB) equations are presented, along with a generalized ω equation, which is a NLB version of Räisänen (1995). Also, an analysis technique, which is used to evaluate when balance is reached independently from using diagnostic balance equations, was developed in part I and will be used here. A description and analysis of the mechanisms (the sequence of physical processes) of dynamical balanced state adjustments in 3D idealized numerical simulations was presented in part I for a reference simulation (which has no rotation), hereafter F0, and a simulation with a typical mid-latitude rotation ($f = 10^{-4}\ s^{-1}$), hereafter F4.

Using the same analysis methods as in part I, the analysis of two simulations with a diabatic heating of meso-β size are presented in section 3.3, both without rotation and with typical mid-latitude rotation ($f = 10^{-4}\ s^{-1}$). In addition, the effect of static stability (section 3.3.2) and the presence of a background wind (section 3.3.3) on the balance state and its adjustment will also be analyzed. The analysis will use the NLB equation and the NLB ω equation, described in part I, in order to compare the model's resulting balance with NLB theory. Results are presented with the same analysis technique used in part I, which involves the time series of several fields most influenced by balanced state adjustments. Results are then related to classical theory. Comparisons are also made against the F0 and F4 simulation analyzed in part I.

3.2 Numerical simulations and NLB diagnostics

The numerical model used is the same as in part I, which is the dynamical core of the Canadian Regional Climate Model (CRCM) as described in Caya and Laprise (1999). The dynamical core of the CRCM is based on the same formulation as that from the

Mesoscale Compressible Community Model (MC2) (Benoit et al., 1997).

Recalling the configuration of the numerical model, the physics package of the model is turned off during the simulations, the atmosphere is dry, and an f-plane is used. The integration timestep used is 60 seconds and data is output each 15 minutes for the meso-α ($\sim$ 1500 km), except 60 seconds for the simulations with the diabatic heating of meso-β ($\sim$ 150 km) size. An artificial diabatic heating is forced into the model at the first timestep and kept constant (in pressure vertical coordinates) throughout the simulation. It is sinusoïdal in the vertical and Gaussian in the horizontal. The heating amplitude at the maximum is set at a value of $21.6K/day$ ($2.5 \times 10^{-4}K/sec$). The main characteristics and initial conditions of the simulations are shown in table 3.1 and 3.2.

Table 3.1 Common characteristics and initial conditions of the numerical simulations.

Horizontal sponge	10 grid points
Vertical sponge depth	15 km
Heating vertical extent	$300 - 800$ hPa
p at heating maximum	522 hPa
Initial vertical motion	0 m/s
Initial surface pressure	Uniform at 1000 hPa

Balanced state reached in the numerical simulations will be compared to NLB as diagnosed by the ω and NLB equations introduced in part I. Note that for simulations with no rotation, only the modified ω equation presented in part I, where all terms multiplied by f are eliminated, will be used.

3.3 Results

This section presents the analysis of the numerical simulations. These simulations explore the effects of the horizontal size of the diabatic heating, the vertical thermodynamic structure (static stability) and the presence of a background horizontal wind (subsec-

Table 3.2 Main characteristics and initial conditions of each analyzed numerical simulation.

Name	Grid	Mesh	Domain	Levels	Coriolis
HRF0	185×185	3 km	555×555 km	59	0 sec^{-1}
HRF4	185×185	3 km	555×555 km	59	10^{-4} sec^{-1}
USF0	92×92	60 km	5550×5550 km	30	0 sec^{-1}
USF4	92×92	60 km	5550×5550 km	30	10^{-4} sec^{-1}
BWF4	92×92	60 km	5550×5550 km	30	10^{-4} sec^{-1}

Name	Length	Heating Hor. Dim.	Init. Hor. Winds	Init. Temp. Prof.
HRF0	10 h	144 km	0 m/s	Isothermal at 0 C
HRF4	10 h	144 km	0 m/s	Isothermal at 0 C
USF0	48 h	1440 km	0 m/s	US Standard Atm.
USF4	24 h	1440 km	0 m/s	US Standard Atm.
BWF4	24 h	1440 km	Uniform 20 m/s	Isothermal at 0 C

tions 3.3.1 to 3.3.3), and results are compared against classical theory. In these analyses the resulting balanced state achieved by the model will be compared to NLB diagnostics using DIONYSOS (Caron et al., 2006). All results shown here use pressure as the vertical coordinate.

3.3.1 Effect of heating size diameter

Diabatic heating zones of small sizes (meso-β and meso-γ: $10 - 200\ km$) is of great interest in recent data assimilation research because operational numerical models will approach meso-γ horizontal resolutions in the next few years. However, there is still debate as to what constitutes the balanced state at these scales.

To help to answer these questions, numerical simulations were performed with a heating size of 144 km and a model horizontal resolution of 3 km and 6 km. Other simulations were also done with heating sizes of 720 km, 360 km and 72 km, but these will not be shown here because they do not add more to the analysis. With a heating size of 144 km (which is 10 times smaller than the F0 simulation) horizontal resolution could not be set 10 times smaller : a ratio of 20 had to be used to prevent major problems in the accuracy of the numerical model solution. The model simulations exhibited non-symmetric response to the symmetric forcing, which is a sign that waves were not properly integrated in time due to the too coarse horizontal resolution. This is why the 144 km heating simulations have a 3 km horizontal resolution instead of 6 km. Because of this, the number of horizontal grid points had to be doubled in each direction to have a proper distance between the heating and the boundaries. Further, the number of vertical levels also had to be almost doubled from 30 to 59 levels to have a proper ratio of horizontal vs vertical resolutions. Simulations in this configuration were done with no rotation, hereafter HRF0, and with rotation ($f = 10^{-4}\ s^{-1}$), hereafter HRF4. These two simulations will be analyzed separately in the following two subsections.

Simulation with no rotation (HRF0)

When the heating size is smaller, the balanced state adjustment occurs much faster. With the 144 km heating size, considered here in an initial isothermal atmosphere, balanced state is reached after only 1h40m, compared to the F0 simulation (1440 km heating size) where it takes 13h30m. Classical theory, from the gravity wave dispersion relationship (part I), predicts that the adjustment is faster for a smaller heating size because gravity waves will have a group velocity and a phase speed close to the speed achieved with the large heating size (since static stability is the same, so will also be the Brunt-Väisälä frequency), which makes for much more effective and rapid propagation of unbalanced energy out of the domain.

What are the main mechanisms leading to a faster balance adjustment? Because the total prescribed heating does not change, the geopotential height tendencies are similar. However, since the horizontal size is smaller, a smaller height change will produce an equivalent horizontal height gradient and corresponding pressure force, and the divergent horizontal winds are therefore produced more quickly. This will lead to a faster increase of divergence/convergence and hence of vertical motion. In fact, the series of physical processes leading to balance are the same, but everything occurs much faster. These statements are confirmed by calculating the relative magnitude of the terms of the relevant equations and by the dispersion relationship.

In the appropriate ω equation for the case of no rotation (part I), horizontal scale ($\triangle x$) appears on both sides of the equation (through the laplacian operator), in the diabatic term and $S\omega$ term, respectively. In the divergence tendency equation (part I), on the other hand, $\triangle x$ only appears on the right hand side of the equation. In table 3.3 is shown the magnitude of terms of ω and divergence equations, with the 1440 km and the 144 km heating sizes, respectively. For the ω equation, the calculation of the relative magnitude of the terms is done after 24h of simulation, while for the divergence tendency equation, it is done before the first overshoot when the field tendencies are constant (at 1h and 14 min, for the 1440 km and the 144 km heating sizes, respectively). The magnitude is

the maximum absolute mean horizontal magnitude of all the vertical levels, in a square of 5x5 points encompassing the center of the heating. Divergence tendency is then $\triangle x$ times (10 times in this case) stronger in the 144 km size than for the 1440 km size, and balanced vertical motion is identical. The adjustment period is then much faster for the small heating size.

Table 3.3 Relative magnitude of the terms related to the impact of horizontal resolution with no rotation.

Balanced omega		
	1440 km	144 km
ω	$-0.14\ Pa/s$	$-0.14\ Pa/s$
$\frac{R}{p}\nabla^2 S\omega$	7×10^{-16}	2×10^{-13}
$= -\frac{R}{p}\nabla^2\left[-\vec{V}\cdot\vec{\nabla}T\right]$	6×10^{-18}	5×10^{-17}
$-\frac{R}{p}\nabla^2\frac{\dot{q}}{c_p}$	7×10^{-16}	2×10^{-13}

Divergence tendency at 1h and 14 min

for the 1440 km and the 144 km heating sizes respectively

	1440 km	144 km
$\frac{\partial D}{\partial t}$	$5 \times 10^{-10}\ sec^{-2}$	$7 \times 10^{-9}\ sec^{-2}$
$= -\nabla^2\phi$	10^{-10}	7×10^{-9}
$+D^2$	2×10^{-12}	4×10^{-11}
$-2\left[\frac{\partial u}{\partial x}\frac{\partial v}{\partial y} - \frac{\partial u}{\partial y}\frac{\partial v}{\partial x}\right]$	2×10^{-12}	6×10^{-12}
$-\vec{V}\cdot\vec{\nabla}D$	2×10^{-12}	1×10^{-11}
$-\omega\frac{\partial D}{\partial p}$	5×10^{-12}	6×10^{-11}
$-\left[\frac{\partial \omega}{\partial x}\frac{\partial u}{\partial p} + \frac{\partial \omega}{\partial y}\frac{\partial v}{\partial p}\right]$	1×10^{-12}	2×10^{-11}

Simulation with rotation $f = 10^{-4}\ s^{-1}$ (HRF4)

Rotation modifies how the heating size affects dynamical balance. The Rossby radius of deformation is on the order of 450 km, which means that Coriolis effects will not

be significant. With the 144 km heating size, considered here in an initial isothermal atmosphere, balanced state is reached after 1h40m, compared to the 1440 km heating size with $f = 10^{-4}\ s^{-1}$, where it takes 16h45m. With a small heating size, balanced state is reached at exactly the same time compared to the simulation with no rotation (HRF0), which is consistent with the Rossby radius of deformation. However, balance occurs much faster when compared with the F4 simulation (1440 km heating size), as was the case with the simulation HRF0. A calculation of the relative magnitude of the terms in the equations is very helpful to examine the effect of heating size on vertical motion and divergence tendencies, which is shown in table 3.4.

One of the effects of the Coriolis force is that the balanced vertical motion will no longer be the same when the heating size changes. This is reflected in the ω equation in table 3.4 where many more terms are present in the equation, hence the horizontal resolution will no longer cancel exactly on both sides of the equation, if these additional terms are large. The first thing to note is that only the large heating size shows a different balanced vertical motion when comparing simulations with rotation vs no rotation. This is because of the temperature advection term, which is non-negligible at the balanced state since there is a non-vanishing horizontal temperature gradient combined with divergent winds (tendencies of these two variables are also non-vanishing). These tendencies are produced because the pressure gradient force has a scale which is comparable to the Coriolis force, while when the heating size is small, the pressure gradient is several orders of magnitude larger : the Coriolis force is then negligible in comparison.

The divergence tendency will also be affected, but only later in the adjustment process, because the only difference with the non-rotating case will be the presence of absolute vorticity.

A summary of the results is shown in table 3.5. The conclusions are similar to those for the simulation with no rotation. The rate of increase in vertical motion is much higher (through strong divergence at the beginning of the simulations) for the small heating size, hence adiabatic cooling dominates over diabatic heating. Also, gravity waves are

Table 3.4 Relative magnitude of the terms related to the impact of horizontal resolution on rotation.

Balanced omega		
	1440 km	144 km
ω	$-0.09\ Pa/s$	$-0.14\ Pa/s$
$\frac{R}{p}\nabla^2 S\omega$	6×10^{-16}	2×10^{-13}
$+f(f+\zeta)\frac{\partial^2\omega}{\partial p^2}$	5×10^{-18}	2×10^{-17}
$-f\omega\frac{\partial^2\zeta}{\partial p^2}$	1×10^{-18}	1×10^{-18}
$-f\frac{\partial}{\partial p}\left[\frac{\partial\omega}{\partial x}\frac{\partial v}{\partial p} - \frac{\partial\omega}{\partial y}\frac{\partial u}{\partial p}\right]$	9×10^{-19}	1×10^{-18}
$= -\frac{R}{p}\nabla^2\left[-\vec{V}\cdot\vec{\nabla}T\right]$	3×10^{-17}	4×10^{-16}
$-\frac{R}{p}\nabla^2\frac{\dot{q}}{c_p}$	7×10^{-16}	2×10^{-13}
$-f\frac{\partial}{\partial p}\left[-\vec{V}\cdot\vec{\nabla}(f+\zeta)\right]$	6×10^{-19}	1×10^{-18}
$+f\frac{\partial}{\partial p}\left[\frac{\partial\zeta_{ag}}{\partial t}\right]$	3×10^{-20}	8×10^{-17}

Divergence tendency at 1h and 14 min

for the 1440 km and the 144 km heating size respectively

	1440 km	144 km
$\frac{\partial D}{\partial t}$	$5 \times 10^{-10}\ sec^{-2}$	$7 \times 10^{-9}\ sec^{-2}$
$= f\zeta$	2×10^{-11}	2×10^{-11}
$-f\zeta_g$	5×10^{-10}	7×10^{-9}
$+D^2$	2×10^{-12}	4×10^{-11}
$-2\left[\frac{\partial u}{\partial x}\frac{\partial v}{\partial y} - \frac{\partial u}{\partial y}\frac{\partial v}{\partial x}\right]$	2×10^{-12}	6×10^{-12}
$-\vec{V}\cdot\vec{\nabla}D$	2×10^{-12}	1×10^{-11}
$-\beta u_{ag}$	0	0
$-\omega\frac{\partial D}{\partial p}$	5×10^{-12}	6×10^{-11}
$-\left[\frac{\partial\omega}{\partial x}\frac{\partial u}{\partial p} + \frac{\partial\omega}{\partial y}\frac{\partial v}{\partial p}\right]$	1×10^{-12}	2×10^{-11}

Table 3.5 Summary of heating size impacts.

	$f = 0\ s^{-1}$		$f = 10^{-4}\ s^{-1}$	
	1440 km	144 km	1440 km	144 km
Time to reach balance	13h30m	1h40m	16h45m	1h40m
Scale of divergence tendencies (sec^{-2}) at 1h (1440 km) and 14 min. (144 km)	5×10^{-10}	7×10^{-9}	5×10^{-10}	7×10^{-9}
Balanced vertical motion at max (Pa/s)	-0.14	-0.14	-0.09	-0.14
Scale of balanced divergence tendency (sec^{-2})	4×10^{-11}	7×10^{-10}	7×10^{-10}	2×10^{-9}

very efficient to drive unbalanced energy out of the domain because the group velocity and phase speed are similar to the case with no rotation.

Balance diagnostics

These simulations have considered a much smaller heating size than the reference simulation. It is of interest to determine if the NLB equation is also valid at this small horizontal scale. For this purpose NLB diagnostics are compared with the model at the balanced state, as was done with the coarser horizontal scale. We are comparing vertical motion at 500 and 700 hPa for the non-rotating (figure 3.1) and the rotating (figure 3.2) simulations at the center of the heating. Also, for the rotating case, we compare absolute vorticity tendency at 400 and 700 hPa (figure 3.3).

The time series of vertical motion have several important characteristics. First, as in the reference simulation, there is a very good agreement between the numerical simulations and the NLB diagnosed values at both of these vertical levels (for simulations both with and without rotation). If fact, these simulations are almost identical. We can

also state that at the center of the heating, the numerical simulation is very close to NLB near 1h30m, but never exactly. This agrees very well with the calculated balance of 1h40m discussed earlier. Also, NLB diagnostics show a diagnosed vertical motion which is constant in time. This indicates that static stability does not change in time, in contrary to the large heating size simulations. This is also expected because temperature tendency is very small (not shown) since the Coriolis force has almost no effect when the heating size is small. On the other hand, the time series of vorticity tendency shows a quite noisy model tendency because model output used to compute tendencies is 1 min. instead of 15 min. used for the larger heating size. Also, quite notably, the agreement between NLB and model vorticity tendency is not too good at 700 hPa (figure 3.3), while vertical motion has a very good agreement (figure 3.2). The exact cause of these differences are still under investigation.

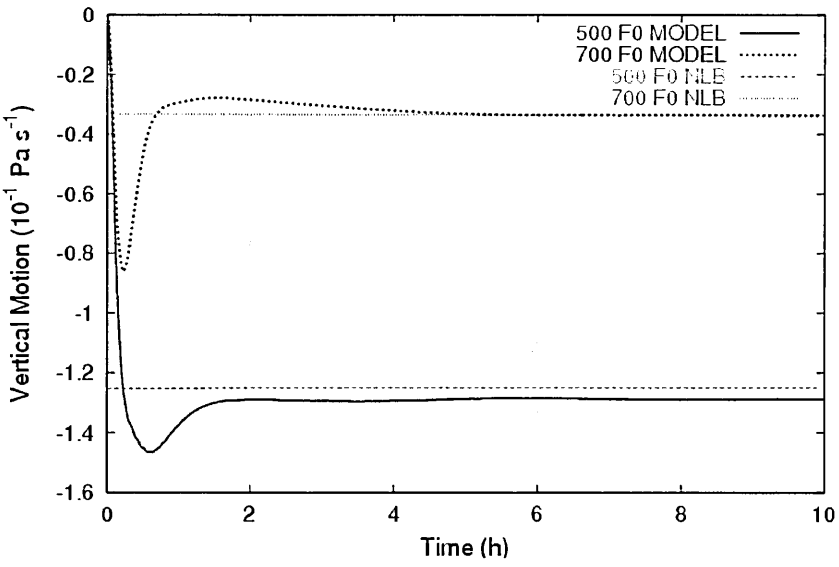

Figure 3.1 Time series of vertical motion ω (10^{-1} Pa s^{-1}) at 500 and 700 hPa comparing model vs NLB vertical motion, simulation HRF0.

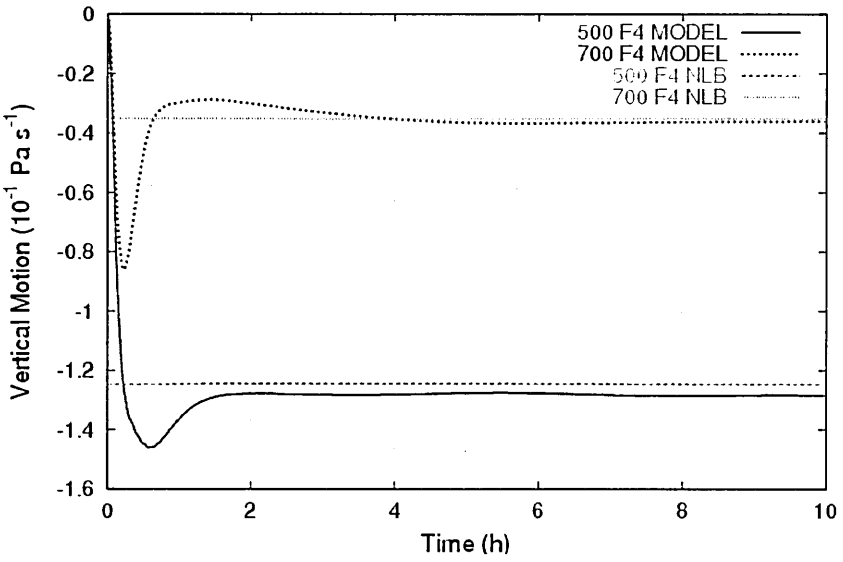

Figure 3.2 Time series of vertical motion ω (10^{-1} Pa s^{-1}) at 500 and 700 hPa comparing model vs NLB vertical motion, simulation HRF4.

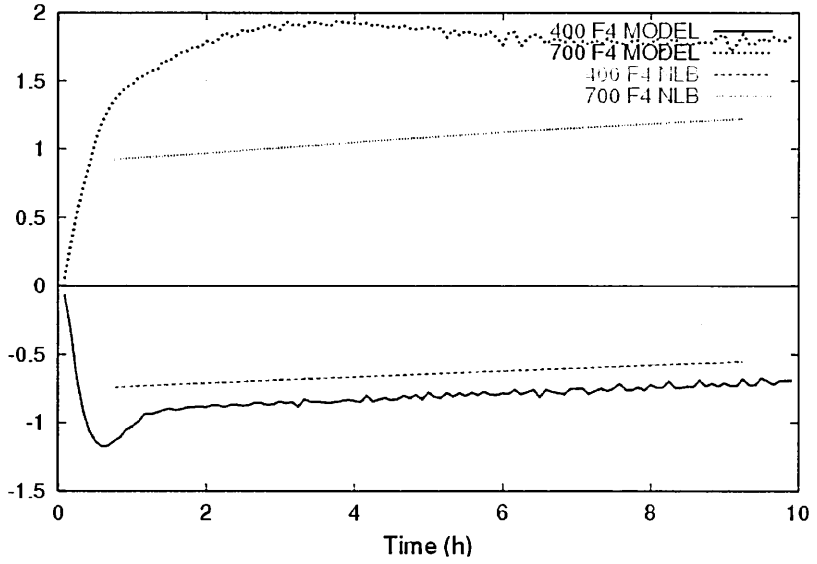

Figure 3.3 Time series of vorticity tendency (10^{-9} s^{-2}) at 400 and 700 hPa comparing model vs NLB vorticity tendency, simulation HRF4.

Summary

In summary, the effect of a smaller heating size diameter is a dynamic balanced state adjustment which occurs a lot faster than for broader heating sizes. It has been explained through the calculation of the magnitude of the terms in the NLB omega equation (table 3.4) that it is because the divergence tendency is much stronger when the heating is small, while vertical motion amplitude is unaffected (no rotation) or slightly affected (rotation). Also gravity waves, which have about the same group velocity and phase speed since static stability is the same, are much more efficient to propagate unbalanced energy out of the domain.

This faster adjustment toward balance is good news for higher resolution model configurations because this means that for meso-γ scales, dynamic balance will be attained very fast for small diabatic heating zones. However, this will not prevent meso-α heating zones (which will also be present in meso-γ simulations) to be much slower in reaching balance.

3.3.2 Effect of vertical thermodynamic structure (static stability)

We have shown previously that the static stability of the atmosphere, and hence its vertical thermodynamic structure, is very important for the dynamical balanced state and its adjustment process (section 2.3). A small difference in stability will mean a very strong feedback in dynamical balance mainly because of adiabatic cooling impact, which generates gravity waves. The static stability will affect the group velocity and phase speed, as well as the frequency, of gravity waves. Thus, from the dispersion relationship, it can be expected that for weaker stability their speed and frequency will be lower, leading to a lower balance adjustment rate. Furthermore, the Rossby radius of deformation will be smaller for the same Coriolis parameter, leading to a greater impact of the Coriolis force on the adjustment rate and more significant inertial gravity wave oscillations.

All numerical simulations described in table 3.2 were also performed with a US Standard Atmosphere (NOAA et al., 1976) vertical temperature distribution (but constant in the horizontal). Both rotating and non-rotating cases have been simulated, hereafter USF0 and USF4 respectively. The F0 simulation has a uniform temperature everywhere in the 3D domain, which means that the atmosphere is very stable compared to the atmosphere in the simulations USF0 and USF4 described here. This should have a great impact on dynamical balance as expected by the analysis of the previous results.

The analysis of the USF0 simulation shows that the balanced state's 3D structure is almost identical to the F0 simulation. However the amplitudes of the dynamical fields are much stronger. This is because a stronger vertical motion is needed to create the same adiabatic cooling in a US Standard Atmosphere, compared to an isothermal atmosphere, to compensate totally for the diabatic heating. This can be seen in the time series of vertical motion at 300 and 500 hPa (figure 3.4). In fact, adiabatic cooling is the same in both F0 and USF0 simulations. Hence the balanced state takes a lot longer to be established when stability is weaker. While balanced state was reached in 13h30m in the F0 simulation, in the USF0 simulation with the US Standard Atmosphere it takes as much as 19h30m.

It takes even longer to achieve balance in a rotating environment, as predicted by classical theory. Simulation F4 ($f = 10^{-4}\ s^{-1}$) reaches a balanced state after 16h45m (for an isothermal atmosphere), but for the USF4 simulation (using a US Standard Atmosphere), the time to achieve balance cannot be determined in the current framework (without changing the prescribed heating intensity) because this simulation produces regions of static instability which cannot be removed since no convection scheme is activated in the model configuration. This means that we can only perform simulations with a heating encompassing all of the troposphere (from 1000 hPa to 300 hPa) and which only develops static instabilities well after 30 h of simulation. In summary, in a weakly stable environment, a balanced state takes much longer to be reached, and this is amplified in a rotating vs a non-rotating environment.

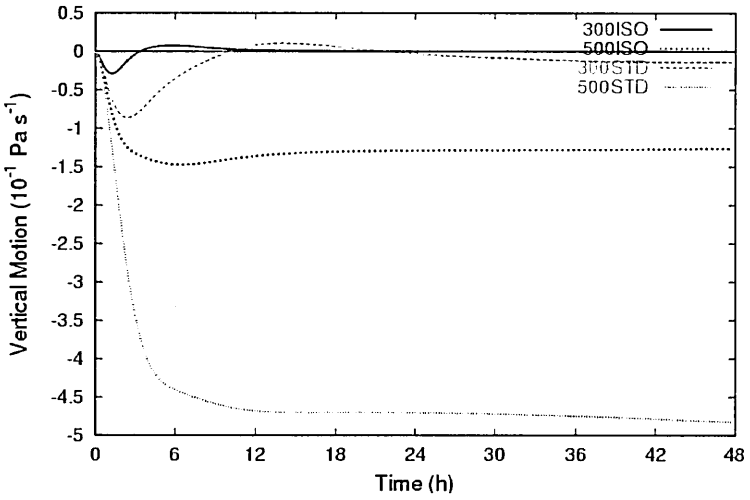

Figure 3.4 Time series of vertical motion ω (10^{-1} Pa s^{-1}) at 300 and 500 hPa for the isothermal (F0) and the US Standard Atmosphere (USF0) simulations (no rotation).

Dynamical balance adjustment processes are very similar in the USF0 simulation compared to the isothermal F0 simulation (in the absence of rotation). The main difference is that the amplitude of the overshoots are much larger and the oscillation frequencies are much higher (this can be especially seen below and above the heating, near the center, see figure 3.4). This is directly related to the strength of the adiabatic cooling which is highly dependent on the static stability (as was mentioned above for the differences in the balanced state).

3.3.3 Effect of the background horizontal wind

A valid question is : what is the effect of a background circulation on dynamical balance? Is the balance (along with its adjustment) different when it is embedded in a background circulation? To answer this question, simulations were done with a background -20 m/s wind (x-component of the wind) in geostrophic balance for the $f = 10^{-4}$ s^{-1} simulation. We will compare this simulation, hereafter BWF4, to the F4 simulation ($f = 10^{-4}$ s^{-1} and no background wind).

After reaching the end of the 24h simulation with a background wind, which is in a balanced state, the atmosphere depicts a totally different 3D structure compared to the F4 simulation. Relative vorticity (figure 3.5) is no longer symmetric around the heating center, while vertical motion is affected to a lesser extent. Its amplitude is indeed only slightly affected because of the vorticity and temperature advection terms in the omega equation. After 24h, the vertical motion has an amplitude which is 14% more than without the background wind, and the 3D structure is no longer totally symmetric around the heating center.

As can be seen in figure 3.7, relative vorticity shows an elongated shape oriented in the same direction as the background wind vector, with a similar horizontal width (perpendicular to the wind vector) as the diabatic heating forcing. In the center of the heating, the balanced state is characterized by vorticity and temperature advection which together compensate exactly the tendencies produced by the diabatic heating, resulting in a dynamical balance which is quite different in structure (compared to the F4 simulation), even if the vertical motion itself is not much affected. The other fields, namely vorticity, temperature and pressure tendencies, are almost zero, which was not the case without the background wind, because of the advection terms in the vorticity and thermodynamic equations (Holton, 1992, pp. 105, 60). We can therefore say that the presence of the background wind affects mainly the rotational and thermodynamical aspects of the balance, but only slightly the divergent aspects.

Adjustment toward a balanced state shows more complex interactions between different processes than in the F4 simulation. The overshoots in the dynamical and thermodynamic fields (especially vorticity and temperature, per discussion above) are creating extrema in the advected values of these fields, hence creating a 3D structure that "self-propagates" away with the background wind through vorticity and temperature advection forcings. When this 3D structure has propagated away (it takes about 30h to propagate completely out of the domain), field tendencies asymptote to constant values and a balanced state is reached.

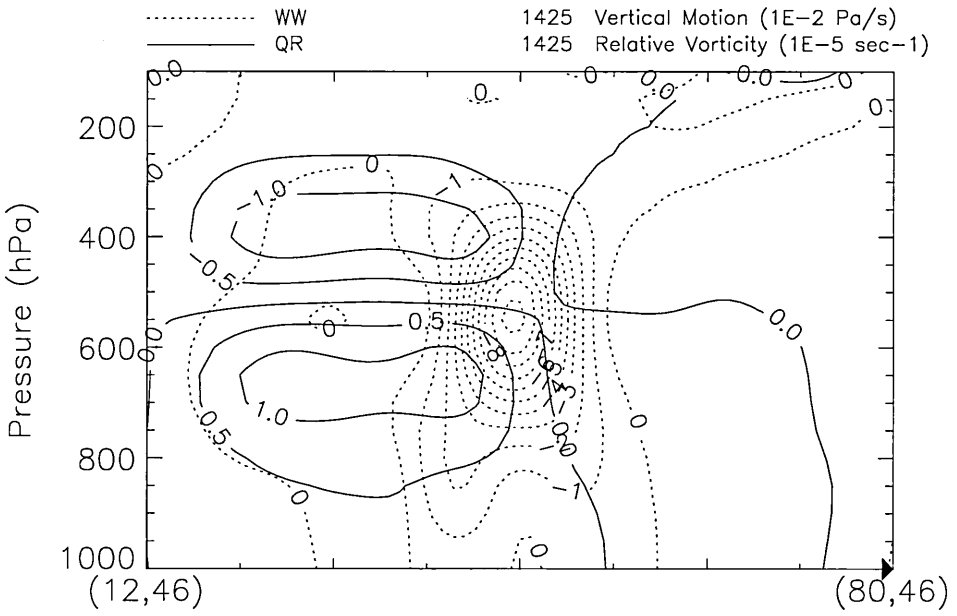

Figure 3.5 Vertical cross-section (west to east) through the center of the heating (on an x-axis) of vertical motion ω ($10^{-2} Pa\ s^{-1}$ dotted lines) and relative vorticity ($10^{-5} s^{-1}$ solid lines) at 24h in the BWF4 simulation (easterly winds of 20 m/s). Vertical axis represents pressure levels.

At the center of the heating core, temperature and vorticity advection terms are together compensating almost exactly the diabatic heating term, as said earlier. When a 20 m/s background wind is present, the vertical motion at 500 hPa (figure 3.6) exhibits significantly less oscillations in time, meaning that dynamical balance is reached much earlier at this location and that the adjustment time is significantly reduced. This is related to vorticity which is advected away through the background wind. Hence, vorticity tendency has vanishsed to near zero after only 8h in the simulation (figure 3.7). This is because of vorticity advection which totally compensates the production of vorticity. This effect then compensates the inertial force, which in turn accelerates the adjustment toward balance.

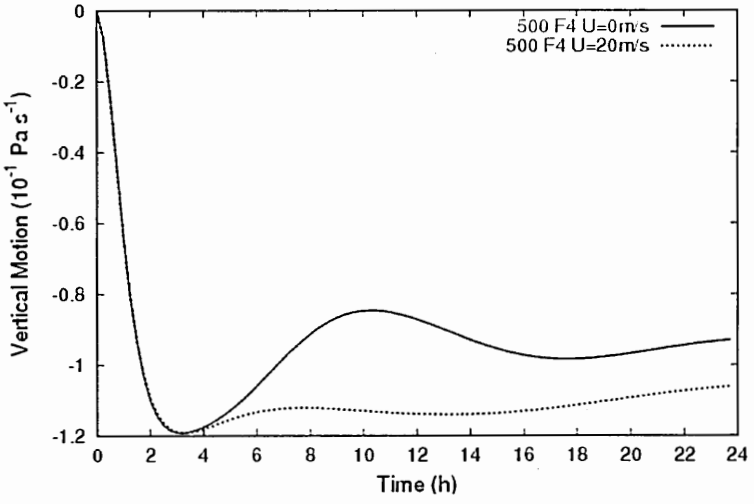

Figure 3.6 Vertical motion ω ($10^{-1}Pa\ s^{-1}$) at 500 hPa with 0 m/s (F4 simulation) and 20 m/s (BWF4 simulation) background winds compared.

As for temperature tendency when dynamical balance is reached, this term is almost zero at the center of the heating while the simulation with no background wind exhibits a constant temperature tendency which is not zero (figure 3.8). This temperature tendency is one to two orders of magnitude less than with no background wind (not shown). Also, as it is the case with vertical motion, oscillations are much reduced during the

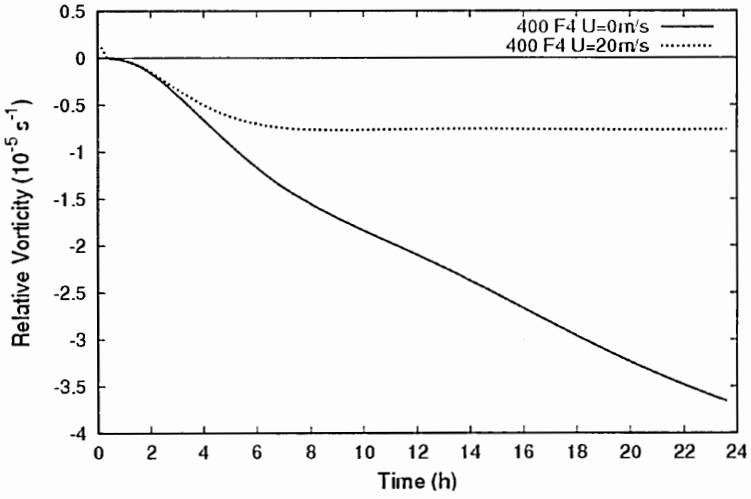

Figure 3.7 Relative vorticity ($10^{-5}s^{-1}$) at 400 hPa with 0 m/s (F4 simulation) and 20 m/s (BWF4 simulation) background winds compared.

adjustment. Absolute vorticity exhibits the same characteristics (not shown), with a constant value at dynamical balance instead of a constant tendency.

In summary, a uniform initial background wind of 20 m/s has mainly an effect on the rotational and thermodynamic aspects of balance. The effect on divergent aspects (vertical motion) are quite smaller : only a 14% increase in the amplitude of vertical motion was observed. The most important effect on the balance adjustment is that the adjustment is much faster because the production of vorticity tendency is compensated totally after 8h in the simulation. The oscillations have then much less amplitude because inertial forces are compensated partially in the overall simulation.

3.4 Conclusions

The impact of several different conditions on dynamical balanced state and adjustment has been presented and compared to the reference and F4 simulations presented in part I. First, the impact of a smaller diabatic heating horizontal size, in the presence

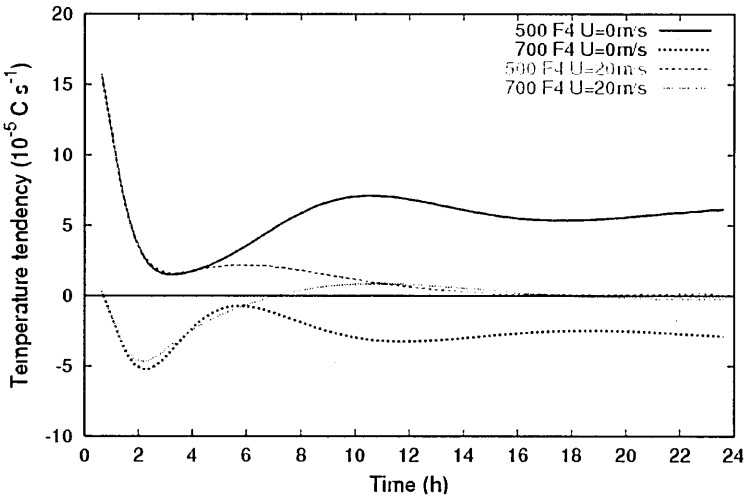

Figure 3.8 Temperature tendency ($10^{-5}C\ s^{-1}$) at 500 and 700 hPa with 0 m/s (F4 simulation) and 20 m/s (BWF4 simulation) background winds compared.

($f = 10^{-4}\ s^{-1}$) or absence of rotation, was presented. It has a significant effect on the physical processes themselves. With tropospheric heating of much reduced horizontal size (meso-β scale), the Coriolis force has a negligible effect, as is expected from the Rossby radius of deformation. This is because the pressure gradient force is several orders of magnitude larger compared to the same force associated to a synoptic scale heating size, while vertical motion is the same, resulting in a Coriolis force which is then several orders of magnitudes smaller than the pressure gradient force. Balanced state and its adjustment is then unaffected by the Coriolis force for a meso-β heating size. Further, for such a heating size, balance adjustment will occur much faster, as predicted by the dispersion relationship, since divergence tendency is much larger because of a strong pressure gradient, while vertical motion is the same. Gravity waves will be much more efficient to propagate unbalanced energy away from the heating source because their phase speed depends almost exclusively on static stability, and not on the heating horizontal size. Since the horizontal size is smaller, gravity waves propagate rapidly away from the heating source region.

Also, the impact of the static stability 3D structure has been directly assessed. It has been shown how important is the static stability on the balance adjustment time and amplitude, as well as on the balanced state itself, as predicted by classical theory. This results in the problem of spurious gravity wave oscillations being much more serious in weaker stability environment (generally this is where precipitation is occurring), and it is highly amplified by the presence of Coriolis.

On the other hand, the presence of a background wind mostly affects the rotational and thermodynamic aspects of the balance. It does affect strongly the adjustment time however since a background wind compensates the fields' tendencies (which are caused by the presence of Coriolis): inertial oscillations are then partially compensated in the overall simulation leading to a faster balance adjustment.

An objective method has been developed to calculate when balance is reached in these idealized numerical simulations and is presented in part I. It has been used as a method independent of the NLB equation. As it is the case with the simulations presented in part I, this method is successful in determining when balance is reached. We can then state that NLB is valid even at smaller scales, i.e., meso-β scales in the context described here.

From the results of this analysis, the problem of dynamical balance adjustment can be important for heating sizes of small horizontal extent (on the order of $100 - 200\ km$) in weaker stability environments, and for very short term forecasts. It is to be noted that there are no significant inertial oscillations associated with balance adjustment at these scales. This is because inertial forces are much weaker than stronger pressure gradient forces created by small heating sizes.

As it is discussed in part I, this work can be extended in many ways. Adding to what is identified in part I, extension of this kind of analysis to real cases (for example on an isolated mesoscale convective system) is the next step, because synthetic cases have many limitations. Nonetheless, they do identify many of the important aspects of dynamical balance.

Acknowledgements. Any comments/questions should be emailed to page.christian@uqam.ca. Luc Fillion has helped with several discussions during the course of this work. This work was funded by the CWRP for research aimed at improving short-term QPF for extreme events. It is part of the Ph.D. Thesis of the first author.

Bibliographie

Benoit, R., M. Desgagné, P. Pellerin, S. Pellerin, Y. Chartier, and S. Desjardins, 1997 : « The Canadian MC2 : A semi-Lagrangian, semi-implicit wide-band atmospheric model suited for fine-scale process studies and simulation ». *Mon. Wea. Rev.*, **125**, 2382–2415.

Caron, J.-F., P. Zwack, and C. Pagé, 2006 : « DIONYSOS : A diagnostic tool for numerically-simulated weather systems ». *Atmos.-Ocean*, submitted. Technical related document see http ://www.dionysos.uqam.ca/doc/Dionysos.pdf.

Caya, D. and R. Laprise, 1999 : « A semi-implicit semi-Lagrangian regional climate model : The Canadian RCM ». *Mon. Wea. Rev.*, **127**, 341–362.

Fillion, L., 2002 : « Variational assimilation of precipitation data and gravity wave excitation ». *Mon. Wea. Rev.*, **130**, 357–371.

Holton, J. R., 1992 : *An introduction to dynamic meteorology*. Academic Press, Inc., 511 pp.

Lorenc, A. C., 2003 : « The potential of the ensemble Kalman filter for NWP–a comparison with 4D-Var ». *Quart. J. Roy. Meteor. Soc.*, **129**, 3183–3203.

Mitchell, H. L., P. L. Houtekamer, and G. Pellerin, 2002 : « Ensemble size, balance, and model-error representation in an Ensemble Kalman Filter ». *Mon. Wea. Rev.*, **130**, 2791–2808.

NOAA, NASA, and USAF, 1976 : U.S. Standard Atmosphere. Report, U.S. Government Printing Office, Washington, D.C.

Polavarapu, S., M. Tanguay, and L. Fillion, 2000 : « Four-dimensional variational data assimilation with digital filter initialization ». *Mon. Wea. Rev.*, **128**, 2491–2510.

Räisänen, J., 1995 : « Factors affecting synoptic-scale vertical motions : A statistical study using a generalized omega equation ». *Mon. Wea. Rev.*, **123**, 2447–2460.

CHAPITRE IV

DIAGNOSING MESOSCALE VERTICAL MOTION : IMPLICATIONS FOR ATMOSPHERIC DATA ASSIMILATION SCHEMES

Christian Pagé, Luc Fillion and Peter Zwack

Abstract

Balance omega equations have recently been used to improve the characterization of balance in the control variable of variational data assimilation methods. We follow the work of Fisher (2003) and its diabatic extension by Fillion (2004a,b) which suggests that in convective regions, a quasi-geostrophic methodology using diabatic forcing terms (from model's convection temperature tendencies) in the omega equation can be applied at the synoptic scale. The present work tries to determine if this methodology can be extended to very high-resolution modelling (1 to 10 km), and if extra terms might be deemed important in the omega equation.

A real case study, using a resolution of 2.5 km, is used to explore numerically these questions. Results show that it is possible at these scales and at least for convective phenomena of length scales $15 - 100$ km, to use a Nonlinear Balance omega diagnostic equation which directly uses the numerical model's temperature tendencies as diabatic forcing. It is shown that this represents an improvement over digital filtering with respect to the 3D structure of vertical motion. Also, our results confirm that the Coriolis force does not play an important role in the resulting balance at these scales, and hence balance is mainly concerned with the divergent part of the wind and not the rotational part, which is confirmed by an analysis of the simulation. Finally, the ageostrophic vorticity tendency term in the omega equation can be important in some situations and an accurate procedure is introduced to compute this term. It is also to be noted that spatial and temporal filtering are needed to achieve these results.

Résumé

Des équations d'omega balancées ont récemment été utilisées pour améliorer la caractérisation de la balance dans la variable de contrôle des méthodes variationnelles d'assimila-

tion de données. Nous continuons le travail de Fisher (2003) et son extension diabatique par Fillion (2004a,b) qui suggèrent que, dans les régions convectives, une méthodologie quasi-géostrophique qui utilise les termes de forçage diabatique (qui proviennent des tendances de température convectives du modèle numérique) dans une équation d'omega peut être utilisée à l'échelle synoptique. La présente recherche tente de déterminer si cette méthodologie peut être étendue à de la modélisation numérique à très fine résolution (1 à 10 km), et si des termes supplémentaires doivent être considérés dans l'équation d'omega.

Une étude de cas réaliste, utilisant une résolution de 2.5 km, est utilisée afin d'explorer numériquement ces questions. Les résultats montrent qu'il est possible à cette échelle, et au moins pour des phénomènes convectifs d'un ordre de grandeur de $15-100$ km, d'utiliser une équation balancée non-linéaire diagnostique d'omega qui utilise directement les tendances de température du modèle numérique comme forçage diabatique dans l'équation. Il est montré que cela représente une amélioration par rapport à l'utilisation d'un filtre digital en rapport à la structure 3D du mouvement vertical. De même, les résultats montrent que la force de Coriolis ne joue pas un rôle important dans la balance résultante à ces échelles, et donc que la balance est principalement reliée à la partie divergente du vent et non pas à la partie rotationnelle, ce qui est confirmé par une analyse de la simulation. Finalement, le terme de tendance du tourbillon agéostrophique dans l'équation d'omega peut être important dans certaines situations, et une méthodologie précise qui permet de calculer ce terme est présentée. Il faut aussi noter qu'un filtrage spatial et temporel est nécessaire afin d'arriver à ces résultats.

4.1 Introduction

Current operational variational data assimilation systems for Numerical Weather Prediction (NWP) all rely on the use of approximate "dynamical balance" concepts. The latter being considered essential so as to enforce a delicate balance between mass and winds so as to avoid excitation of fast gravity wave noise in the early stage of the forecast. Before the advent of operational variational data assimilation approaches, the notion of dynamical balance was represented by the Nonlinear Normal Mode Initialization (NNMI) scheme based on Machenhauer's (1977) or Baer and Tribbia's (1977) balance schemes (see Temperton, 1988). In the pre-variational analysis period (i.e. when optimal interpolation analysis schemes were used), NNMI schemes were applied to fields of initial conditions (e.g. winds, temperature, moisture, surface pressure). The resulting analysis fields were then referred to as initialized initial conditions (i.e. balanced initial conditions).

In operational variational analysis context however, balance concepts were rather introduced as simple relationships applied to analysis increments rather than to the full predictive variables. With this respect, Parrish and Derber (1992) first introduced the notion of balanced and unbalanced analysis variable components before correlation modeling assumptions are introduced. Similar simple balance concepts were quickly adopted and used in the Canadian 3D-Var analysis system (see Gauthier et al., 1999). Later, Derber and Bouttier (1999), exploited inherent balance relationships assumed to exist in their ensemble of lagged-forecasts. A regression approach was developed to capture the linear relationship contained in the forecast error samples between mass and winds for instance. Sophisticated linear regression relationships were then introduced in the then operational European Centre for Medium-range Weather Forecasts (ECMWF) three-dimensional variational analysis system (i.e. 3D-Var) with significant success. As part of this new approach, it was shown that linear regressions were capable of representing expected geostrophic relationships among mass and rotational wind components over mid-latitudes from an ensemble of lagged forecasts.

Recently, in an attempt to improve ECMWF background error covariances, Fisher (2003) (hereafter referred to as F03) introduced the quasi-geostrophic (QG) set of balanced equations explicitly in the definition of the balanced part of the analysis variables. As shown by F03, quite similar analysis increments resulted from this new analysis procedure as compared to the previous operational use of linear regressions mentioned above. A noticeable distinction however was obtained for the divergent part of the wind increments and, consequently, vertical motion increments. As one would expect from balanced considerations at synoptic scales treated by ECMWF analysis, the QG-Omega equation enforced coherent divergent flow structures depending on the basic-state considered (see Fig. 17 from F03).

Very recently, additional major NWP centers joined the group of centers operating with benefits a 4D-Var data assimilation system after initial implementations performed at ECMWF and Météo France; e.g. the Japan Meteorological Agency now runs 4D-Var for their operational mesoscale and global data assimilation systems; the Met-Office in England runs 4D-Var since 5 October 2004 and MSC in Dorval now runs a global operational 4D-Var system since 15 March 2005. As a natural extension for operational regional data assimilation, MSC now considers the development of a limited area 4D-Var analysis system (hereafter referred to as Meso4dvar). The primary goal of this new development project is to replace the current operational regional 3D-Var system which suffers from being totally dependent of the global variational analysis system, and especially upon its low horizontal resolution (triangular truncation at wavenumber 108, T108). For this system, Fillion (2004a) introduced the extension of F03 ideas together with the introduction of diabatic forcing of balanced vertical motion. These ideas are currently being examined in a continental version of Meso4dvar (inner loop resolution set at 35 km). The latter, because of its spatial horizontal extension (which covers essentially all of North America), allows the coherent introduction of the QG omega equation in a satisfactory manner. What turns out to be more unknown at this point however, is the degree of extension of the original ideas of F03 in the context of truly mesoscale versions of 3D and 4D-Var systems. This directly concerns the local version of

the Meso4dvar project at MSC where the forecast model is run at 2.5 km and the inner loop of the 3D-Var analysis system still waits to be determined. This local version covers for instance the southern part of Quebec region and is intended to be used for forecasts up to 24h. Figure 4.1 shows both continental and local analysis/forecast domains just described. With regard to the above discussion on balance operators introduced in the analysis variables, it is yet not known if a similar diagnostic omega equation can be used to accurately represent background error correlations at such fine scales.

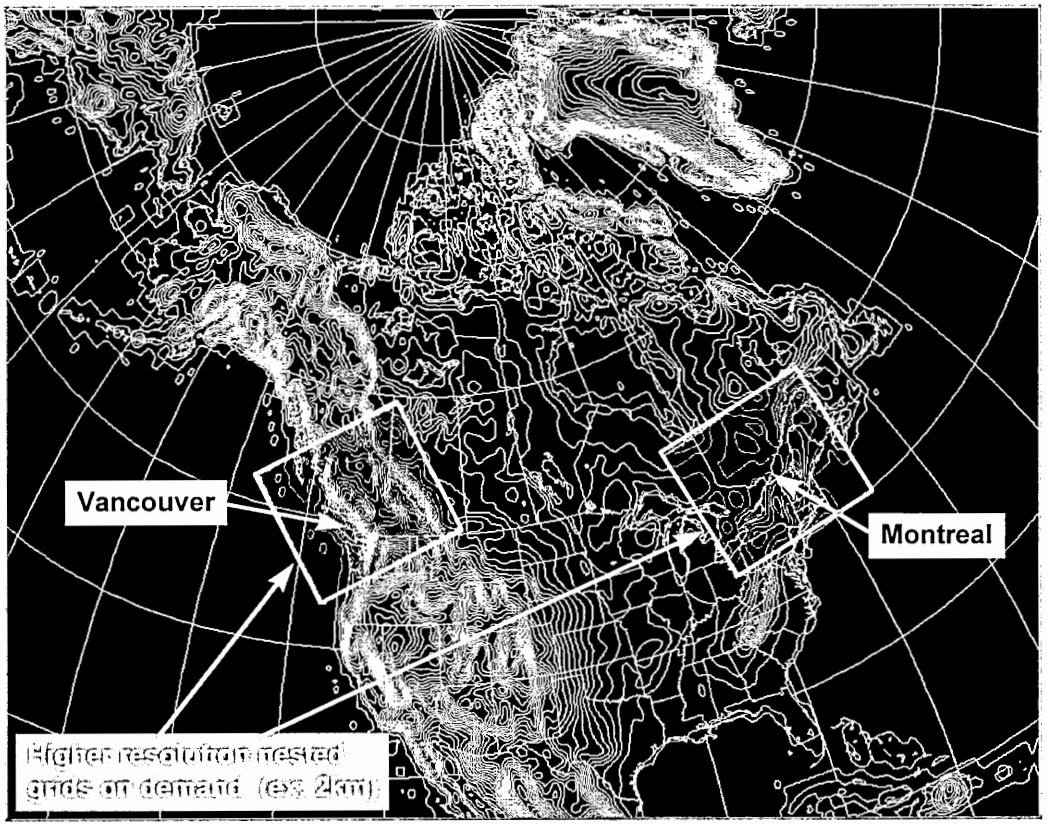

Figure 4.1 Target Grid for Regional 48H Forecast at 10 km using GEM-LAM

In view of these primary goals in mind, it becomes important to examine the possibility to establish if some form of "balanced" omega diagnostic equation exists at the mesoscale for instance. Without going into complex scaling arguments typical of previous theoretical studies on the possible balanced properties of mesoscale flows, we pose the problem

rather directly in terms of empirically studying summertime mesoscale systems as they emerge from mature runs with a "state-of-the-art" mesoscale forecast model.

It can already be expected that moist physics for instance will be necessary at these scales in the omega equation. In addition we expect that the relative importance of the terms in the omega equation will be quite different for the synoptic-scale (phenomena of length scales $150-1000\ km$) compared with the meso-β scale ($15-100\ km$). We propose here to determine if a nonlinear balance (hereafter referred to as NLB) omega equation can be deduced and to what extent it can be used to diagnose mesoscale vertical motions in a simulated real case using a multi-nested mesoscale model (resolutions of $1-15\ km$). Also, the relative importance of the various terms in the NLB omega equation will be assessed. It is important to mention that the diagnosed mesoscale vertical motion from the omega equation represents the effect of the diabatic heating on the vertical motion at scales larger than the individual convective elements whose vertical motion is driven by local buoyancy. An attempt to validate the diagnosed nonlinear balance omega vertical motion is also performed using a specially designed method (through divergent winds). This method uses a set of experiments, which can assess the importance of information derived from divergent winds in the analysis of a forecast in convective situations. The experiments are initialized using a 5h forecast of a pilot model at the same resolution, but with divergent winds derived from either the 5h forecast of the pilot model or from a diagnostic of nonlinear balance using the diabatic temperature tendencies as forcing. These simulations are also compared against a simulation using zero wind divergence.

The numerical model and simulations are described in section 4.2 along with the nonlinear balance omega equation. The case study is presented in section 4.3. The accuracy of the NLB omega diagnostics, calculated with the model's convection-induced temperature tendencies, along with comparisons against digitally-filtered and unfiltered omega vertical motion and the experiments on divergent winds, are discussed in section 4.4.

4.2 Methodology

4.2.1 Nonlinear Balanced equations

Our approach here doesn't make a-priori scaling assumptions to derive balance conditions but rather estimates a-posteriori the relevant scaling that prevails. Our objective is to characterize the balance of terms that may exists under summertime mesoscale convection in view of possible diagnostic relationships that could be used for advanced variational atmospheric data assimilation at such spatial and temporal resolutions.

It can be shown (see appendix) that an omega equation can be derived using the equations of motion, energy, ideal gas and continuity by only using the hydrostatic approximation (and neglecting the term involving directly β). The resulting equation takes the form:

$$\begin{aligned}\frac{R}{p}\nabla^2 S\omega + f(f+\zeta)\frac{\partial^2\omega}{\partial p^2} - f\omega\frac{\partial^2\zeta}{\partial p^2} - f\frac{\partial}{\partial p}\left[\frac{\partial\omega}{\partial x}\frac{\partial v}{\partial p} - \frac{\partial\omega}{\partial y}\frac{\partial u}{\partial p}\right] \\ = -\frac{R}{p}\nabla^2\left[-\vec{V}\cdot\vec{\nabla}T\right] - \frac{R}{p}\nabla^2\frac{\dot{q}}{c_p} - f\frac{\partial}{\partial p}\left[-\vec{V}\cdot\vec{\nabla}(f+\zeta)\right] \\ - f\frac{\partial}{\partial p}\left[\vec{k}\cdot\vec{\nabla}\times\vec{F}\right] + f\frac{\partial}{\partial p}\left[\frac{\partial\zeta_{ag}}{\partial t}\right] \quad (4.1)\end{aligned}$$

All the symbols have their usual meteorological meaning (e.g., Holton, 1992, p. 476-479) except for $\vec{F}$ which represents frictional forcings. Such an equation was used for diagnostic studies in the past for instance by Pauley and Newman (1992) and Räisänen (1995) at synoptic scales. We use (4.1) for mesoscale conditions.

The last right-hand side term of equation (4.1), $f\frac{\partial}{\partial p}\left[\frac{\partial\zeta_{ag}}{\partial t}\right]$, must be evaluated. The methodology used to evaluate this term involves an iterative procedure, described as follows. First, equation (4.1) is solved to get ω_b^1 using the approximation:

$$\frac{\partial\zeta_{ag}}{\partial t} = 0 \quad (4.2)$$

where the subscript b stands for balance (for reasons that will become clear later) and the superscript 1 identifies the first iteration. Once ω_b^1 is known, the following definition

is used:

$$\frac{\partial \zeta_{ag}}{\partial t} = \frac{\partial \zeta}{\partial t} - \frac{\partial \zeta_g}{\partial t} \tag{4.3}$$

where ζ_{ag}, ζ, and ζ_g are the ageostrophic, relative and geostrophic vorticities, respectively. The term $\frac{\partial \zeta}{\partial t}$ is evaluated using the complete vorticity tendency equation:

$$\left.\frac{\partial \zeta}{\partial t}\right|_b = -\vec{V}\cdot\vec{\nabla}(f+\zeta) + (f+\zeta)\frac{\partial \omega_b^1}{\partial p} - \omega_b^1\frac{\partial \zeta}{\partial p} - \left(\frac{\partial \omega_b^1}{\partial x}\frac{\partial v}{\partial p} - \frac{\partial \omega_b^1}{\partial y}\frac{\partial u}{\partial p}\right) + \left(\vec{k}\cdot\vec{\nabla}\times\vec{F}\right) \tag{4.4}$$

where it is assumed that vorticity is a balanced quantity. The term $\frac{\partial \zeta_g}{\partial t}$ remains to be evaluated. Using the geostrophic wind definition:

$$\vec{V_g} = \frac{1}{f}\vec{k}\times\vec{\nabla}\phi, \tag{4.5}$$

and applying the rotational operator $\left(\vec{k}\cdot\vec{\nabla}\times\right)$ to equation (4.5) gives:

$$\zeta_g = \frac{1}{f}\nabla_h^2\phi - \frac{1}{f^2}\beta\frac{\partial \phi}{\partial y}, \tag{4.6}$$

where ∇_h^2 is a horizontal laplacian operator and the Coriolis parameter is assumed only a function of the y coordinate. Applying $\frac{\partial}{\partial t}$ to (4.6) gives:

$$\frac{\partial \zeta_g}{\partial t} = \frac{1}{f}\nabla_h^2\left(\frac{\partial \phi}{\partial t}\right) - \frac{1}{f^2}\beta\frac{\partial}{\partial y}\left(\frac{\partial \phi}{\partial t}\right). \tag{4.7}$$

Unfortunately for horizontal scales considered here, the terms involving $\frac{\partial \phi}{\partial t}$ cannot be evaluated directly using numerical model data because of numerical problems, which are related, in part, to the fact that ϕ reacts very rapidly to gravity waves propagation, which is not the case with ζ and $\frac{\partial \zeta}{\partial t}$ (not shown). To overcome these problems, the following methodology is used. We start with the complete divergence equation, which can be derived by taking the divergence of the basic horizontal equations of motion. We thus have:

$$\frac{\partial D}{\partial t} + \nabla^2\phi - f\zeta + D^2 - 2\left[\frac{\partial u}{\partial x}\frac{\partial v}{\partial y} - \frac{\partial u}{\partial y}\frac{\partial v}{\partial x}\right] + \vec{V}\cdot\vec{\nabla}D + \frac{\partial f}{\partial y}u - \frac{\partial f}{\partial x}v + \omega\frac{\partial D}{\partial p} + \left[\frac{\partial \omega}{\partial x}\frac{\partial u}{\partial p} + \frac{\partial \omega}{\partial y}\frac{\partial v}{\partial p}\right] - \vec{\nabla}\cdot\vec{F} = 0 \tag{4.8}$$

As a first approximation, keeping only the rotational part of the wind in (4.8) and using Helmholtz's decomposition of the wind to get Charney's (1955) equation:

$$\nabla^2\phi_b = f\nabla^2\psi + 2\Big[\frac{\partial^2\psi}{\partial x^2}\frac{\partial^2\psi}{\partial y^2} - \Big(\frac{\partial^2\psi}{\partial x\partial y}\Big)^2\Big] + \frac{\partial f}{\partial y}\frac{\partial\psi}{\partial y} + \frac{\partial f}{\partial x}\frac{\partial\psi}{\partial x} \tag{4.9}$$

Applying $\dfrac{\partial}{\partial t}$ to (4.9):

$$\nabla^2\Big(\frac{\partial\phi}{\partial t}\Big)\Big|_b = f\nabla^2\Big(\frac{\partial\psi}{\partial t}\Big) + 2\Big[\frac{\partial^2}{\partial x^2}\Big(\frac{\partial\psi}{\partial t}\Big)\frac{\partial^2\psi}{\partial y^2} + \frac{\partial^2\psi}{\partial x^2}\frac{\partial^2}{\partial y^2}\Big(\frac{\partial\psi}{\partial t}\Big) - 2\frac{\partial^2}{\partial x\partial y}\Big(\frac{\partial\psi}{\partial t}\Big)\frac{\partial^2\psi}{\partial x\partial y}\Big] + \beta\frac{\partial}{\partial y}\Big(\frac{\partial\psi}{\partial t}\Big) \tag{4.10}$$

The ∇^2 operator can be inverted in (4.10) to evaluate $\dfrac{\partial\phi}{\partial t}\Big|_b$, and thus, $\dfrac{\partial\zeta_g}{\partial t}\Big|_b$ in (4.7) and $\dfrac{\partial\zeta_{ag}}{\partial t}\Big|_b$ in (4.3) can be estimated. The term $\dfrac{\partial\psi}{\partial t}$ is calculated using horizontal winds time tendencies. The boundary conditions used to invert the ∇^2 are $\phi\overline{f}^{-1}$ for (4.9) and $\dfrac{\partial\phi}{\partial t} = 0$ for (4.10). Once $\dfrac{\partial\zeta_{ag}}{\partial t}\Big|_b$ is known, it is put back into the omega equation (4.1) to evaluate ω_b^2. Only two iterations were found sufficient for convergence of iterative procedure. As will be shown in section 4.4, using only the time derivative of Charney's equation in (4.3) proves to be sufficient to significantly improve ω diagnosis for mature convective systems. A refinement of the procedure would be to keep all terms involving divergence in (4.8) as estimated for the current iteration; i.e. ω_b^k. This latter aspect is however not considered in the present study due to the sufficient accuracy obtained.

In the proposed iterative scheme, the omega equation (4.1) can exhibit problems when the ellipticity condition is not met, which is when:

$$S \leq 0 \tag{4.11}$$

or

$$\frac{RSf}{p}(\zeta + f) \leq \frac{f^2}{4}\Big|\frac{\partial V}{\partial p}\Big|^2 \tag{4.12}$$

To ensure convergence in these situations, the stability (S) and/or relative vorticity (ζ) are slightly modified (following Räisänen (1995, p. 2450)) when one or both conditions are met. Ellipticity classification is discussed in Mikhaïlov (1980). In the case discussed

here, a mean (per output timestep) of 9% of the points in the domain exhibited this problem and needed these modifications.

Going back to the mesoscale data assimilation problem, the full equation (4.1) may appear too complicated to use in a minimization context like the variational analysis approach, especially if it must be solved at each iteration in the mesoscale extension of F04's scheme. However, as will be demonstrated, by examining the a-posteriori magnitudes of all terms of (4.1), the full equation reduces to a very simple form that in principle is more practical and encouraging to use in a variational context.

4.2.2 Numerical model and simulations

Numerical simulations are performed using the Global Environmental Multiscale (GEM) model in its regional configurations (REG) (Côté et al., 1998) and Limited-Area (LAM) (Gravel et al., 2004; Erfani et al., 2005). The GEM-LAM is run for $6h$, using, as analysis, a $12h$ forecast of the GEM-REG valid on July 7th 2004 at 12 UTC. The LAM model grid has 564 x 494 horizontal grid points with 58 vertical levels, with a resolution of 2.5 km using an integration time step of 1 minute. Convection is explicit and the model is non-hydrostatic. The LAM horizontal boundary conditions are updated every hour. A 3h cutoff time digital filter is used for initialization of the LAM model to ensure that gravity waves resulting from the initial conditions do not contaminate the forecast. The model simulation is output every 5 min.

To assess the impact of the initial divergent winds on the forecast, as well as to assess the usefulness of the diagnosed balanced divergent winds, additional experiments were designed. These experiments are summarized in Table 4.1, where a LAM2 domain is nested within the the LAM domain described above. The LAM2 domain is centered in the LAM domain and 3D grid points in both domains are colocated. The dimensions are 534x464, which is smaller than the LAM pilot grid for nesting purposes. No digital filter is used in these LAM2 simulations. The analysis used for these LAM2 simulations is the LAM $5h$ forecast, valid at 17 UTC, except for the divergent winds. Hence, ther-

modynamics (temperature and humidity) as well as pressure and rotational winds are from the LAM $5h$ forecast (no microphysics fields are available in the analysis). The LAM2 simulations are initialized at 17 UTC, and the LAM simulation is used as the pilot model. The nonlinear balance diagnostics of the divergent winds use explicit diabatic temperature tendencies from the pilot LAM simulation (perfect case), combined with pressure, rotational wind, temperature and moisture of the LAM2 (adiabatic) analysis.

Table 4.1 Configurations for special divergent wind experiments

Experiment	Divergent Winds
LAM2S1	From pilot LAM (reference)
LAM2S2	From Nonlinear Balance Diagnostics of pilot LAM
LAM2S3	Set to zero

4.2.3 Evaluating diagnostics of balanced omega

The accuracy of the vertical motion from the nonlinear balance (NLB) omega equation is evaluated by comparison with the model's vertical motion for (a) ensembles of rapidly developing storm cells as well as for (b) ensembles that have lasted for a longer period. In these latter areas the accuracy of the diagnostics of the NLB vertical motion can be assessed by a comparison with the model's vertical motion.

For comparisons and calculations, the output of the LAM simulation, which is internally horizontally filtered by using cubic splines, is first vertically interpolated to 20 vertical pressure levels (50 to 1000 hPa with an interval of 50 hPa), then temporally interpolated between the output time steps (every 5 min.), and finally horizontally filtered using a Shuman numerical filter which removes wavelengths equal to or less than $5\triangle x$. This filtered model output is then used in the NLB omega equation, which is solved iteratively using sequential over-relaxation and whose results are then filtered again using the same Shuman filter. This latter filtering was necessary because the calculations in (4.1) are quite sensitive to numerical noise generated by the high order spatial derivatives. It is

to be noted that a careful examination of the filtering effects revealed that the most important filtering processes are the time interpolation and the $5\triangle x$ Shuman filter on NLB diagnostics output. Other filters have very limited impact (results not shown). The digital filter initialization is of widespread use in variational analysis schemes for synoptic scales at operational centers referred to in section 4.1. Because of clear separation of timescales between the gravity wave "noise" and synoptic scale "signal", the use of Huang and Lynch's (1993) digital filter approach is justified and very efficient. At mesoscale however, it is clear that an overlap of these timescales exists and, except by significantly reducing the cutoff period, its application needs to be revisited. For these reasons, our NLB vertical motions will also be compared to digitally filtered vertical motions (3h time span for both 3h and 1h cutoff periods), as well as against the unfiltered model's vertical motion.

4.3 Case Study description

The case studied (July 7, 2004) was a region of very weak pressure and temperature gradients within a very weak surface low-pressure system over the middle Mississippi Valley and adjacent states, where deep convection has occurred (figure 4.2). This weak low-pressure region was connected to a weak trough from a low-pressure centre over the Great Lakes. There was also a weak temperature gradient and high humidity value in the region where convection was initiated later in the simulation. Horizontal winds at the surface were light, while in the rest of the troposphere they were on the order of 10 to 20 m/s with some maxima on the order of 25 m/s in the upper troposphere. Several mesoscale "fronts" (significant humidity, pressure and temperature gradients over small distances) developed during the integration and one of these mesoscale "front" was associated with very strong convection.

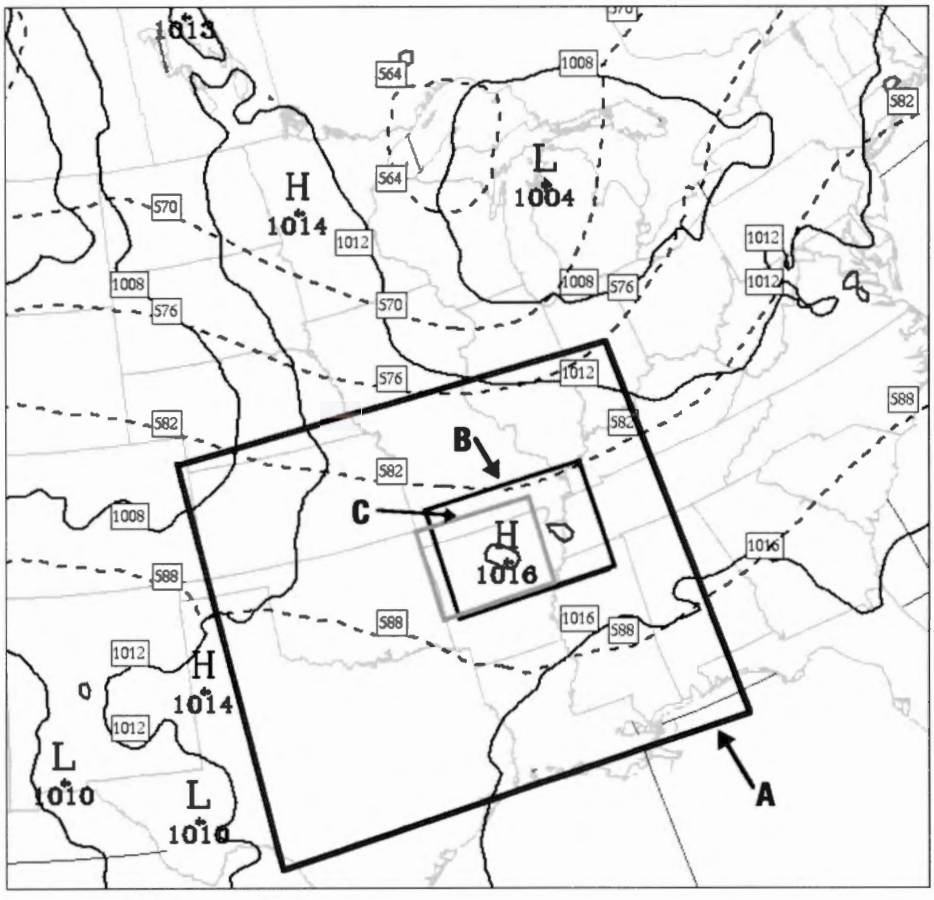

Figure 4.2 A portion of the GEM-REG pilot model domain is shown, along with Mean Sea-Level pressure (solid) and Geopotential Height at 500 hPa (dashed). This is a 17h forecast valid at 17 UTC July 7th 2004. GEM-LAM domain is highlighted (A), along with regions of interest, referenced thereafter (B and C).

4.4 Results and discussions

4.4.1 Importance of information from divergent winds on convection evolution

As a simple illustration of the impact of divergent wind information on convection evolution, three numerical simulations have been designed. One of the simulation is using the nonlinear balance diagnosed divergent part of the winds in the analysis, while the other is using the pilot model (reference), and another one has zero divergent winds (see table 4.1). The vertical motions as output from these simulations are then compared.

The LAM2S2 simulation (balanced divergent winds), when compared to the LAM2S1 reference simulation, shows that the regions of significant upward vertical motion are slightly displaced spatially, and that this displacement increases slowly with time. The vertical motion's 3D structure is quite similar (see figure 4.3), even at the smallest scales, which is confirmed by a mean correlation of 0.70 after 45 min. of simulation (0.83 after 30 min.).

On the other hand, the LAM2S3 simulation (zero divergent winds) shows that convection is generated correctly in the first minutes of integration, but that after 20 minutes the 3D structures and the regions affected by convection are very different from the reference simulation (see dashed lines compared to solid lines of figure 4.4 vs figure 4.3). Convection is also generated at different locations than that of the reference simulation. It is only at the largest scales that the coverage and intensity of convection are spatially similar, but only for the first 30 min. of simulation. This is confirmed with the correlation against the reference run, which is only 0.13 after 45 min. (0.20 after 30 min.).

These results emphasize clearly the important role of divergent winds for the evolution of convection at these scales. Even when all the other pieces of information (temperature, moisture, rotational winds, pressure) are correctly taken into account, a lack of proper treatment of divergent winds can be detrimental. At synoptic scale, the ratio of the spin-up time of numerical models and the life time of meteorological systems which involve

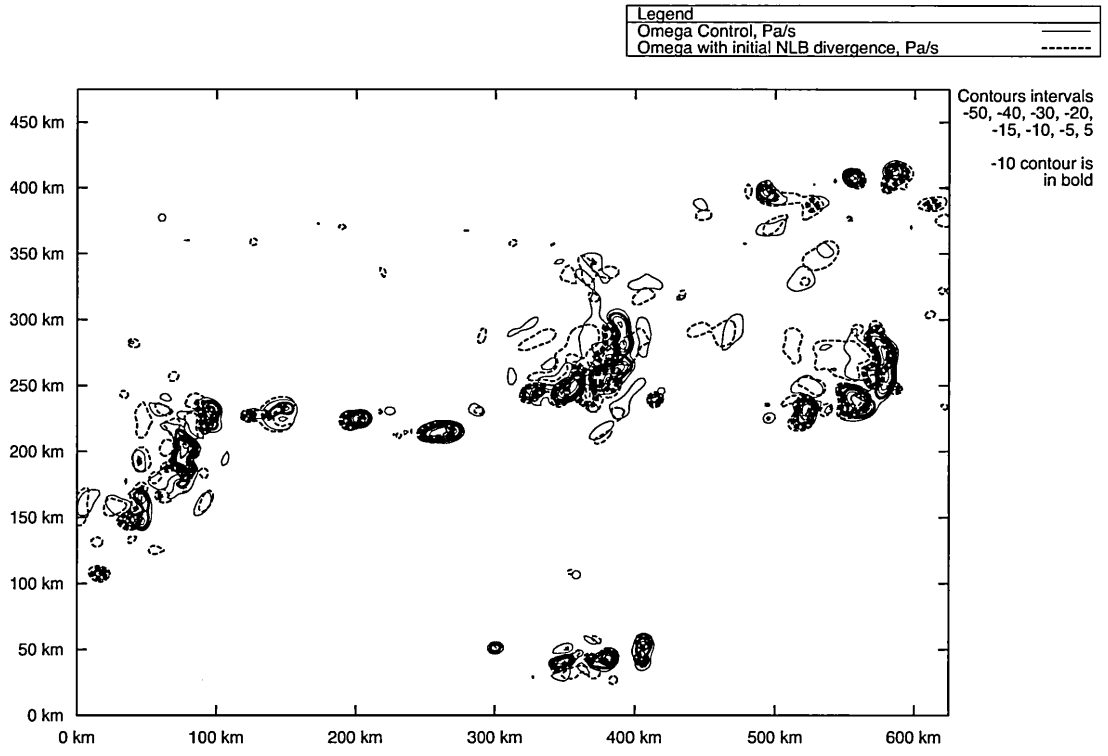

Figure 4.3 GEM-LAM Model LAM2S1 (solid) and LAM2S2 (dashed) vertical motions at 750 hPa over a subdomain of the model around the Mississipi Valley (region B highlighted in figure 4.2). Negative contours are dashed. 45 $min.$ forecast valid at 17h45 UTC July 7th. Contours -50 to 50 Pa/s are shown (interval 5).

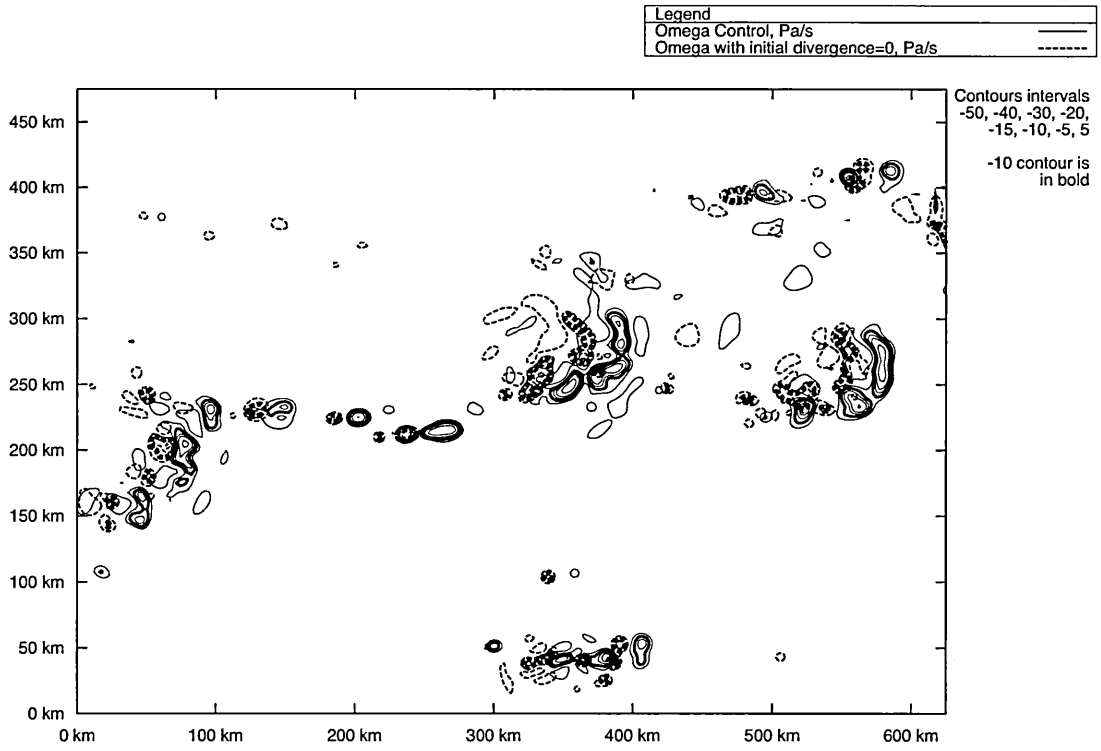

Figure 4.4 GEM-LAM Model LAM2S1 (solid) and LAM2S3 (dashed) vertical motions at 750 hPa over a subdomain of the model around the Mississipi Valley (region B highlighted in figure 4.2). Negative contours are dashed. 45 *min.* forecast valid at 17h45 UTC July 7th. Contours -50 to 50 Pa/s are shown (interval 5).

convection is quite small. On the contrary, at the scales examined here, this ratio is much larger because the life time of ensembles of convective cells is on the order of 45 minutes. This has drastic consequences for atmospheric data assimilation at the mesoscale. Often of secondary importance in treatment in the analysis scheme at synoptic scale, it now becomes of primary importance at mesoscale.

4.4.2 Accuracy of calculated balanced omega using model diabatic temperature tendencies

At 17 UTC, after $5h$ of integration, intense convection occurs throughout much of the LAM domain. Figure 4.5 shows the model's 750 hPa omega vertical motion superimposed on the NLB diagnosed omega vertical motion in a region of active convection (region B highlighted in figure 4.2). For the majority of convective ensembles (especially the older ones), the agreement between the model's and the nonlinear balanced omega vertical motion is very good. This is also confirmed by vertical cross-sections and profiles (figures 4.6 and 4.7). This means that the model vertical motion is nearly balanced even at these scales, and that the model's temperature tendencies due to convection (directly from the model's physics) can be used in the omega equation (4.1). For the period between 15:20 UTC and 18 UTC (between $3h20$ and $6h$ of integration), the mean correlation between the nonlinear and the model omega is 0.92, while the mean ratio of the root mean squares is 1.07. Other experiments have also been performed using the GEM-REG at 15 km resolution, which uses a parameterized convection scheme, and the results show a similar accuracy of the diagnosed balanced omega vertical motion (not shown). This latter result directly support F04's diabatic approach. We stress here that this result has important implications for variational data assimilation and particularly supports the methodology suggested by F04 to the extent that these physical time tendencies can be actually incorporated in the analysis procedure.

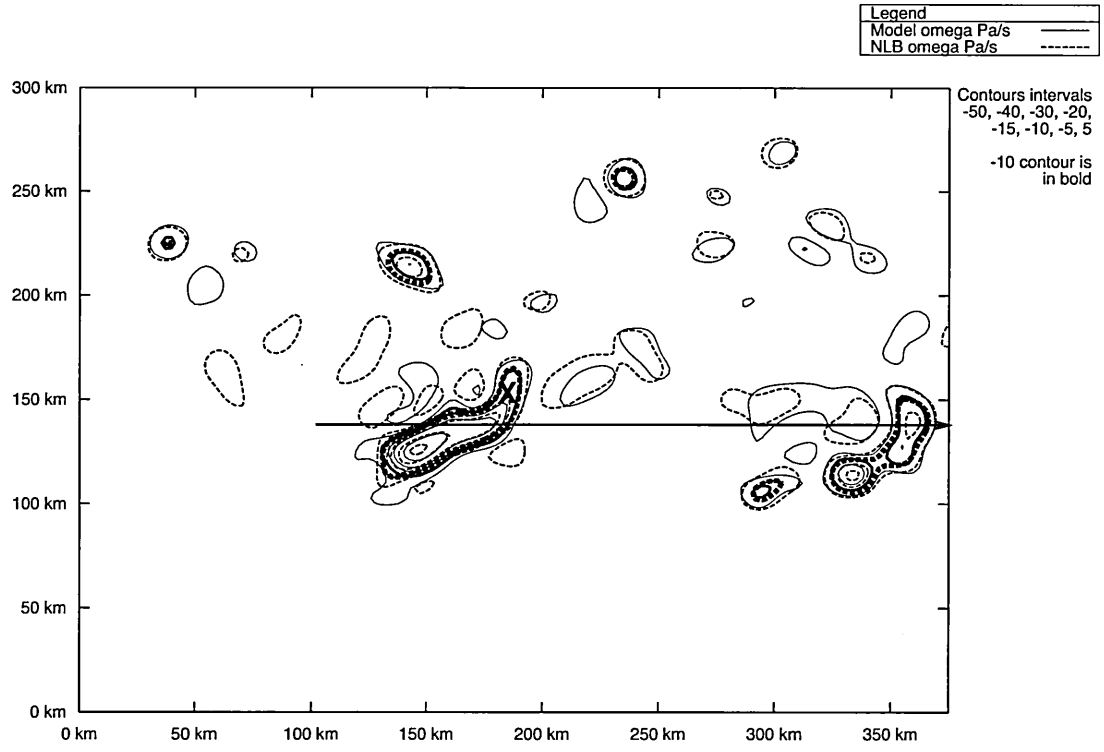

Figure 4.5 GEM-LAM Model (solid) and NLB diagnosed (dashed) vertical motions at 750 hPa over a subdomain of the model around the Mississipi Valley (region B highlighted in figure 4.2). Negative contours are dashed. $5h$ forecast valid at 17 UTC July 7th. Contours -50 to 50 Pa/s are shown (interval 5).

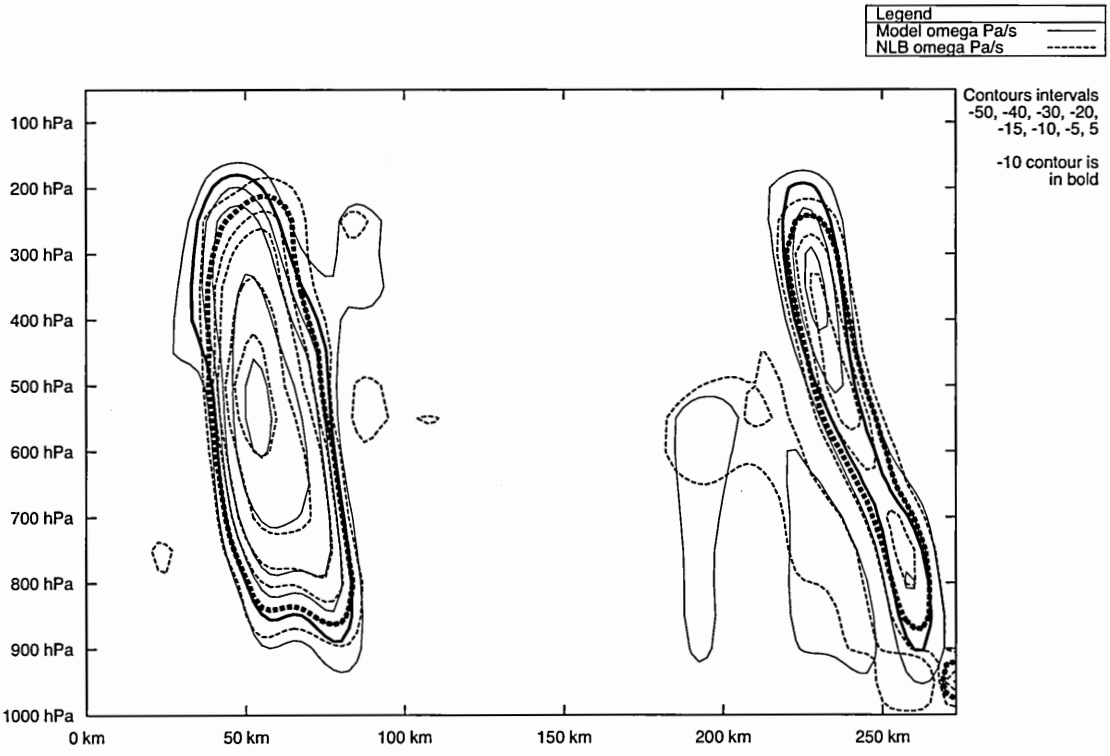

Figure 4.6 Same as fig. 4.5, but a vertical cross-section following the arrow on fig. 4.5.

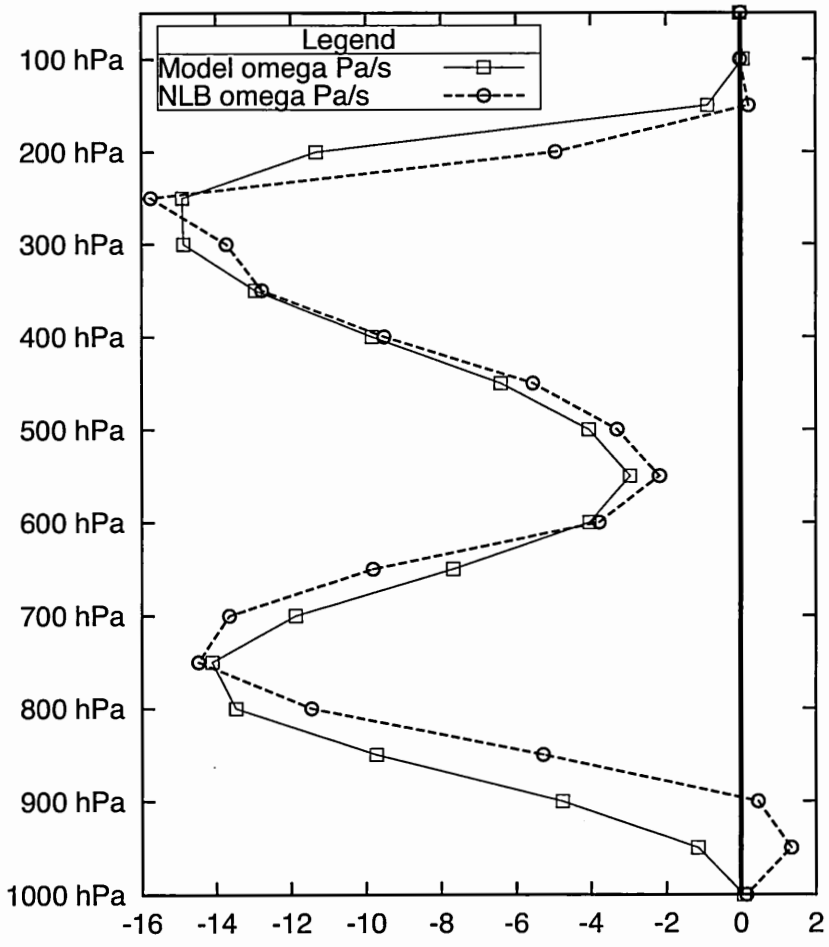

Figure 4.7 Same as fig. 4.5, but a vertical profile at X indicated in fig. 4.5. Horizontal axis is in Pa/s.

4.4.3 Discussion of nonlinear balance at these scales

With the exception of the forcing due to friction forcing (which was not neglected in the equation), the relative magnitudes of the left-hand and right-hand terms of the NLB omega equation (4.1) were evaluated at 17 UTC ($5h$ forecast). These magnitudes are shown in Table 4.2 for grid points where the NLB vertical motion has an absolute value of at least 5 Pa/s.

Table 4.2 Relative magnitude of the NLB omega equation terms using LAM simulation.

Nonlinear Balanced omega	
$\frac{R}{p}\nabla^2 S\omega$	10^{-11}
$+f(f+\zeta)\frac{\partial^2\omega}{\partial p^2}$	10^{-16}
$-f\omega\frac{\partial^2\zeta}{\partial p^2}$	10^{-16}
$-f\frac{\partial}{\partial p}\left[\frac{\partial\omega}{\partial x}\frac{\partial v}{\partial p}-\frac{\partial\omega}{\partial y}\frac{\partial u}{\partial p}\right]$	10^{-15}
$=-\frac{R}{p}\nabla^2\left[-\vec{V}\cdot\vec{\nabla}T\right]$	10^{-12}
$-\frac{R}{p}\nabla^2\frac{\dot{q}}{c_p}$	10^{-11}
$-f\frac{\partial}{\partial p}\left[-\vec{V}\cdot\vec{\nabla}(f+\zeta)\right]$	10^{-15}
$+f\frac{\partial}{\partial p}\left[\frac{\partial\zeta_{ag}}{\partial t}\right]$	10^{-12} at maximum

Clearly from (4.1), only the first left-hand-side term and the diabatic right-hand terms are dominant in regions of strong vertical motion.

$$\frac{R}{p}\nabla^2 S\omega = -\frac{R}{p}\nabla^2\frac{\dot{q}}{c_p}. \tag{4.13}$$

However, the Laplacian of temperature advection, as well as the ageostrophic tendency terms on the right-hand-side become significant in a few convective ensembles, accounting for as much as 20% of the total vertical motion. If follows that the inclusion of the balanced ageostrophic vorticity tendency term in the omega equation can improve the balanced vertical motion by as much as 20%.

These results raise the following questions. It has just been shown that balance, at

these scales, is mainly related to the divergent part of the wind. However, including the NLB ageostrophic vorticity tendency term in the omega equation, derived from the time tendency of the NLB equation (equation (4.9)), improves the results. Because the approximations needed to derive Charney's NLB equation should not be fulfilled at these horizontal and temporal scales (Holton, 1992, p. 383-388), why does the inclusion of the time tendency of Charney's NLB equation in the omega equation improves the results?

At these scales, the NLB vorticity tendency (4.4) is a good approximation of the model vorticity tendency, which is confirmed by figures 4.8 and 4.9, which are representative of the overall results. This is also confirmed by a mean correlation of 0.67 and a mean root mean square fraction of 0.84, over the forecast hours $3h20$ to $6h$ of the simulation and between the vertical levels 300 hPa to 800 hPa. However, the model's ageostrophic vorticity tendency is totally different from the NLB one, which means that the residue of the NLB equation is very significant. However, this doesn't imply that the NLB equation is not valid and cannot be used at these scales. Rather, this is because the model geopotential height is highly unbalanced, hence its height tendency also. Fortunately, it is possible to calculate a balanced height tendency using only the rotational part of the wind, which is less affected by unbalanced motions, using equations (4.3) to (4.10). Thus, using this methodology, it is possible to recover the balanced part of the model's height tendency, and, through the NLB equation, improves the NLB vertical motion representation. This is especially true at the center of very active ensembles of storm cells where the ageostrophic vorticity tendency term is more important. Finally, a methodology to recover the balanced temperature and height using the NLB equation, in a similar way as described above for its tendency, is also possible in theory.

4.4.4 Comparison of balanced vs. digitally filtered and unfiltered model vertical motion

As mentioned in the previous section, because of its important use in current synoptic-scale 3D-4D-Var at operational centers, we examine the use of digital filter technique in our context. In this section, a comparison will be made between the diagnosed balanced

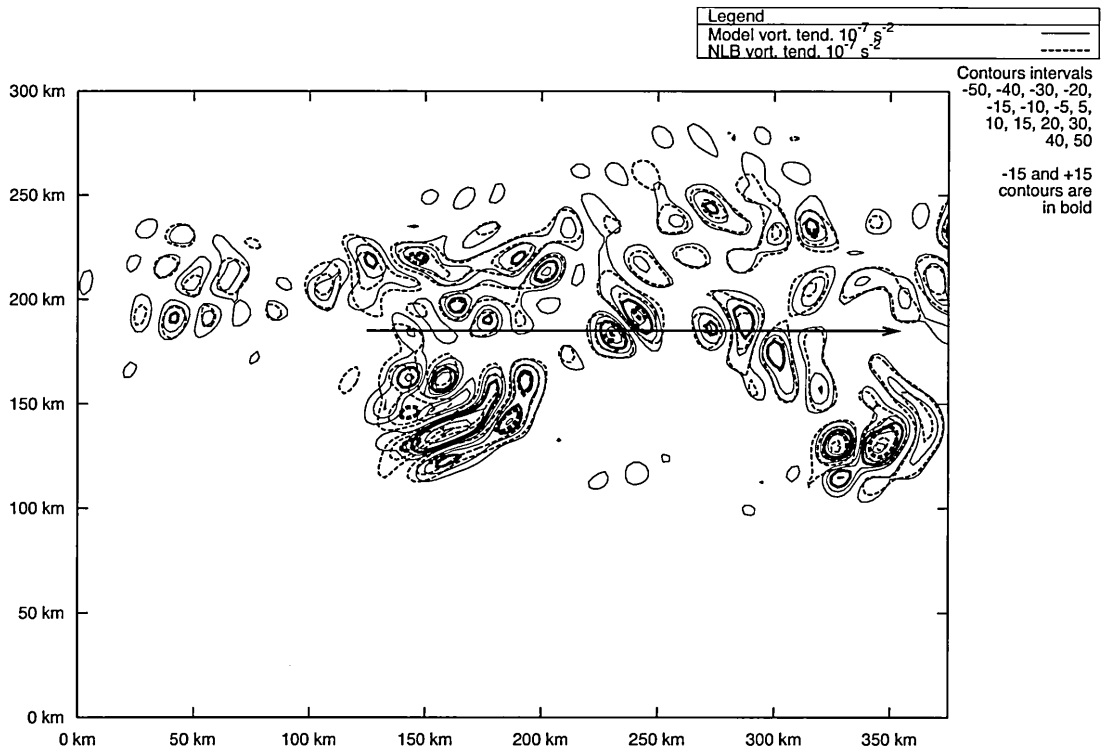

Figure 4.8 GEM-LAM Model (solid) and NLB diagnosed (dashed) vorticity tendency at 750 hPa over a subdomain of the model around the Mississipi Valley (region B highlighted in figure 4.2). $5h$ forecast valid at 17 UTC July 7th. Contour interval $5X10^{-7}s^{-2}$.

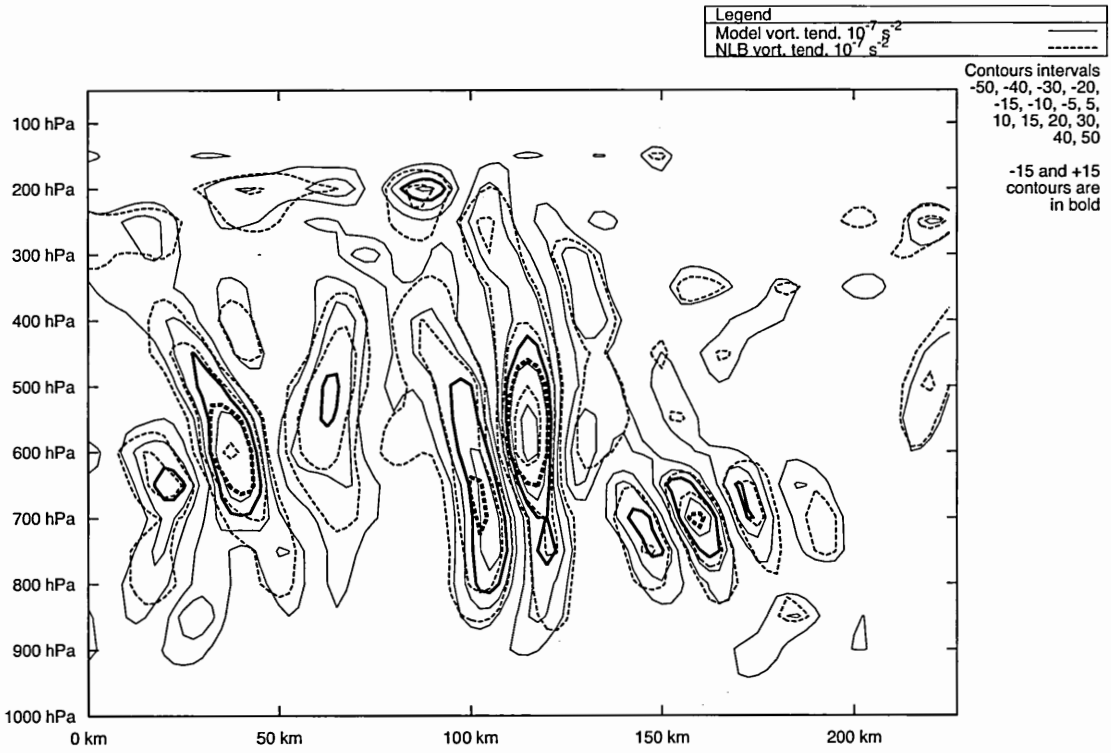

Figure 4.9 Same as fig. 4.8, but a vertical cross-section following the arrow on fig. 4.8.

vertical motion, filtered spatially using a $5\triangle x$ horizontal Shuman filter at 1.5 hours into the simulation, and vertical motion calculated using a digital filter with two different cut-offs ($1h$ and $3h$) as well as with the unfiltered instantaneous model vertical motion which, as previously mentioned, was spatially filtered internally using cubic splines.

It is to be noted that the effect of using the model's internal cubic spline filter, as well as using the Shuman filter, on model output prior to diagnostic calculations, are not very significant overall (not shown). They affect primarily the top (in the vertical) of diabatic temperature tendencies where the vertical gradients can be very large in some places.

A comparison, shown for region C highlighted in figure 4.2, between the balanced and 3-hour digitally filtered vertical motions (figures 4.10 and 4.11) shows that the latter is much weaker than the former and the spatial correlation is not very good (table 4.3). The unfiltered instantaneous vertical motion is, on the other hand, better spatially and vertically correlated (figures 4.12 and 4.13) with the balanced one. However the amplitudes are much larger, which is possibly the result of gravity wave oscillations and balance adjustments. Temporal animations (not shown) also reveal what are probably gravity wave signatures (especially in cell complex in the left part of the domain of figure 4.12). The use of $3h$ cutoffs, although justifiable for coarser grids simulations is here, as expected, not appropriate. The $1h$ cutoff digitally filtered vertical motion has a behavior between these two extremes, and it is better correlated (figures 4.14 and 4.15) with the balanced vertical motion than the 3h cutoff one. However the amplitudes are too weak. Table 4.3 shows the mean correlations and absolute mean values of these vertical motions and summarizes those results. It is clear from these results that the use of the NLB omega equation produces more accurate results than the digital filter used here.

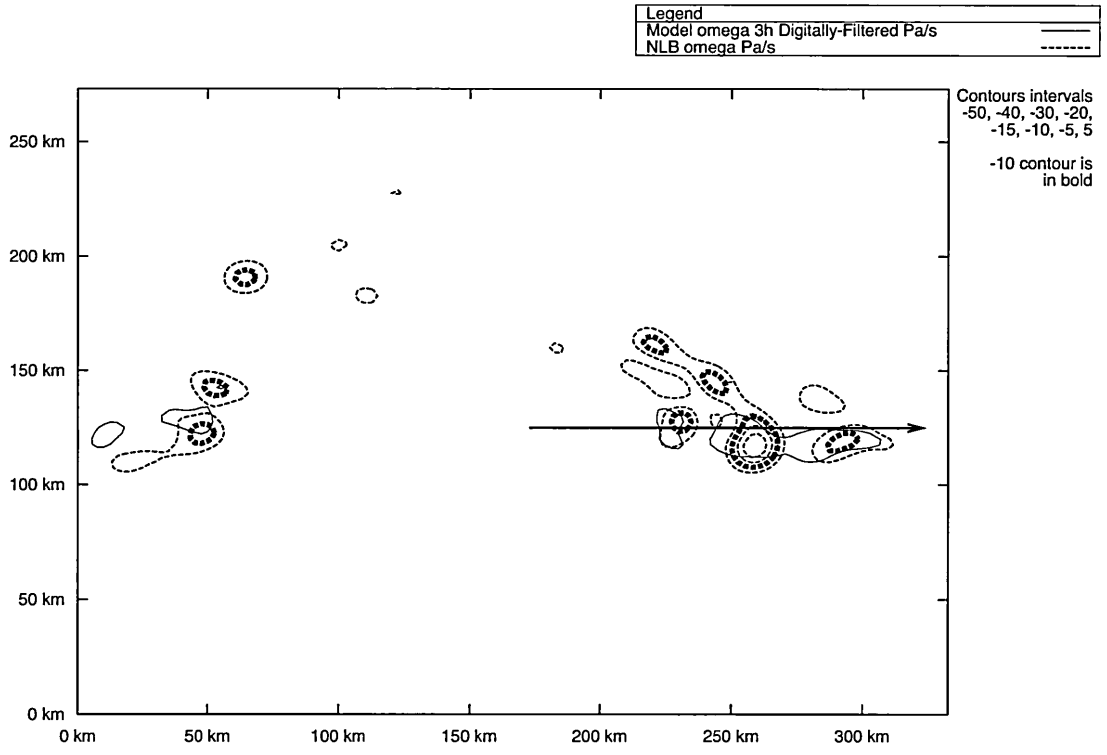

Figure 4.10 GEM-LAM Model digitally filtered $3h$ cutoff (solid) and NLB diagnosed (dashed) vertical motions at 750 hPa over a model subdomain (shown for region C highlighted in figure 4.2). Valid at 13:30 UTC July 7th, 2004 ($1h30$ forecast). Contours -50 to 50 Pa/s are shown (interval 5).

Table 4.3 Comparing vertical motions with NLB vertical motion: digitally filtered using 1h and 3h cutoff periods (3h time span) as well as not digitally filtered.

	Correlation	Ratio of mean RMS
Digital Filter 3h	0.70	0.56
Digital Filter 1h	0.84	0.97
No digital filter	0.87	1.28

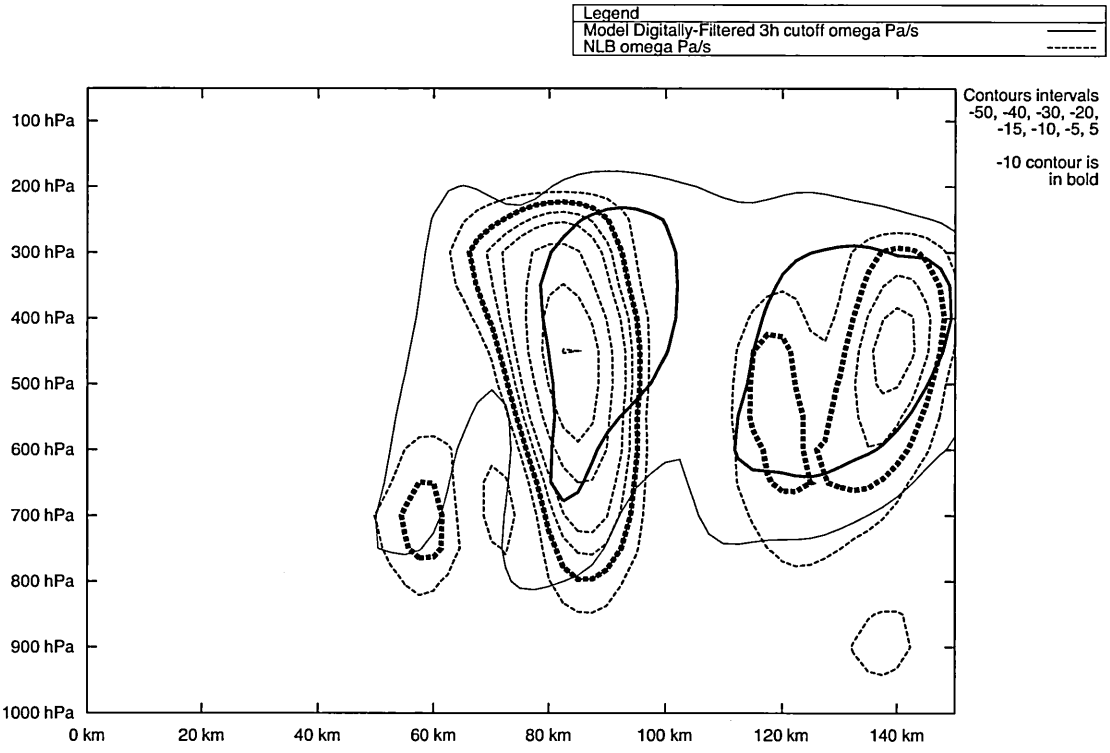

Figure 4.11 Same as fig. 4.10, but a vertical cross-section following the arrow on fig. 4.10.

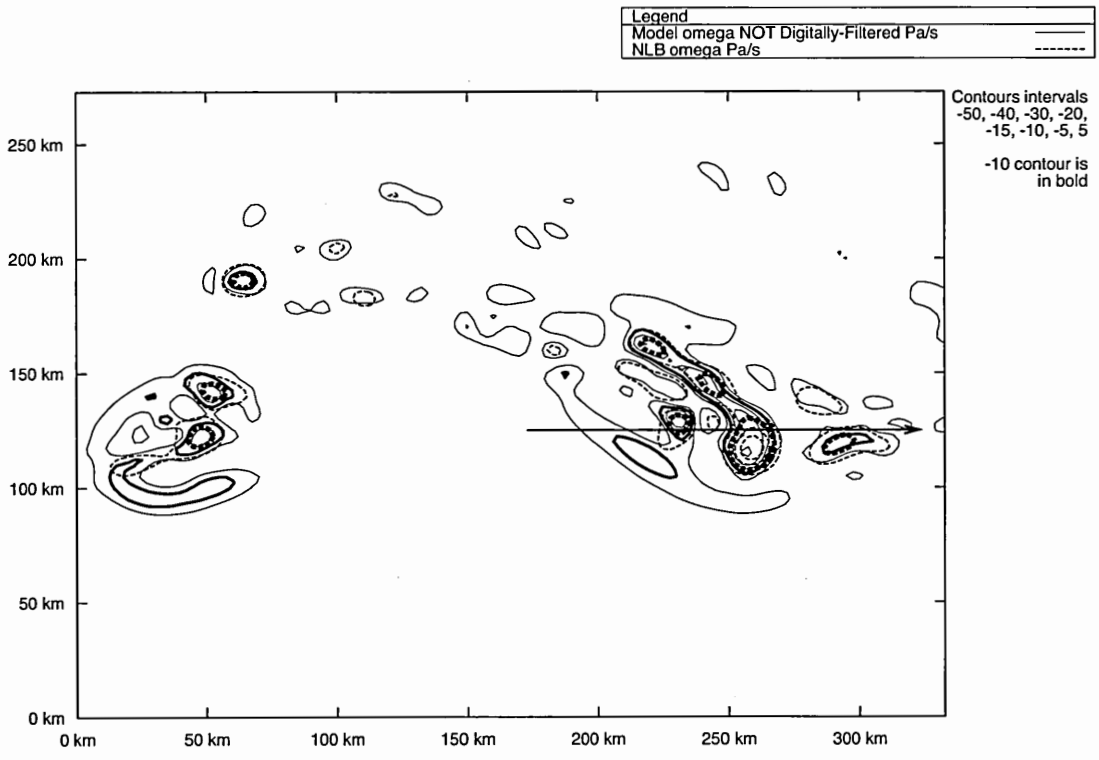

Figure 4.12 Same as fig. 4.10 except the model vertical motion is unfiltered.

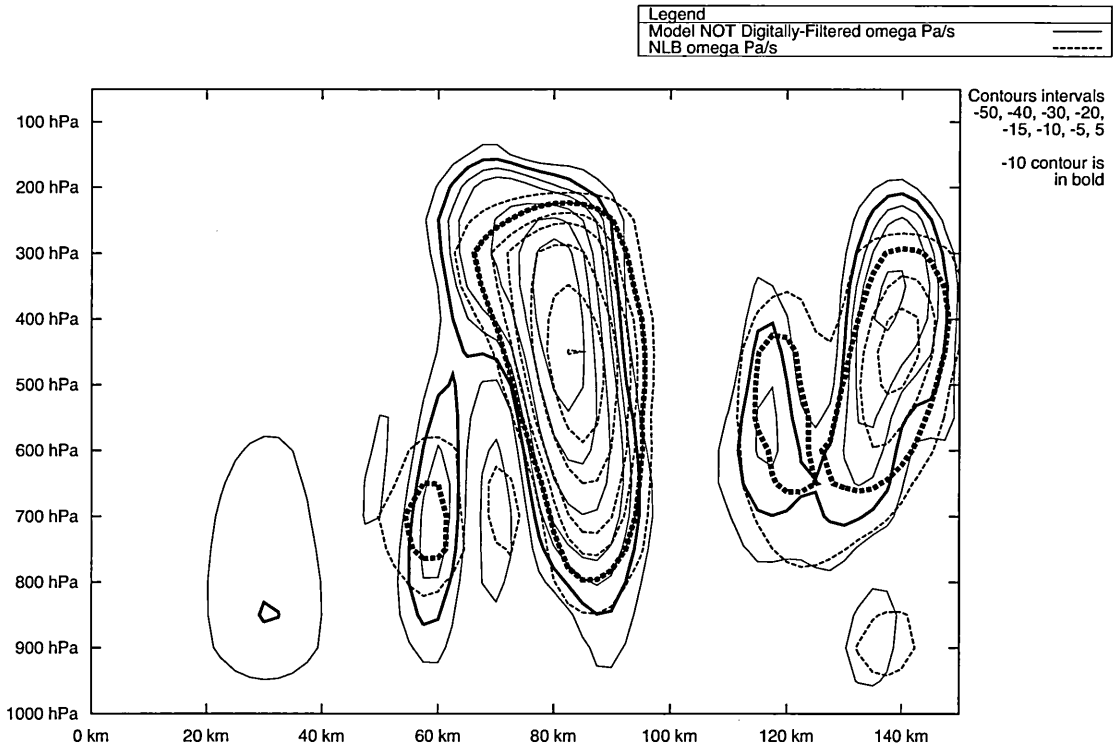

Figure 4.13 Same as fig. 4.12, but a vertical cross-section following the arrow on fig. 4.12.

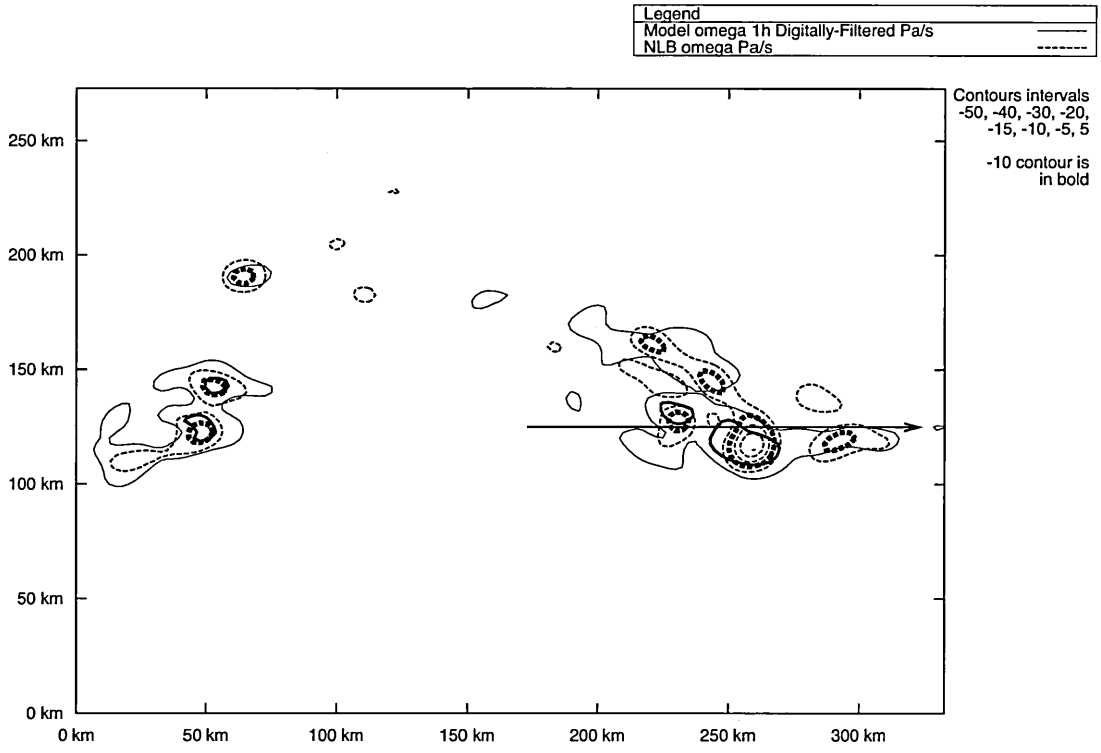

Figure 4.14 Same as fig. 4.10 except the model vertical motion is using a $1h$ cutoff digital filter.

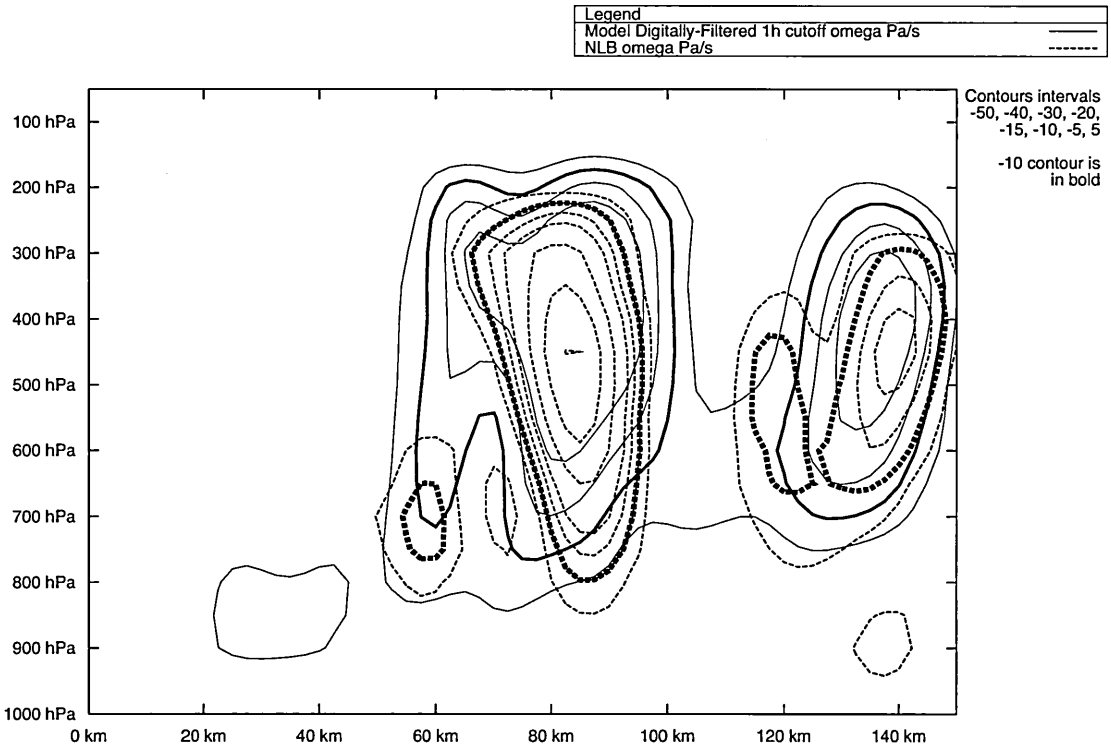

Figure 4.15 Same as fig. 4.14, but a vertical cross-section following the arrow on fig. 4.14.

4.5 Discussions and conclusions

Balance issues in variational data assimilation methods are a challenge at mesoscale (model resolutions of $1 - 10\ km$). It is true that the balance problem is not as critical in 4D-var vs 3D-var, because 4D-var methods can generate better balanced initial conditions. However, the poor accuracy of linearization of moist physical processes such as deep convection in 4D-var makes the approach presented here appealing. Currently, for mesoscale context (as can be judged from the last HIRLAM 2004 workshop in England), either a digital filter approach is used or these issues are simply not dealt with. It is of primary importance to address diabatic balance issues since balance provides the link between the model dynamics and physical processes. Balance may also help to sustain existing analyzed storm cells after initial time and reduce the propagation of unwanted gravity waves.

A set of experiments using the GEM-LAM pilot model, nonlinear balance and zero divergent winds showed that even with all the correct thermodynamics and dynamic fields as initial conditions, the accuracy of the divergent part of the wind is crucial. Nonlinear balance diagnostics with the methods presented in this paper were able to retrieve, from the other model's variables and the convective scheme, much of the needed divergent wind information with respect to the forecast of the evolution of convection.

The work presented here demonstrates that, for sustained summer convective circulations, an accurate diagnostic equation for ω can be used for meso-β scales (phenomena of $15 - 100\ km$ length scales). It also shows that in such cases, the numerical model's physical tendencies, through its diabatic temperature tendencies, can be used directly in a nonlinear balance omega equation to calculate a balanced omega vertical motion, and therefore, balanced horizontal divergent winds. This omega vertical motion is in dynamical balance with the model's diabatic temperature tendencies. Using a complete form of the omega equation (see (4.1)), results reveal that, in convective situations, only the first term on the left-hand side of the nonlinear omega equation is significant. On the right-hand side, apart from the Laplacian of diabatic temperature tendencies which

is the dominant term, the Laplacian of temperature advection and the ageostrophic vorticity tendency terms can be important (up to 20% of the total for the latter) in some regions, Overall however they are much smaller. The resulting ω-equation takes the simple form :

$$\nabla^2 S\omega = -\nabla^2 \left[-\vec{V} \cdot \vec{\nabla} T\right] - \nabla^2 \frac{\dot{q}}{c_p} + \frac{fp}{R} \frac{\partial}{\partial p} \left[\frac{\partial \zeta_{ag}}{\partial t}\right] \tag{4.14}$$

A comparison was made between balanced vertical motion with unfiltered model and digitally filtered vertical motion ($1h$ and $3h$ cutoff periods using a $3h$ time span and 1 min time steps ; i.e. 180 temporal points used in the filter). Results indicate that a $3h$ cutoff period is much too long for simulations using a horizontal resolution of 2.5 km. Although the amplitudes are still damped, a $1h$ cutoff for the digital filter is a good compromise because it retains most of the 3D structure. Unfiltered vertical motion has amplitudes that are much too large, which is probably a result of balance adjustments. Using a NLB omega equation, including as forcing the model's diabatic temperature tendencies, is an appealing alternative.

The case study presented here is almost purely convective. Hence this work should be extended to more cases, especially baroclinic cases and others that would involve significant upper atmosphere dynamics such as jets.

These results are very encouraging because it shows that even if diabatic temperature tendencies from the model's physics are very local and involve sharp gradients, they can be used to calculate a balanced vertical motion and therefore horizontal divergent winds, which are in dynamical balance with the model's physics. Spatial and temporal filtering are needed to achieve these results. This result is true at least for the chosen case study, for both explicit and parameterized convective schemes, at model resolutions ranging from 2.5 to 15 km.

Although results presented here have significant accuracy to be envisaged as a useful tool for balance constraint in mesoscale data assimilation schemes, increasing the vertical resolution as compared to the one used here (i.e. 20 vertical levels) can potentially bring higher accuracy of diagnosed vertical motion. We leave these aspects for a future study.

Acknowledgements. This work is part of the Ph.D. Thesis of the first author. Thanks are due to Amin Erfani, Sylvie Gravel and Michel Desgagné for GEM model support, as well as to Yves Chartier for help on several technical issues. This work was funded partially by the Canadian Foundation for Climate and Atmospheric Sciences (CFCAS).

4.6 Appendix: Complete omega equation derivation

Starting with the equation of motion in isobaric coordinates and in vectorial form:

$$\frac{d\vec{V}}{dt} + f\vec{k} \times \vec{V} + \vec{\nabla}_p \phi + \vec{F} = 0 \tag{4.15}$$

Expanding the total derivative gives:

$$\underbrace{\frac{\partial \vec{V}}{\partial t}}_{A} + \underbrace{\vec{V} \cdot \vec{\nabla}_p \vec{V}}_{B} + \underbrace{\omega \frac{\partial \vec{V}}{\partial p}}_{C} + \underbrace{f\vec{k} \times \vec{V}}_{D} + \underbrace{\vec{\nabla}_p \phi}_{E} + \underbrace{\vec{F}}_{F} = 0 \tag{4.16}$$

The operator $\vec{k} \cdot \vec{\nabla}_p \times$ is then applied to (4.16). We will develop each term separately. Now, let's develop term A:

$$\vec{k} \cdot \vec{\nabla}_p \times \frac{\partial \vec{V}}{\partial t} = \frac{\partial}{\partial t}\left(\vec{k} \cdot \vec{\nabla}_p \times \vec{V}\right) = \frac{\partial \zeta}{\partial t} \tag{4.17}$$

Now, developing term B: We must use the vectorial identity:

$$\left(\vec{V} \cdot \vec{\nabla}_p\right)\vec{V} = \frac{1}{2}\vec{\nabla}_p\left(\vec{V} \cdot \vec{V}\right) + \zeta\vec{k} \times \vec{V} \tag{4.18}$$

Term B can thus be given by:

$$\vec{k} \cdot \vec{\nabla}_p \times \left(\vec{V} \cdot \vec{\nabla}_p \vec{V}\right) = \frac{1}{2}\vec{k} \cdot \vec{\nabla}_p \times \left[\vec{\nabla}_p\left(\vec{V} \cdot \vec{V}\right)\right] + \vec{k} \cdot \vec{\nabla}_p \times \left(\zeta\vec{k} \times \vec{V}\right) \tag{4.19}$$

The first right-hand-side term goes to zero, and using the identity $\vec{\nabla} \times \vec{\nabla} A = 0$, term B can be expressed as:

$$\vec{k} \cdot \vec{\nabla}_p \times \left(\vec{V} \cdot \vec{\nabla}_p \vec{V}\right) = \vec{k} \cdot \vec{\nabla}_p \times \left(\zeta\vec{k} \times \vec{V}\right) \tag{4.20}$$

Using another vectorial identity:

$$\vec{\nabla} \times \left(\vec{A} \times \vec{B}\right) = \vec{A}\left(\vec{\nabla} \cdot \vec{B}\right) - \vec{B}\left(\vec{\nabla} \cdot \vec{A}\right) - \left(\vec{A} \cdot \vec{\nabla}\right)\vec{B} + \left(\vec{B} \cdot \vec{\nabla}\right)\vec{A} \tag{4.21}$$

Term B can thus be expressed as:

$$\vec{\nabla}_p \times (\zeta\vec{k} \times \vec{V}) = \zeta\vec{k}(\vec{\nabla}_p \cdot \vec{V}) - \vec{V}(\vec{\nabla}_p \cdot \zeta\vec{k}) - (\zeta\vec{k} \cdot \vec{\nabla}_p)\vec{V} + (\vec{V} \cdot \vec{\nabla}_p)\zeta\vec{k} \tag{4.22}$$

Re-arranging some terms and applying $(\vec{k} \cdot)$ to the equation, gives:

$$\vec{k} \cdot \vec{\nabla}_p \times (\zeta\vec{k} \times \vec{V}) = \vec{k} \cdot \vec{k}\zeta(\vec{\nabla}_p \cdot \vec{V}) - \vec{k} \cdot \vec{V}(\vec{\nabla}_p \cdot \zeta\vec{k}) - \vec{k} \cdot (\zeta\vec{k} \cdot \vec{\nabla}_p)\vec{V} + \vec{k} \cdot (\vec{V} \cdot \vec{\nabla}_p\zeta)\vec{k} \tag{4.23}$$

But, $\vec{k} \cdot \vec{V} = 0$. the final term B thus becomes:

$$\vec{k} \cdot \vec{\nabla}_p \times (\zeta\vec{k} \times \vec{V}) = \zeta(\vec{\nabla}_p \cdot \vec{V}) + (\vec{V} \cdot \vec{\nabla}_p\zeta) \tag{4.24}$$

Now, developing term C:

$$\vec{k} \cdot \vec{\nabla}_p \times \left(\omega\frac{\partial\vec{V}}{\partial p}\right) = \vec{k} \cdot \left[\vec{\nabla}_p\omega \times \frac{\partial\vec{V}}{\partial p} + \omega\vec{\nabla}_p \times \frac{\partial\vec{V}}{\partial p}\right] \tag{4.25}$$

Substituting the definition of vorticity ζ gives the final term C:

$$\vec{k} \cdot \vec{\nabla}_p \times \left(\omega\frac{\partial\vec{V}}{\partial p}\right) = \vec{k} \cdot \left[\vec{\nabla}_p\omega \times \frac{\partial\vec{V}}{\partial p}\right] + \omega\frac{\partial\zeta}{\partial p} \tag{4.26}$$

Now, developing term D, by expanding the term:

$$\vec{k} \cdot \vec{\nabla}_p \times (f\vec{k} \times \vec{V}) = \vec{k} \cdot [f\vec{k}(\vec{\nabla}_p \cdot \vec{V}) - \vec{V}(\vec{\nabla}_p \cdot f\vec{k}) - (f\vec{k} \cdot \vec{\nabla}_p)\vec{V} + (\vec{V} \cdot \vec{\nabla}_p)f\vec{k}] \tag{4.27}$$

Expanding, and eliminating terms involving $\vec{k} \cdot \vec{k}$ gives the final term D:

$$\vec{k} \cdot \vec{\nabla}_p \times (f\vec{k} \times \vec{V}) = f(\vec{\nabla}_p \cdot \vec{V}) + (\vec{V} \cdot \vec{\nabla}_p)f \tag{4.28}$$

The term E vanishes because of vectorial identity. Combining all terms A to F thus gives:

$$\frac{\partial\zeta}{\partial t} + \zeta(\vec{\nabla}_p \cdot \vec{V}) + (\vec{V} \cdot \vec{\nabla}_p\zeta) + \vec{k} \cdot \left[\vec{\nabla}_p\omega \times \frac{\partial\vec{V}}{\partial p}\right] + \omega\frac{\partial\zeta}{\partial p} + f(\vec{\nabla}_p \cdot \vec{V}) + (\vec{V} \cdot \vec{\nabla}_p)f + \vec{k} \cdot \vec{\nabla} \times \vec{F} = 0 \tag{4.29}$$

Re-arranging terms to express the vorticity equation in a familiar form, and omitting the p subscript to the $\vec{\nabla}$ operator, gives:

$$-(f + \zeta)\vec{\nabla}_p \cdot \vec{V} - \omega\frac{\partial\zeta}{\partial p} + \vec{k} \cdot \left(\frac{\partial\vec{V}}{\partial p} \times \vec{\nabla}\omega\right) = \frac{\partial\zeta}{\partial t} + \vec{V} \cdot \vec{\nabla}(f + \zeta) - \vec{k} \cdot \vec{\nabla} \times \vec{F} \tag{4.30}$$

Taking the vertical derivative $\frac{\partial}{\partial p}$ of the vorticity equation (4.30), and expanding the tilting-twisting term, gives:

$$-\frac{\partial}{\partial p}\Big[(f+\zeta)\vec{\nabla}\cdot\vec{V}\Big]-\frac{\partial\omega}{\partial p}\frac{\partial\zeta}{\partial p}-\frac{\omega\partial^2\zeta}{\partial p^2}-\frac{\partial}{\partial p}\Big(\frac{\partial\omega}{\partial x}\frac{\partial v}{\partial p}-\frac{\partial\omega}{\partial y}\frac{\partial u}{\partial p}\Big)= \\ \frac{\partial}{\partial p}\Big(\frac{\partial\zeta}{\partial t}\Big)+\frac{\partial}{\partial p}\big[\vec{V}\cdot\vec{\nabla}(f+\zeta)\big]-\frac{\partial}{\partial p}\big(\vec{k}\cdot\vec{\nabla}\times\vec{F}\big) \quad (4.31)$$

Using the continuity equation $\vec{\nabla}\cdot\vec{V}=-\frac{\partial\omega}{\partial p}$ and the definition of the geostrophic vorticity $\zeta=\zeta_g+\zeta_{ag}$ and $\zeta_g=\frac{1}{f}\nabla^2\phi$ gives:

$$\frac{\partial}{\partial p}\Big[(f+\zeta)\frac{\partial\omega}{\partial p}\Big]-\frac{\partial\omega}{\partial p}\frac{\partial\zeta}{\partial p}-\omega\frac{\partial^2\zeta}{\partial p^2}-\frac{\partial}{\partial p}\Big(\frac{\partial\omega}{\partial x}\frac{\partial v}{\partial p}-\frac{\partial\omega}{\partial y}\frac{\partial u}{\partial p}\Big)= \\ \frac{1}{f}\frac{\partial}{\partial t}\Big(\nabla^2\frac{\partial\phi}{\partial p}\Big)+\frac{\partial}{\partial p}\big[\vec{V}\cdot\vec{\nabla}(f+\zeta)\big]-\frac{\partial}{\partial p}\big(\vec{k}\cdot\vec{\nabla}\times\vec{F}\big)+\frac{\partial}{\partial p}\Big(\frac{\partial\zeta_{ag}}{\partial t}\Big) \quad (4.32)$$

Expanding the first two left-hand-side terms gives:

$$(f+\zeta)\frac{\partial^2\omega}{\partial p^2}-\omega\frac{\partial^2\zeta}{\partial p^2}-\frac{\partial}{\partial p}\Big(\frac{\partial\omega}{\partial x}\frac{\partial v}{\partial p}-\frac{\partial\omega}{\partial y}\frac{\partial u}{\partial p}\Big)= \\ \frac{1}{f}\frac{\partial}{\partial t}\Big(\nabla^2\frac{\partial\phi}{\partial p}\Big)+\frac{\partial}{\partial p}\big[\vec{V}\cdot\vec{\nabla}(f+\zeta)\big]-\frac{\partial}{\partial p}\big(\vec{k}\cdot\vec{\nabla}\times\vec{F}\big)+\frac{\partial}{\partial p}\Big(\frac{\partial\zeta_{ag}}{\partial t}\Big) \quad (4.33)$$

Using the hydrostatic approximation $\frac{\partial\phi}{\partial p}=-\frac{1}{\rho}$ and $\rho=\frac{p}{RT}$, and the thermodynamic equation $\frac{\partial T}{\partial t}=S\omega-\vec{V}\cdot\vec{\nabla}T+\frac{\dot{q}}{c_p}$, the equation becomes:

$$\frac{R}{pf}\nabla^2 S\omega+(f+\zeta)\frac{\partial^2\omega}{\partial p^2}-\omega\frac{\partial^2\zeta}{\partial p^2}-\frac{\partial}{\partial p}\Big(\frac{\partial\omega}{\partial x}\frac{\partial v}{\partial p}-\frac{\partial\omega}{\partial y}\frac{\partial u}{\partial p}\Big)= \\ \frac{R}{pf}\nabla^2\big(-\vec{V}\cdot\vec{\nabla}T\big)-\frac{R}{pf}\nabla^2\frac{\dot{q}}{c_p}+\frac{\partial}{\partial p}\big[\vec{V}\cdot\vec{\nabla}(f+\zeta)\big]-\frac{\partial}{\partial p}\big(\vec{k}\cdot\vec{\nabla}\times\vec{F}\big)+\frac{\partial}{\partial p}\Big(\frac{\partial\zeta_{ag}}{\partial t}\Big) \quad (4.34)$$

Finally multiplying by f, modifying the sign of the vorticity advection term, and re-arranging the terms gives the final complete omega equation:

$$\frac{R}{p}\nabla^2 S\omega+f(f+\zeta)\frac{\partial^2\omega}{\partial p^2}-f\omega\frac{\partial^2\zeta}{\partial p^2}-f\frac{\partial}{\partial p}\left[\frac{\partial\omega}{\partial x}\frac{\partial v}{\partial p}-\frac{\partial\omega}{\partial y}\frac{\partial u}{\partial p}\right] \\ =-\frac{R}{p}\nabla^2\left[-\vec{V}\cdot\vec{\nabla}T\right]-\frac{R}{p}\nabla^2\frac{\dot{q}}{c_p}-f\frac{\partial}{\partial p}\left[-\vec{V}\cdot\vec{\nabla}(f+\zeta)\right] \\ -f\frac{\partial}{\partial p}\left[\vec{k}\cdot\vec{\nabla}\times\vec{F}\right]+f\frac{\partial}{\partial p}\left[\frac{\partial\zeta_{ag}}{\partial t}\right] \quad (4.35)$$

Thus, this complete (primitive) omega equation can be derived using the equations of motion, energy, ideal gas and continuity by only using the hydrostatic approximation.

Bibliographie

Baer, F. and J. J. Tribbia, 1977 : « On complete filtering of gravity modes through nonlinear initialization ». *Mon. Wea. Rev.*, **105**, 1536–1539.

Charney, J., 1955 : « The use of the primitive equations of motion in numerical prediction ». *Tellus*, **7**, 22–26.

Côté, J., J.-G. Desmarais, S. Gravel, A. Méthot, A. Pantoine, M. Roch, and A. Staniforth, 1998 : « The operational CMC-MRB Global Environmental Multiscale (GEM) model. Part I : Design considerations and formulation. ». *Mon. Wea. Rev.*, **126**, 1373–1395.

Derber, J. D. and F. Bouttier, 1999 : « A reformulation for the background error covariance in the ECMWF global data assimilation system ». *Tellus*, **51**, 195–222.

Erfani, A., J. Mailhot, S. Gravel, M. Desgagnés, P. King, D. Sills, N. McLennan, and D. Jacob, 2005 : « The high resolution limited area version of the Global Environmental Multiscale model (GEM-LAM) and its potential operational applications ». *Preprints, 11th Conference on Mesoscale Processes, 24-28 October 2005*, Amer. Meteor. Soc., Albuquerque, NM, 1M.4.

Fillion, L., 2004a : « Balanced mass and moisture constraint in variational data assimilation ». *High Resolution Data Assimilation Workshop, 1-4 Km Resolution. HIRLAM Workshop, 15-17 Nov 2004*, HIRLAM, Exeter, UK.

———, 2004b : « Issues regarding the assimilation of precipitation. 6th international workshop on adjoint applications in dynamic meteorology ». *6th International Workshop on Adjoint Applications in Dynamic Meteorology, 24-28 May 2004*, Acquafredda di Maratea, Basilicata, Italy.

Fisher, M., 2003 : « Background error covariance modeling ». *Recent Developments in Data Assimilation for Atmosphere and Ocean*, ECMWF, Reading, UK, 45–63.

Gauthier, P., C. Charette, L. Fillion, P. Koclas, and S. Laroche, 1999 : « Implementation of a 3D variational data assimilation system at the Canadian Meteorological Centre. Part I : The global analysis ». *Appl. Opt.*, **37**, 103–156.

Gravel, S., A. Erfani, and U. Gramann, 2004 : « A comparison of an interactive and non-interactive approach to mesoscale forecasting using the IOP-2B of MAP ». *Preprints, 11th Conference on Mountain Meteorology and the Annual Mesoscale Alpine Program (MAP), 20-25 June 2004*, Amer. Meteor. Soc., Bartlett, NH, 17.4.

Holton, J. R., 1992 : *An introduction to dynamic meteorology*. Academic Press, Inc., 511 pp.

Huang, X.-Y. and P. Lynch, 1993 : « Diabatic Digital-Filtering Initialization : Application to the HIRLAM Model ». *Mon. Wea. Rev.*, **121**, 589–603.

Machenhauer, B., 1977 : « On the dynamics of gravity oscillations in a shallow water model with application to normal mode initialization ». *Contrib. Atmos. Phys.*, **50**, 253–271.

Mikhaïlov, V., 1980 : *Equations aux dérivées partielles*. Editions Mir, Moscou, 390 pp.

Parrish, D. F. and J. D. Derber, 1992 : « The National Meteorological Center spectral statistical interpolation analysis system ». *Mon. Wea. Rev.*, **120**, 1747–1763.

Pauley, P. M. and S. J. Newman, 1992 : « A comparison of quasigeostrophic and nonquasi- geostrophic vertical motions for a model-simulated rapidly intensifying marine extratropical cyclone ». *Mon. Wea. Rev.*, **120**, 1108–1134.

Räisänen, J., 1995 : « Factors affecting synoptic-scale vertical motions : A statistical study using a generalized omega equation ». *Mon. Wea. Rev.*, **123**, 2447–2460.

Temperton, C., 1988 : « Implicit normal mode initialization ». *Mon. Wea. Rev.*, **115**, 1013–1031.

CHAPITRE V

CONCLUSION GÉNÉRALE

Résumé

Cette recherche a permis principalement de développer une méthodologie appropriée pour caractériser l'état balancé dans les modèles numériques de prévision à méso-échelle pour des phénomènes météorologiques ayant un diamètre aussi petit que de l'ordre de 15 km, ainsi que d'utiliser des relations de balance dynamique dans les modèles numériques à une résolution horizontale de 2.5 km. Les *contributions* les plus importantes sont : l'identification précise de la suite des processus physiques impliqués dans l'ajustement vers un état balancé dans les modèles numériques en lien avec la théorie classique d'ajustement linéaire ; la caractérisation de l'état balancé à méso-échelle dans des simulation idéalisées ; la caractérisation de l'état balancé à méso-échelle dans un contexte de simulation réaliste d'un cas de convection profonde d'été ; l'importance de l'information apportée par les vents divergents pour les prévisions de précipitations à méso-échelle ; la démonstration qu'il est possible d'utiliser les tendances de température issues de la convection dans le modèle en combinaison avec l'équation de balance non-linéaire et une équation complète décrivant le mouvement vertical, afin de déterminer des vents divergents balancés ayant une bonne précision. Les limites de la recherche portent à la fois sur certains aspects des simulations idéalisées, sur la méthode d'évaluation des vents divergents balancés et sur le type de situation réelle présentée ici. Des études complémentaires permettraient d'approfondir quelques-unes des limites identifiées.

Abstract

The research proposes an appropriate methodology to characterize balanced state in numerical models for mesoscale meteorological phenomena that have a diameter as small as 15 km, as well as to utilize dynamical balance relationships in numerical models having a horizontal resolution of 2.5 km. The most important contributions of this work are: precise identification of the sequence of physical processes involved in the adjustment toward a balanced state in numerical models, with comparisons made with classical linear adjustment theory; the characterization of balanced state at mesoscale in idealized simulations; the characterization of balanced state at mesoscale in the context of realistic simulations of a strong summer convective case situation; determination of the importance of information brought by divergent winds for quantitative precipitation forecasts at the mesoscale; the demonstration that it is possible to use temperature

tendencies issued directly from the model convection in combination with the nonlinear balance equation and a complete vertical motion equation to calculate the balanced divergent winds with a good accuracy. The limits of the research deal with certain aspects of the idealized simulations, the method used to calculate the balanced divergent winds and the type of the simulated realistic case presented here. Further research may take into account some of these caveats.

5.1 Contributions

Dans un cadre général, la présente recherche a permis de caractériser l'état balancé à méso-échelle, dans les modèles numériques à résolution horizontale de l'ordre de 2.5 km, pour des systèmes météorologiques ayant un diamètre aussi petit qu'environ 15 km. C'est principalement la balance impliquant la partie divergente du vent qui a été caractérisée. Il a été montré qu'il est possible d'utiliser la théorie de balance non-linéaire, à cette échelle, en combinaison avec les tendances diabatiques de température issue du modèle numérique afin de fournir une information utile sur la balance dynamique du modèle. De plus, il a aussi été démontré que les parties divergente et balancée du vent est une information importante influençant la qualité des prévisions de précipitations à court terme et à méso-échelle dans une simulation numérique.

À la lumière des objectifs spécifiques initiaux, les retombées atteintes sont les suivantes :

D'une part, les mécanismes physiques impliqués dans le processus d'ajustement vers l'état balancé ont été précisément identifiés dans des simulations numériques idéalisées réalisées avec le modèle MRCC, et mis en relation avec la théorie classique d'ajustement linéaire, autant à l'échelle synoptique qu'à méso-échelle. Ceci permet de relier les mécanismes physiques de l'ajustement et la production d'ondes de gravité, prévues par la théorie classique. En modifiant certains paramètres des simulations, tels que la stabilité statique, la présence d'un vent de base, la latitude ainsi que la taille horizontale du réchauffement, leur influence sur l'état balancé et son ajustement a été examinée. Ainsi, lorsque la taille du réchauffement est de fine échelle, la latitude (force de Coriolis) n'a qu'une influence très limitée sur les mécanismes d'ajustement et sur l'état balancé. Aussi, le temps d'ajustement vers l'état balancé est très réduit par rapport aux simulations à plus grande échelle. De plus, la stabilité statique de l'atmosphère a une influence significative sur le temps d'ajustement ainsi que sur l'état balancé lui-même. En effet, une stabilité statique plus faible augmente significativement l'amplitude des oscillations et leur période.

D'autre part, l'étude d'un cas réel de convection profonde d'été, tel que simulé par le modèle GEM en mode aire limitée (résolution horizontale de 2.5 km), a permis de caractériser l'état balancé pour des ensembles convectifs ayant une taille de 15 à 100 km. Pour la situation étudiée ici, le type de balance à cette échelle est principalement relié à la divergence. Il a aussi été montré que l'information apportée par les vents divergents pour la prévision à court terme du mouvement vertical (et donc de la précipitation) est très grande. En effet, sans cette information, la prévision se dégrade très rapidement, même si tous les autres champs atmosphériques sont supposés parfaitement connus. Heureusement, il est possible de calculer les vents divergents balancés, à cette échelle, en utilisant une équation du mouvement vertical complète en combinaison avec l'équation de balance non-linéaire et en utilisant les tendances de température des processus diabatiques, directement issues du modèle numérique. Il faut signaler que seuls quelques termes de l'équation complète du mouvement vertical sont importants à cette échelle et pour le type de situation étudié. En effet, les termes du membre gauche de l'équation impliquant la force de Coriolis sont tous négligeables. Finalement, il a également été montré qu'en imposant une balance des vents divergents au temps initial d'une simulation numérique à petite échelle, calculés avec la méthodologie présentée dans la présente recherche, les prévisions de précipitations (évaluées par l'intermédiaire du mouvement vertical) sont remarquablement similaires à celles d'une simulation de contrôle.

Ce projet de recherche est innovateur tant au niveau de l'utilisation des relations impliquant une balance non-linéaire à petite échelle, que de l'utilisation des tendances de température issues directement de la convection du modèle dans des équations représentant un type de balance dynamique à cette échelle.

5.2 Applications

La recherche réalisée s'inscrit dans le cadre plus large de l'assimilation variationnelle de données à méso-échelle (résolution horizontale de 2.5 km), ainsi que des problèmes de balance dynamique anticipés au niveau de l'assimilation variationnelle de données de précipitations à cette échelle de même qu'à l'échelle synoptique. La caractérisation qui a

été réalisée permet de mieux comprendre les mécanismes d'ajustement vers un état balancé, pour des phénomènes de réchauffement de l'atmosphère d'un diamètre de l'ordre de 15 à 1500 km et ce, en relation et en accord avec la théorie classique d'ajustement. Les résultats présentés ici permettent donc de mieux appréhender la problématique de l'assimilation de données à méso-échelle, spécialement au niveau de l'assimilation des données de précipitations. Ces résultats montrent aussi que cette technique peut aussi être utilisée à l'échelle synoptique, où les problèmes d'assimilation de données de précipitations se posent également.

Par ailleurs, l'importance de l'information apportée par les vents divergents, au niveau des prévisions de précipitations, a été clairement démontrée lors d'une simulation d'un cas réel par le modèle GEM-LAM. L'approche, présentée ici, a montré qu'il est possible de restituer les vents divergents balancés en utilisant les tendances de températures, causées par les processus diabatiques, directement issues du modèle numérique. La précision des vents divergents balancés déterminés par cette approche est très satisfaisante. De plus, cette approche est avantageuse par rapport à l'utilisation d'un filtre digital, car notre approche récupère de l'information physique dans un contexte de balance non-linéaire, contrairement au filtre digital qui a une réponse purement mathématique dépendant seulement des fréquences des ondes présentes dans la simulation. La méthode présentée ici agit donc comme un filtre « physique » qui tient mieux compte de la physique des phénomènes. Cette méthode sera certainement reprise, et incorporée aux méthodes variationnelles d'assimilation de données 3D à méso-échelle.

5.3 Limites et extension de la recherche

Les limites de la recherche portent à la fois sur certains aspects des simulations idéalisées, de la méthode d'évaluation des vents divergents balancés et sur le type de situation réelle présentée ici.

La validité des résultats découlant des simulations idéalisées est limitée par le fait que seule la partie dynamique du modèle numérique MRCC a été utilisée. En effet, la partie

physique a été désactivée. Par conséquent, il n'y a pas d'interaction de l'atmosphère avec la surface, d'effet diurne, de processus micro-physiques, et l'atmosphère ne contient pas d'humidité. Cependant, les résultats obtenus doivent être analysés avec ces limites prises en considération. En effet, les simulations idéalisées ont été effectuées avec ces limites afin de mieux isoler la dynamique de l'ajustement pris isolément, et afin de permettre l'étude détaillée des mécanismes physiques en jeu dans un contexte simplifié. Les résultats obtenus lors de ces simulations idéalisées sont alors utiles pour la deuxième partie de la présente recherche, en autant que ces limites soient considérées.

D'autre part, la méthodologie de calcul des vents divergents balancés nécessite un ajustement artificiel de termes dans l'équation du mouvement vertical balancé de type elliptique à certains endroits dans le domaine de simulation. Cependant, cet ajustement a déjà été utilisé par Räisänen (1995), et, dans la présente recherche, n'a été appliqué que pour une moyenne de 9% des points de grille du domaine de simulation. Cependant, cette limite est peu importante car les termes en question sont plusieurs ordres de grandeur plus petits que les termes importants. De même, les équations utilisées sont définies sur des coordonnées verticales de pression, et non pas sur la coordonnée verticale du modèle. Ceci peut potentiellement introduire des erreurs si cette méthodologie est utilisée sur des régions où le relief est significatif. Il faudra alors ré-écrire ces équations et modifier cette méthodologie en travaillant directement avec les coordonnées du modèle numérique.

Une autre limite de cette recherche est que celle-ci ne permet pas de démontrer qu'il sera possible d'utiliser directement des observations directes du dégagement de chaleur latente dans une analyse variationnelle. La présente étude ne porte que sur la caractérisation de la balance entre un dégagement de chaleur latente estimé par la représentation de la convection telle que décrite par le modèle, selon la méthode de Fillion et al. (2005), mais à plus petite échelle (avec un modèle numérique de résolution horizontale de 2.5 km).

Finalement, le cas réel tel que simulé par le modèle GEM-LAM, est un cas d'atmosphère très convective, éloigné des zones baroclines, des forts gradients de pression et de courant-jets importants dans les hauts niveaux de l'atmosphère, et également sur une zone où le

relief est peu accentué. Par conséquent, les résultats obtenus au niveau du type de balance pour des systèmes météorologiques d'un diamètre de l'ordre de 15 à 100 km, ainsi qu'au niveau des vents divergents balancés, sont limités à ce type de situation météorologique. Pour compléter la présente recherche, la méthodologie employée ici devrait être appliquée à d'autres types de situations météorologiques et sur d'autres régions.

Bibliographie

Fillion, L., M. Tanguay, N. Ek, C. Pagé, et S. Pellerin, 2005 : « Balanced coupling between vertical motion and diabatic heating for variational data assimilation ». *The International Symposium on Nowcasting and Very Short Range Forecasting, WMO Workshop, 5-9 Sep 2005*, World Meteorological Organization, Toulouse, France.

Räisänen, J., 1995 : « Factors affecting synoptic-scale vertical motions : A statistical study using a generalized omega equation ». *Mon. Wea. Rev.*, **123**, 2447–2460.